# TABLE OF CONTENTS

# LIST OF FIGURES

## CHAPTER 5

# LIST OF TABLES

# CHAPTER ONE

# DEFINING THE PROBLEM

# CHAPTER 1

# DEFINING THE PROBLEM

## 1.1    INTRODUCTION

Aluminum alloys have been used in many high technology sectors such as automotive, marine and aerospace industries due to their exceptional properties. These properties comprise light weight due to the low density of aluminum, good formability, high corrosion resistance, high electrical and thermal conductivity, high stiffness and improved high temperature strength [1]. Pure aluminum is very soft and ductile and therefore cannot be used in applications that require high yielding strength, especially under high temperature conditions. The mechanical properties of aluminum alloys may be improved by means of addition of alloying elements or heat treatment, to increase the hardness, toughness or yield strength of these alloys [2].

Aluminum alloys are divided into two categories, wrought alloys and cast alloys. Among different foundry alloys, aluminum casting alloys are very popular, as they have the highest castability ratings, possess good fluidity and comparably low melting points. For these reasons, cast iron and steel components are being increasingly replaced by aluminum alloys, particularly in the automotive industry. Choosing one casting alloy over another tends to be determined by the relative ability of the alloy to meet one or more of the characteristics required for a specific application [4].

Aluminum-silicon (Al-Si) alloys are the largest group of cast aluminum alloys and constitute 85% to 90% of all aluminum castings. Addition of Si increases the fluidity and

decreases solidification shrinkage; Si increases the strength and stiffness, but reduces the ductility. Depending on the silicon content, Al-Si alloys are divided into three groups: hypoeutectic alloys with a Si content of between 5 and 10%, eutectic alloys with 11-13% Si, and hypereutectic alloys, with a Si content of between 14 and 20% [6]. Silicon has a lower density compared to aluminum, and is one of the few elements which may be added to it without the loss of a weight advantage [5].

Aluminum-copper (Al-Cu) casting alloys are characterized by their superior strength and excellent ductility. The copper content of Al-Cu casting alloys is usually 4wt% to 8wt% which makes them expensive alloys. As a result of the elevated density of Cu, 8.92 g/cm3, the high Cu content of Al-Cu alloys increases the weight of the cast parts manufactured from these alloys, thereby leading to increased fuel consumption. Also, copper has a significant impact on the strength and hardness of aluminum castings at both ambient and elevated temperatures. The mechanical properties of these alloys may be improved via age hardening through the formation of $Al_2Cu$ precipitates following aging treatment [3].

The major alloying elements used to impart particular properties to aluminum are silicon (Si), magnesium (Mg), manganese (Mn) and copper (Cu). Silicon imparts good fluidity to the alloy. Magnesium and copper are hardening elements which strengthen the alloy following heat treatment through precipitation or age hardening. Manganese is used to control the type of iron phases formed in the alloy. Small amounts of Mn play a positive role in combining with iron (Fe) to form the Chinese script α-Fe intermetallic phase instead

of the detrimental platelet-like β-Fe phase. The α-Fe phase is much more compact and less detrimental to the mechanical properties [7]. Iron is occasionally used to give the material special qualities. For example, in the case of die casting alloys, iron is added to reduce die soldering.

Other alloying elements used in combination with one or more of the major alloying elements include bismuth (Bi), boron (B), chromium (Cr), lead (Pb), nickel (Ni), titanium (Ti) and zirconium (Zr). They are usually used in very small amounts (<0.1 percent by weight), although B, Pb and Cr levels may go up to 0.5 percent, in special cases, to enhance properties such as castability, machinability, heat- and corrosion-resistance, and tensile strength [8].

Alloying additions are used to enhance the structure and mechanical properties of aluminum casting alloys. Strontium (Sr) is added to Al alloys containing Si to modify the morphology of the Si particles from coarse, brittle flakes to a finer spherical form. Also, the absorption of Sr by iron intermetallics, results in refining their morphology [9-10].

Titanium is added either individually or in combination with boron to refine the grain structure of the α-Al matrix, as it creates many nuclei in the melt, which encourages the formation of small equiaxed grains of α-Al, rather than the coarse, columnar grain structure that is produced in the absence of grain refinement.

Zirconium (Zr) is usually contained in aluminum alloys in an amount of 0.1 to 0.25 wt%. Segregations of the $Al_3Zr$ phase particles or dispersoids formed are finer than those of Mn aluminides (10-100 nm) [12]. However, the effect of precipitation hardening due to

segregations of the Al$_3$Zr phase is not high because of the low content of Zr in the alloys just like in the case of Mn aluminides; however, the effect of the finer zirconium aluminide segregations on the process of recrystallization in deformed semi-products and, accordingly, on their grain structure is considerably stronger. Zirconium is normally added to aluminum to form a fine precipitate of intermetallic particles that inhibit recrystallization [14]. Additionally it has been shown that it increases the resistance to over-aging when it is added to binary Al-Sc alloys [13].

Nickel (Ni), one of the important additions, is added to Al-Cu and Al-Si alloys to improve hardness and strength at elevated temperatures and to reduce the coefficient of expansion, as the existing Al-Si-Cu and Al-Si-Mg alloy systems lose strength above 150°C [11]. Also, Ni and Zr when added to Al-Si alloys precipitate in the form of Al3Ni and Al$_3$Zr, respectively.

Mischmetal consists of a combination of rare earth metals like lanthanum (La), cerium (Ce), neodymium (Nd) and praseodymium (Pr). Besides modifying the eutectic silicon, it can form a fine dispersion of coherent intermetallic compounds which strengthen the grain boundaries, increasing the strength of the Al-Si alloys at elevated temperatures. Sharan and his co-workers investigated the modification effect of rare earth additions in hypoeutectic and hypereutectic Al-Si alloys, they found that with up to 0.2% rare earth metal additions to hypoeutectic Al-Si alloys, some refinement in primary α-Al and the eutectic structure occurred, leading to an increase in the tensile strength by 36% and the percentage elongation by 2 to 3 times [57, 58, 59, 60]. The addition of rare earth metals

leads to the improvement in the hardness of Al alloys because the rare earth metals can react easily with Al to form high melting point and infusible dispersed intermetallic compounds, which leads to grain refining and the strengthening of the grain boundary regions. The change in the microstructure (such as grain refining, improved grain orientation and proper secondary phase distribution) results in an appreciable enhancement in the alloy properties [63].

In this study, the tensile properties of an Al-2%Cu based alloy were investigated. Coded alloy 220, and with a composition of Al-2.4%Cu-1.2%Si-0.4Mg-0.4%Fe-0.6%Mn-0.15%Ti, this base alloy was used to prepare other alloys by adding Sr, Ti, Zr, Ni, V, Cr and La to the melt, individually or in different combinations. Test bar castings were made using the low-pressure die casting (LPDC) technique which provides several advantages, among them high productivity and reduced machining costs. The LPDC test bars obtained were used for tensile testing.

## 1.2    OBJECTIVES

The present study was undertaken to investigate the effects of alloying elements on the mechanical properties of Al-2%Cu based 220 alloys subjected to different heat treatment conditions, and tested at both ambient and high temperature. The main objectives of the study therefore covered:

- Investigating the influence of the addition of different elements (Ti, Zr, V, Ni, Sr, La, and Cr) on the tensile properties (UTS, YS, El %) of 220 (Al-2%Cu) type base alloys at room temperature.

- Investigating the influence of these additions on tensile properties (UTS, YS, El %) of the 220 alloys at high temperature, stabilized for 1 hr and 200 hrs at 250°C before testing.

- Examining the microstructural features of the alloys used to acquire a better understanding of the phases and intermetallics present in the structure.

- Analyzing the alloy quality obtained under the various alloy/heat treatment conditions employed, through the use of suitably proposed quality indices, in order to recommend the optimum metallurgical conditions for improving the properties for 220 type casting alloys used in specific application.

# CHAPTER TWO

# SURVEY OF THE LITERATUR

# CHAPTER 2

# SURVEY OF THE LITERATURE

## 2.1    ALUMINUM ALLOYS

Aluminum alloys are divided into two main groups: aluminum wrought alloys and aluminum casting alloys [15]. Aluminum wrought alloys are available primarily in the form of worked products which have been subjected to plastic deformation by cold and hot working processes such as rolling, extrusion, and drawing either singly or in combination, so as to transform cast aluminum ingots into the desired product form. The microstructural changes associated with the working and with any accompanying thermal treatments are used to control certain properties and characteristics of the worked (or wrought) product or alloy. Examples of wrought products include plates or sheets, extruded shapes such as window frames, and forged automotive and airframe components.

As mentioned in Chapter 1, cast aluminum alloys are the most versatile of all common foundry alloys due to their excellent castability, low melting temperature, low gas solubility, and high strength-to-weight ratio, all of which are accompanied by good machinability and satisfactory thermal and electrical conductivity. In automotive applications, these alloys are used primarily for engine components, including engine blocks, cylinder heads, and pistons.

Aluminum casting alloys are grouped into nine different series of alloys, namely, 1xx.x series, 2xx.x series, 3xx.x series, and so on. The principal alloying element or elements in each series characterizes that series, as shown in Table 2.1 [16]. The alloy

designation system is derived from the Aluminum Association. Whereas wrought alloys follow a four-digit system, a three-digit system is used for cast alloys. These digits are followed by a letter that denotes the temper or heat treat condition. The first digit indicates the principal alloying element. The second and third digits are capricious numbers given to identify a specific alloy in the series. The number following the decimal point indicates whether the alloy is a casting (0) or an ingot (1or 2). A capital letter prefix indicates a modification to a specific alloy. Thus an Al-Cu alloy would belong to the 2xx.x series, whereas an alloy containing Al-Si-Mg or Al-Si-Cu, or Al-Si-Cu-Mg would belong to the 3xx.x series, and so on [15, 16].

Table 2-1: Cast aluminum alloy designation system. [16]

| Alloy Series | Principal Alloying Element |
|:---:|:---:|
| 1xx.x | Aluminum (99.00% minimum) |
| 2xx.x | Copper |
| 3xx.x | Silicon plus copper (and, or) magnesium |
| 4xx.x | Silicon |
| 5xx.x | Magnesium |
| 6xx.x | Unused series |
| 7xx.x | Zinc |
| 8xx.x | Tin |
| 9xx.x | Other elements |

## 2.2    ALUMINUM-COPPER CASTING ALLOYS

Copper has the single greatest impact of all alloying elements on the strength and hardness of aluminum casting alloys, in both as-cast and heat-treated conditions, and at ambient and elevated service temperatures. Copper improves the machinability of aluminum alloys by increasing the matrix hardness, making it easier to generate small cutting chips and fine machined finishes. On the downside, copper reduces the resistance to corrosion and hot cracking, or hot tearing and, in certain alloys and tempers, it increases the stress corrosion susceptibility. Copper is generally used to increase the tensile strength and hardness through heat treatment.

Copper has a maximum solubility in solid aluminum of approximately 5.7 wt% at the eutectic temperature of 548°C, as shown in Figure 2.1 [17]. The aluminum rich α-Al phase forms initially during the solidification of hypoeutectic alloys containing less than 33.2% Cu; subsequently the remaining liquid separates at the eutectic temperature into α-Al and the Al2Cu intermetallic phase designated θ. The composition of the θ ($Al_2Cu$) phase ranges from 52.5 to 54.1% Cu corresponding to the eutectic temperature and room temperature, respectively.

Aluminum-copper (Al-Cu) alloys have marginal castability relative to almost any of the alloys containing silicon. These alloys have limited fluidity and require careful gating and generous riser feeding during solidification to ensure casting soundness. In addition, it should be kept in mind that pressure-tight parts of intricate design are difficult to obtain, and their resistance to hot tearing is relatively poor; they are also susceptible to stress

11

corrosion cracking in the fully-hardened condition. As a result, the binary Al-Cu casting alloys are infrequently used, in actual fact, while most commercial alloys are alloyed with other additives, mainly silicon (Si) and magnesium (Mg).
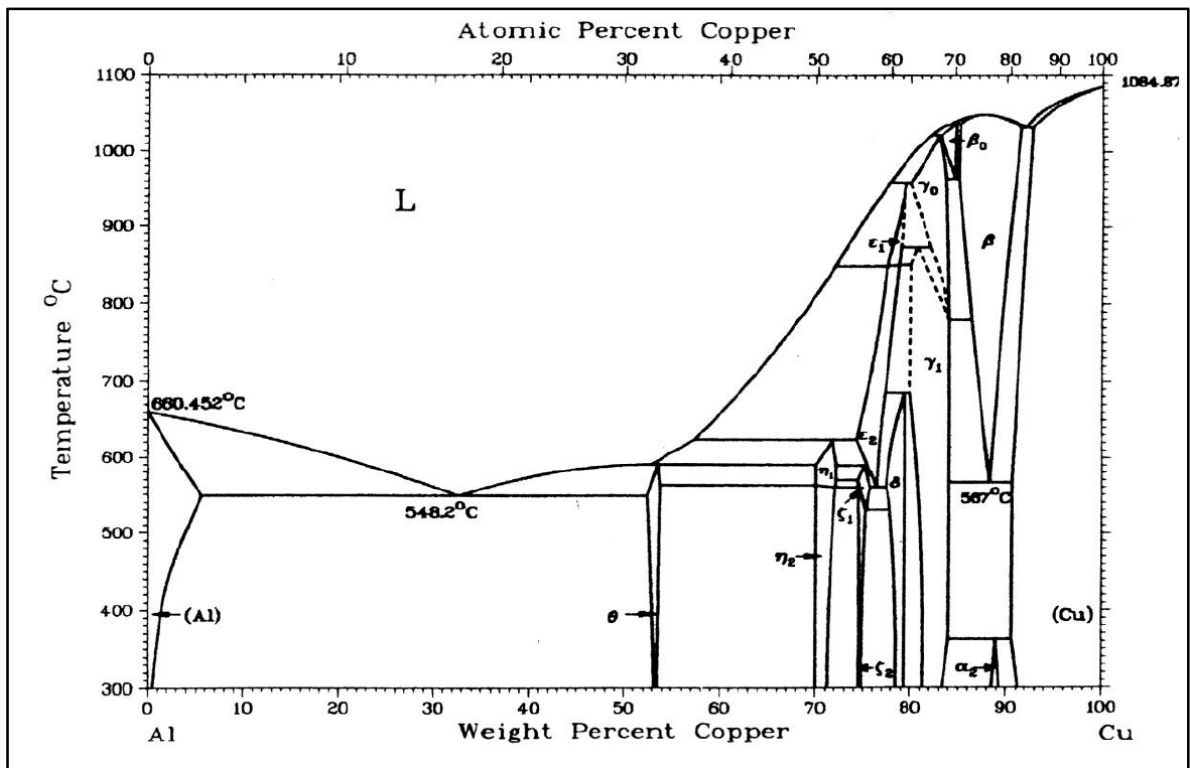


**Figure 2-1: Phase diagram of the Al-Cu alloy system [17].**

The addition of Si and Mg to Al-Cu based alloys results in the formation of a family of Al-Cu-Si-Mg alloys which has widespread applications, especially in the automotive and aerospace industries based on the superiority of their mechanical properties, castability, weldability and machinability. The metallurgical parameters controlling the quality and mechanical properties of these alloys, namely, heat treatment, addition of alloying

elements, and the type and volume fraction of iron-intermetallics formed are discussed in the following subsections.

### 2.2.1  HEAT TREATMENT OF AL-CU-SI-MG ALLOYS

Heat-treatment is commonly used to improve the mechanical properties of cast aluminum alloys [20]. Heat-treatment improves the strength of aluminum alloys through a process known as precipitation-hardening which occurs during the heating and cooling of an aluminum alloy and in which precipitates are formed in the aluminum matrix [21]. The improvement in properties as a result of heat treatment depends upon the change in solubility of the alloying constituents with temperature. Figure 2.2 illustrates the major steps of the heat treatment process normally used to improve the mechanical properties of aluminum alloys. During solution heat treatment, the atoms of the hardening elements (such as Cu and Mg) are put in solid solution, using a solution treatment temperature just below the eutectic temperature, and a solution time long enough to allow solutionizing of the second phase constituents to form a supersaturated solid solution. The next step is quenching, where the alloy casting is rapidly quenched to retain the supersaturated solid solution at room temperature. Finally, the sample is subjected to an aging treatment, during which the hardening precipitates are formed when the sample is heated to a lower temperature than the solution temperature (termed artificial ageing) or left to age at room temperature (called natural aging) [18, 19, 20].

The main reason for carrying out heat treatment is to obtain an increase in strength. Different heat treatment processes (or tempers) are available, depending on the casting

process and desired properties of the alloy. In the T5-treatment, the aging treatment is carried out at temperatures above ambient, typically in the range of 150-200˚C. The heat treatment is carried out at these relatively low temperatures to eliminate growth. The T5 temper is also used to stabilize the castings dimensionally (improving the mechanical properties). The T6 treatment is the one most commonly used for Al-Cu-Si-Mg casting alloys with the intent of obtaining the best compromise between strength and ductility [11, 22]. The stabilization T7 temper is conducted at higher aging temperatures (200-240°C) than the T6 temper (150-180°C), causing overaging and a consequent reduction in the hardening effect. The T7 treatment is usually carried out to improve some specific characteristic such as corrosion resistance and/or to increase the stability and performance of the casting at elevated temperatures [19].
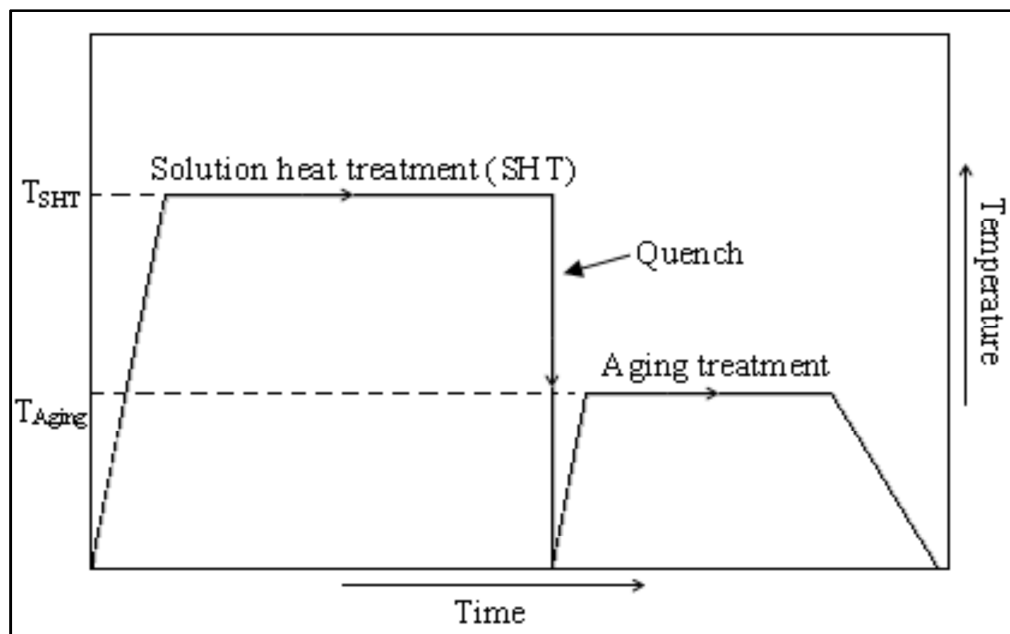


**Figure 2-2: Diagram showing the three steps for precipitation hardening [18].**

Aluminum-copper cast alloys are considered to be heat-treatable alloys. Figure 2.3 displays the temperature ranges of the heat treatment applied to Al-Cu alloys [19]. For example, the solution heat treatment range of Al-4.5Cu alloy is 515°C to 550°C in which the Cu completely dissolves thereby producing a complete solid solution. This solid solution will become supersaturated as the temperature decreases to below 515°C. In order to produce age-hardening, the alloy should be aged within a temperature range of 150°C to 220°C for a pre-determined aging period. Aluminum castings are heat treated for homogenization; stress relief; improved dimensional stability and machinability; optimized strength, ductility, toughness and corrosion resistance [23].
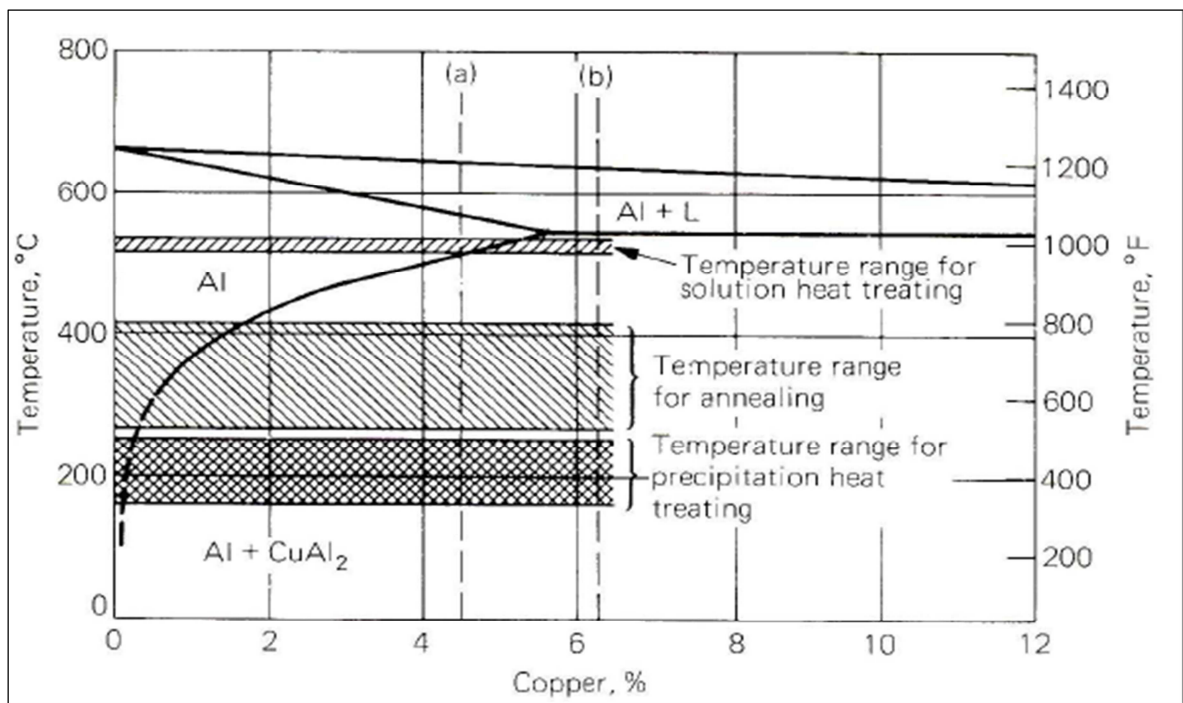


**Figure 2-3: The temperature ranges of heat treatment in Al-Cu system alloys [19].**

The three basic stages of the T6 heat treatment, i.e. solution heat-treatment, quenching, and precipitation hardening through artificial aging, are shown schematically in Figure 2.4, and reviewed in the following sections in the context of Al-Cu-Si-Mg alloys.
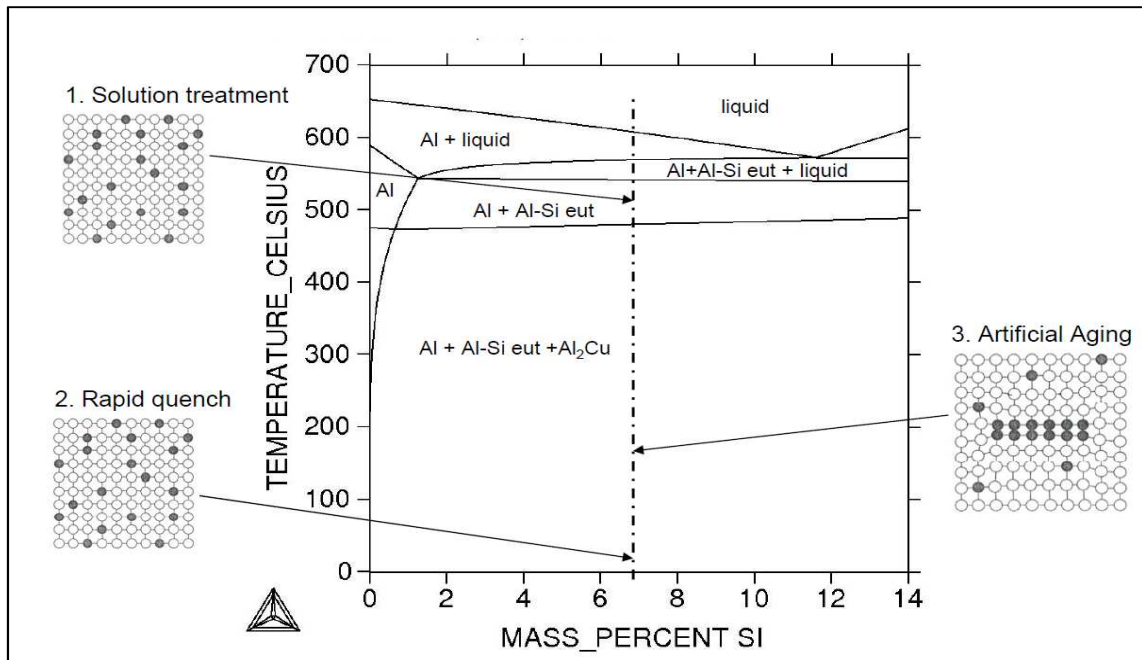


**Figure 2-4: The T6 heat treatment process. [12]**

### 2.2.1.1    *SOLUTION HEAT TREATMENT*

The main function of solution heat treatment is to maximize the solubility of elements in the matrix such as Cu and Mg, to dissolve and alter the intermetallics which are formed during solidification, to increase the homogeneity of the microstructure, and to spheroidize the eutectic Si particles [18]. Solution heat treatment is controlled by temperature and time. The solution treatment temperature is a critical parameter in Cu-containing alloys due to the occurrence of incipient melting. From the investigations of

Reiso et al. [24], the incipient melting takes place at and above the corresponding eutectic temperature as a result of the reduction in the Gibbs free energies. The detrimental effect of incipient melting on the mechanical properties arises from the void formation which may be attributed to the difference in density between the Cu-rich phase particles (θ, S, Q) and the matrix, and the insufficient time available for the aluminum atoms to diffuse back into the volume occupied by the particles in order to accumulate this same volume. The time required for solution heat treating depends on the type of product, alloy, casting or fabricating procedure used and thickness insofar as it influences the pre-existing microstructure [20]. These factors establish the proportions of the solutes that are in or out of solution and the size and distribution of the precipitated phases [18, 19].

Solution heat treatment can be used to dissolve the β-$Al_5FeSi$ phase and thus reduce the harmful effect of its platelet morphology which leads to a deterioration in the mechanical properties and an increase in the shrinkage porosity. It has been found that solution temperatures below 500°C (i.e. equilibrium heat treatment) cannot dissolve the β-$Al_5FeSi$ phase. The dissolution of the phase is accelerated as the solution temperature increases. The process of the dissolution of β-iron platelets starts with necking, then fragmentation, and finally spheroidization [25, 26].

The solution heat treatment process may be carried out either in a single step or in multiple steps. The single-step treatment for Al-Cu alloys is normally limited to 495°C, because a higher temperature might lead to the incipient melting of the copper phase. On the other hand, heat treatment at temperatures of 495°C, or less, is not sufficient to

maximize the dissolution of the copper-rich phases or to modify the morphology of the silicon particles. In order to overcome this problem, a two-step solution heat treatment was proposed by Sokolowski et al. [27], where the second-stage is maintained at temperatures below 525°C. In general, only the conventional single-stage solution heat treatment of 8h at 495°C for 319 aluminum alloys is carried out to avoid the incipient melting of the copper phase.

### 2.2.1.2    *QUENCHING*

Quenching is the step which follows solution heat treatment. The purpose of this process is to preserve the solid solution formed at the solution heat treating temperature by means of rapid cooling to some lower temperature, usually close to room temperature. When the casting is cooled from the solution temperature, the solubility of the hardening elements decreases. Solutes are lost from the enriched α-Al solid solution by precipitation [18, 20]. In most instances, to avoid those types of precipitation that are detrimental to the mechanical properties or to corrosion resistance, the solid solution formed during solution heat treatment must be quenched rapidly enough without any interruption to produce a supersaturated solution at room temperature. Because of a high level of supersaturation and a high diffusion rate for most Al-Si casting alloys at temperatures between 450°C and 200°C, the quench rate is critical as the precipitates form rapidly. At higher temperatures the supersaturation is too low and at lower temperatures the diffusion rate is too low for precipitation to be critical; 4°C/s is a limiting quench rate above which the yield strength increases slowly with further increase in quench rate [18]. Quenching rate greatly

influences the microstructure and properties of super high strength aluminum alloys, namely, the ultimate strength and yield strength. With decrease in the quenching rate, the strength of the casting/sample decreases [28].

### 2.2.1.3  *AGING (PRECIPITATION HEAT TREATMENT)*

Aging is the final stage in the heat treatment of cast aluminum alloys. After solution treatment and quenching, strengthening can be completed either at room temperature (natural aging) or by applying a precipitation heat treatment (artificial aging).

Age hardening or precipitation hardening is produced by phase transformations making uniform dispersion of coherent precipitates in a softer matrix. Aging at, for example, 100°C – 260°C is called artificial aging because the alloy is heated to produce precipitation. The use of a lower aging temperature allows for the properties to be more uniform. When heat-treated alloys are aged at room temperature, this is called natural aging. The alloy properties are dependent on the aging temperature and aging time. Typically the hardness and strength of the alloy increases initially with time and particle size until it reaches the peak where maximum strength is obtained (termed peak aging). Further aging will decrease the strength and hardness (termed overaging).

Cuniberti et al. [29] studied the influence of natural aging on precipitation hardening of an Al–Mg–Si alloy using mechanical testing and quantitative transmission electron microscopy, and found that natural aging increases yield stress and reduces ductility, which is attributed to the formation of Mg/Si clusters. Their findings are in

keeping with those of Mohamed and Samuel [18], in which the precipitation of metastable Mg-rich phases was reported to depend on the Mg-to-Si ratio. The excess of Si in solid solution can significantly alter the kinetics of precipitation and the phase composition.

The hardening of Al-Cu alloys is achieved by the precipitation of the hardening phase $\theta$ (Al$_2$Cu) out of the supersaturated solid solution (S.S.S), in a special sequence as follows:

$$S.S.S \rightarrow GPZ\ I \rightarrow \theta" \ (GPZ\ II) \rightarrow \theta' \rightarrow \theta \ (Al2Cu)$$

Here, the precipitation sequence in the Al-Cu system starts with the formation of fully coherent Guinier-Preston zones (GPZ I) which are clusters of copper atoms which have acquired a disc-like shape. The GPZ I phases are ultimately replaced by the coherent $\theta"$ phases as aging progresses, the coherent $\theta"$ phases are tetragonal in structure. As the aging process develops further, the final metastable $\theta'$ phase is formed. This phase is a semi-coherent one displaying a tetragonal structure and an Al$_2$Cu composition [19, 30, 31, and 32].

The addition of Si and Mg to Al-Cu alloys alters the precipitation-hardening system of these alloys substantially. The precipitation-hardening characteristics of the resulting Al-Cu-Si-Mg alloys often appear to be relatively complex. This complexity may be attributed to the formation of several hardening phases including $\theta'$ (Al$_2$Cu), $\beta"$ (Mg$_2$Si), S' (Al$_2$CuMg), and the quaternary phase AlMgSiCu which is designated as the Q (Al$_5$Mg$_8$Si$_6$Cu$_2$) or $\lambda$ (Al$_5$Mg$_8$Si$_6$Cu$_2$) phase [33, 34].

Suzuki et al. [35] reported that the precipitation sequence of Al-2%Cu-0.9%Mg-0.25%Si results in the formation of S' ($Al_2CuMg$) and β' ($Mg_2Si$) phase precipitates. Increasing the Si content up to 0.5%, however, promotes the precipitation of θ' ($Al_2Cu$) and Q ($Al_5Mg_8Si_6Cu_2$) while suppressing the formation of the S' and β' phase precipitates. Li et al. [36] concluded that the improvement observed in the mechanical properties of Al-7%Si-0.5%Mg foundry alloys through the addition of Cu may be attributed to the increase in the density of β" precipitates and the precipitation of Q phase precursors in addition to the precipitation of the θ' phase at higher Cu contents.

### 2.2.2 EFFECT OF ALLOYING ELEMENTS

The properties of aluminum casting alloys can be improved upon through the appropriate control of several metallurgical parameters involved in the production of these castings. One such parameter involves the addition of suitable alloying elements. Alloys containing Cu and Mg show a greater response to heat treatment as a result of the presence of both elements. These alloy types display excellent strength and hardness values although at some sacrifice to ductility and corrosion resistance. While the properties in the as-cast condition are acceptable for certain applications, the alloys are typically heat-treated for optimal properties. Thus, the addition of alloying elements to aluminum is the principal method used to produce a selection of different materials that can be used in a wide range of structural applications.

Silicon (Si) has a good influence in that it reduces the melting temperature of aluminum alloys and improves the fluidity [39], to form a eutectic, and to promote the

formation of strengthening precipitates through the expected reaction of Si and Mg present in solid solution [40]. These alloys have several advantages such as high strength, low weight, high castability, good weldability, good thermal conductivity, excellent corrosion resistance and have acceptable mechanical and physical properties at high temperatures up to 250°C [41]. Higher tensile strength can be attributed mainly to the presence of spheroidized Si particles that provide substantial dispersion hardening [40].

However, Al-Si alloys are limited to applications which can work under temperatures up to 250°C [37]; above this temperature the alloy loses coherency between the aluminum solid solution matrix and the precipitated particles which then rapidly coarsen and dissolve again into the solid solution, resulting in an alloy having an undesirable microstructure for high temperature applications [38].

Adding copper (Cu) to aluminum alloys has many positive benefits which enhance the mechanical properties. First, it increases the alloy strength at both room and high temperatures whether these alloys are heat treated after casting or not [43]. However, it was found that the addition of copper to aluminum reduces the ability of the alloy to corrosion resistance [42].

When the Cu content is above its solubility limit in Al, the precipitation of the second phase θ also contributes to the strengthening effect. During solution treatment, Cu dissolves rapidly into the aluminum matrix despite the short solution treatment time employed and this element is critical in facilitating age hardening, particularly when Mg and Si are also present. The strengthening effect of Cu in Al-Si alloys is linked to the

precipitation of the secondary eutectic phases of intermetallic $Al_2Cu$ or $Al_5Cu_2Mg_8Si_6$ that form during aging (T6 heat treatment).

In addition to Cu, the addition of transition elements such as nickel (Ni) is considered to be effective for increasing the room and the high temperature strength of cast Al–Si alloys by forming stable aluminides [44]. As with the as-cast condition, the ductility of alloys aged to a T6 temper decrease gradually as the Cu content is increased [40]. Nickel is added to Al-Cu and Al-Si alloys to improve hardness and strength at elevated temperatures and to reduce the coefficient of expansion, as the existing Al-Si-Cu and Al-Si-Mg alloy systems lose strength above 150°C [11].

Magnesium (Mg) is added to aluminum alloys in order to increase the strength and corrosion resistance, and to enhance their weldability [45]. In addition, Mg increases the hardness of Al-Cu alloys, especially in castings; however, with a decrease in the ductility and impact resistance [45]. Even small amounts of Mg can have a profound effect on age hardening [40]. Tavitas-Medrano et al. [46] reported that small additions of 0.4 weight percent of Mg increase the response of the alloy to artificial aging, thereby increasing the achievable tensile strength and micro-hardness values, however, at the expense of reduced elongation and impact toughness.

Manganese (Mn) is highly soluble in aluminum, so that when a casting is quenched after solution heat treatment, most of the added Mn is substantially retained in solid solution [22]. Manganese increases the strength of the alloy either in solid solution or by modifying the morphology of the iron intermetallic phases which are formed after the heat

treatment. Small amounts of Mn play a positive role in combining with Fe to form the Chinese script α-iron intermetallic phase instead of the plate-like β-iron $Al_5FeSi$ phase. The α-iron $Al_{15}(Fe,Mn)_3Si_2$ phase is much more compact and less detrimental to the mechanical properties [47].

Zirconium (Zr) is usually contained in aluminum alloys in an amount of 0.1 to 0.25 wt%. Segregations of the $Al_3Zr$ phase are finer in size than those of the Mn aluminides (10 – 100 nm) [12]. However, the effect of precipitation hardening due to segregations of the $Al_3Zr$ phase is not high because of the low content of Zr in the alloys similar to the case of Mn aluminides, but the effect of the finer $Al_3Zr$ segregations on the process of recrystallization in deformed semi-products and, accordingly, on their grain structure is considerably stronger. Zirconium is normally added to aluminum to form a fine precipitate of intermetallic particles that inhibit recrystallization [14]. Additionally it has been shown that it increases the resistance to over-aging when it is added to binary Al-Sc alloys [13]. Also, Ni and Zr when added to Al-Si alloys precipitate in the form of $Al_3Ni$ and $Al_3Zr$, respectively.

Strontium (Sr) is added to Al-Si casting alloys to modify the morphology of the Si particles from coarse brittle flakes to a finer fibrous form that leads to an enhancement in the tensile properties, in particular, the ductility of the alloy [48]. Addition of Sr to the melt changes the mode of eutectic nucleation; as a result, it reduces the overall surface slumping and redistributes porosity in the casting [38].

Titanium (Ti) is added either individually or in combination with boron ($TiB_2$) to refine the grain structure of the α-Al matrix, as it creates many nuclei in the melt, which encourages the formation of small equiaxed grains of α-Al, rather than the coarse, columnar grain structure that is produced in the absence of grain refinement. In Al-Si alloys such as A356 and A357, best results are obtained by adding 10-20 ppm of boron in the form of Al-5Ti-1B or Al-3Ti-1B rod. For Al-Cu and Al-4.5%Cu-0.5%Mn alloys, best results are achieved with the addition of less than 0.05% Ti and 10-20 ppm of boron, added in the form of Al-5Ti-1B or Al-3Ti-B rod. For Al-Si-Cu alloys, such as A319 (Al-3%Cu-5.5%Si) alloy, 10-20 ppm of boron in the form of Al-5Ti-1B or Al-3Ti- 1B rod provides the best results [49, 50].

Vanadium (V) is added to aluminum alloys in order to increase grain refining during solidification due to the formation of the $Al_{11}V$ intermetallic phase [59]. Early researches studied the effect of adding vanadium to aluminum alloys and proved that traces of V in such alloys improves the mechanical properties, in particular the alloy strength [51] and enhances its plasticity behavior [55,56].

Chromium (Cr) is added to many alloys of the Al-Mg, Al-Mg-Si and Al-Mg-Zn groups, where it is added in amounts generally not exceeding 0.35%. In excess of these limits, it tends to form very coarse constituents with other impurities or additions such as manganese, iron, and titanium. Chromium typically forms the compound $CrAl_7$, which displays extremely limited solid-state solubility and is therefore useful in suppressing grain-growth tendencies. Thus it is used to control grain structure, to prevent grain growth in Al-

Mg alloys, and to prevent recrystallization in Al-Mg-Si or Al-Mg-Zn alloys during hot tearing or heat treatment [61].

Lanthanum (La) and cerium (Ce), or rare earth elements in Al alloys interact preferentially with other elements to form intermetallic compounds which concentrate in the grain boundary regions and result in hindering grain boundary movement by slip. As a result, the strength of the alloy is improved at elevated temperature. Sharan and Prasad [57] investigated the influence of rare earth fluorides in hypoeutectic Al-7.5%Si alloy, and reported that the tensile strength increased by 36% and the percentage elongation by about 2 to 3 times its original value due to the addition of up to 0.2% rare earth fluorides to the alloy. Ravi et al. [62], found that the addition of mischmetal up to 1 wt% results in an increase in the tensile properties and hardness by up to 20% in Al-7Si-0.3Mg alloy, attributed to the refinement of the microstructure and the formation of intermetallic compounds between Al and Si, Mg, Fe, Ce, and La. Mischmetal addition above 1 % was observed to decrease the tensile properties, but increased the hardness. Owing to the formation of Ce- and La-containing hard and stable intermetallic compounds in the aluminum matrix, a certain amount of Mg was consumed from the aluminum matrix in order to form these compounds. This reduced the amount of the precipitation hardening $Mg_2Si$ phase, thus reducing the strength of the alloy [62].

The addition of rare earth metals leads to the improvement in the hardness of Al alloys because the rare earth metals can react easily with Al to form high melting point and infusible dispersed intermetallic compounds, which leads to grain refining and the

strengthening of the grain boundary regions. The change in the microstructure (such as grain refining, improved grain orientation and proper secondary phase distribution) results in an appreciable enhancement in the alloy properties [63].

### 2.2.3   EFFECT OF IRON INTERMETALLIC PHASES

Iron is one of the most common impurities found in aluminum alloys, frequently appearing as intermetallic second phases in combination with aluminum and other elements. The less common Fe-rich intermetallic phases are $\delta$-$Al_4FeSi_2$ and $\pi$-$Al_8Mg_3FeSi_6$, while the more outstanding and commonly observed ones are $\alpha$-$Al_{15}(Fe,Mn)_3Si_2$ and $\beta$-$Al_5FeSi$ [52,68]. In Figure 2.5, the $\alpha$-Fe phase appears as Chinese script particles while the platelet-like $\beta$-Fe phase appears as needles [26]. The brittle $\beta$-Fe intermetallic phase platelets act as stress raisers during service and adversely affect mechanical properties. It was reported that increasing the iron content from 0.5 to 1.2% in Al-Si casting alloys dramatically reduces the mechanical properties, particularly ductility, due to the formation of the $\beta$-Fe phase [53]. Bonsack [54] found that in Al-Si alloys with Fe contents higher than 0.5%, the formation of the $\beta$-Fe phase increases strength values and slightly decreases ductility; when the Fe content exceeds 0.8%, however, the ductility decreases significantly. In Al-Si-Cu alloys, increasing the Fe content continuously decreases ductility, and drastically so for Fe contents above 0.9% [52]. The coarse $\beta$-Fe phase platelets interfere with liquid flowing into interdendritic channels; this reduces feeding during solidification and consequently promotes the formation of porosity [64, 69].
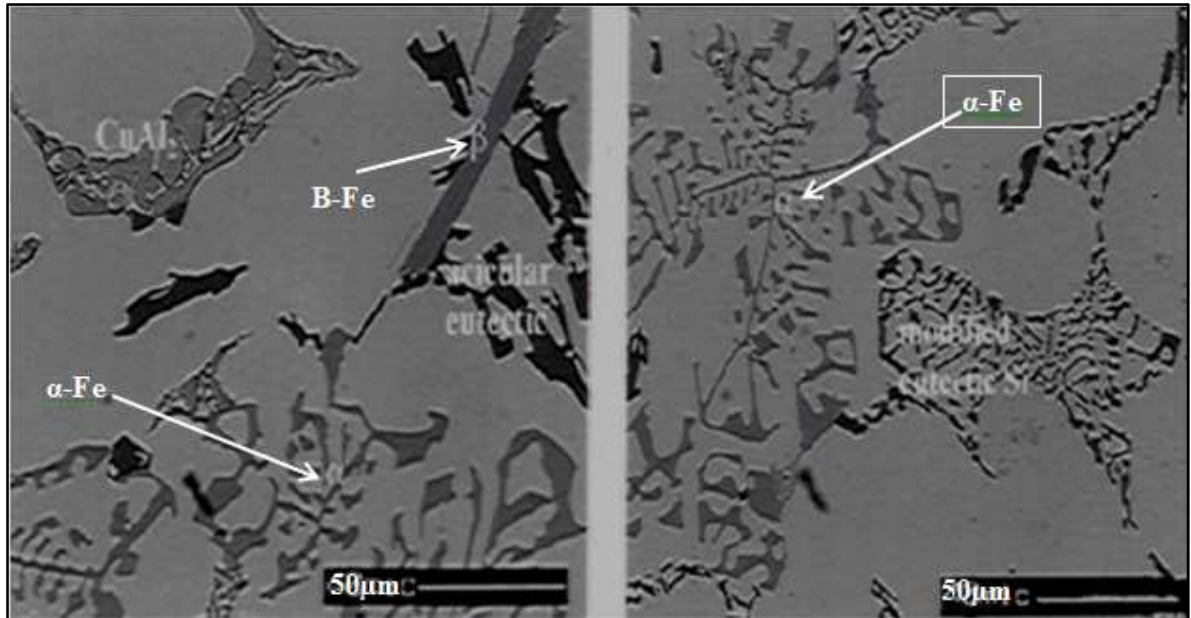
**Figure 2-5: As-cast 319 alloys showing the morphology of β-Fe and α-Fe intermetallic[26].**

The critical iron content at which the β-Fe phase appears has been the subject of much debate in the literature. The β-Fe phase is most associated with Fe contents of more than 1% [52]. Backerud et al. [6] reported, however, that an iron content of 0.48% is sufficient to form the β-Fe phase during solidification of the 356 aluminum alloy. In fact, the critical iron content at which the β-Fe phase forms is strongly dependant on the cooling rate. Lakshmanan et al. [67] reported that, at low cooling rates (0.1°C/s), the β-Fe phase is favored, at high cooling rates (10°C/s), the β-Fe phase is inhibited, but at very high cooling rates (20°C/s), the β-Fe phase is strongly favored. Neutralization of Fe through the promotion of the less harmful α-Fe Chinese script phase is sought at the expense of the brittle needlelike β-Fe phase with the goal of improving strength, ductility and other properties. Small amounts of manganese (usually Mn:Fe = 0.5) play a positive role in

combining with iron to form the less harmful α-Fe Chinese script phase instead of the brittle β-Fe phase [24, 54].

At higher Mn:Fe ratios and/or in the presence of chromium, however, the iron, manganese and chromium form another version of the α-Fe phase, $\alpha\text{-Al}_{15}(\text{Fe,Mn,Cr})_3\text{Si}_2$, termed sludge, displaying a star-like morphology. These sludge particles are extremely hard and thus have a detrimental effect on mechanical properties and machinability. The formation of these particles may be controlled by calculating the sludge factor which correlates the %Fe, %Mn, and %Cr levels, as follows [65, 66]:

$$\text{Sludge Factor (S.F.)} = 1 \text{ x wt\% Fe} + 2 \text{ x wt\% Mn} + 3 \text{ x wt\% Cr} \qquad (2.1)$$

The critical sludge factor beyond which sludge is formed equals 1.8 if a casting temperature of 650°C or more is maintained. However, for holding temperatures lower than this value, a critical sludge factor of 1.4 is recommended, since sludge formation is a temperature-dependent process in combination with the Fe, Mn, and Cr concentrations.

### 2.2.4   POROSITY FORMATION

Porosity is one of the critical factors which is central to the quality of the casting. This parameter may be detrimental not only to the surface quality after machining but also to the mechanical properties and corrosion resistance of alloys.

Porosity in castings occurs because of the rejection of gas from the liquid metal during solidification and/or the inability of the liquid metal to feed through the interdendritic regions to compensate for the volume shrinkage associated with solidification. Hydrogen is the only gas capable of dissolving to any significant extent in molten aluminum, resulting in outgassing, which leads to the formation of porosity and ultimately to reduced mechanical properties and diminished corrosion resistance [78].

#### 2.2.4.1       *THEORY OF POROSITY FORMATION*

The formation of porosity in solidifying metals is the result of two mechanisms: (i) shrinkage, resulting from the volume decrease accompanying solidification;  this type of porosity can also occur as "microshrinkage" or "microporosity", dispersed in the interstices of dendritic solidification regions, typically found in alloys with a large difference between their solidus and liquidus temperatures. Limited or inadequate liquid metal feeding in the dendrite solidification area gives rise to shrinkage; and   (ii) gas porosity, resulting from the decrease in the solubility of hydrogen in aluminum during solidification.

According to Campbell [79], the growth tendency of pores is described generically by the following equation:

$$P_g + P_s > P_{atm} + P_H + P_{s-t} \qquad\qquad 2.2$$

Where $P_g$ = equilibrium pressure of dissolved gases in the melt;

$P_s$ = pressure drop due to shrinkage;

$P_{atm}$ = pressure of the atmosphere over the system;

$P_H$ = pressure due to the metallostatic head;

$P_{s-t}$ = pressure due to surface tension at the pore/liquid interface.

The dissolved gas pressure, $P_g$, and pressure drop due to shrinkage, $P_s$, are the major driving forces in the formation of porosity. For a particular casting design, $P_{atm}$ and $P_H$ are constants, and a decrease in $P_{s-t}$, as observed for modifiers such as sodium or strontium, can lead to the increased probability of pore formation.

The pore growth process has been depicted schematically by Kubo and Pehlke [80], as shown in Figure 2.6. In (a), the gas porosity nucleates at the base of the dendrite arms. The synergistic effect between shrinkage and gas pores overcomes the large amount of negative free energy required to form a gas-metal surface, thereby facilitating the nucleation shown in Figure 2.6(a). As solidification proceeds, the degree of porosity increases as a result of the higher potential for gas evolution. The radius of the porous area

becomes large enough to decrease the contribution of interfacial energies, and thus the porosity becomes detached from the dendrites, as shown in (b). At a still further stage of solidification, neighbouring dendrites collide, making interdendritic feeding difficult. At this stage, the porosity is thought to grow so as to compensate for solidification shrinkage, as shown in Figure 2.6(c).
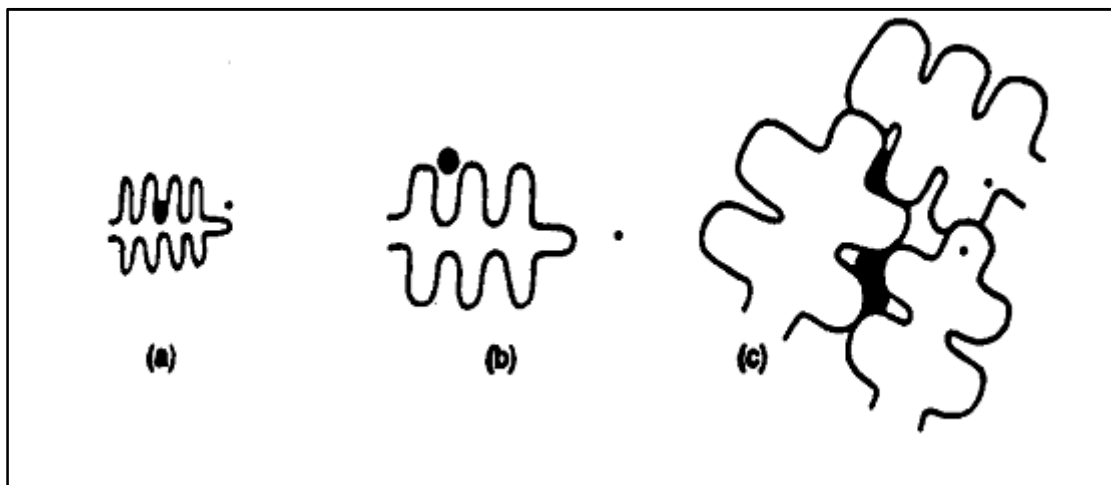


**Figure 2-6: The growth process of porosity formation. [79]**

Roy et al. [81, 82], reported that the addition of Mg to 319 alloy reduces the percentage porosity without a noticeable change in pore size and shape. They also observed that in materials containing a very low level of hydrogen, shrinkage pores are seen to nucleate at the interface of the blocky $Al_2Cu$ particles. According to Edwards et al. [83], the effect of magnesium on micro-porosity formation in Al-Si-Cu casting alloys is not consistent. However, in most of the alloys, Mg appears to decrease the porosity by amounts ranging from 0.01% to 0.3%.

### 2.2.5  QUALITY OF CAST ALUMINUM ALLOYS

The Quality index (Q) represents a numerical value that defines the quality of an aluminum alloy/casting, and is related to the UTS and plastic strain of the material to fracture (Ef). Drouzy et al. [70, 71] developed an empirical formula to characterize the mechanical performance (quality) of Al-7%Si-Mg casting alloys, using the following equations.

$$Q = UTS + d \log (Ef) \qquad\qquad \text{Eqn. (2.2)}$$

where Q and UTS are in MPa, d is a material constant equal to 150 MPa for Al-7%Si-Mg alloys, and Ef is the elongation to fracture in a tensile test.

$$YS = a\ UTS - b \log (Ef) + c \qquad\qquad \text{Eqn. (2.3)}$$

where the coefficients a, b, and c were calculated as 1, 60, and -13 respectively, for Al-7%Si-Mg alloys, with b and c expressed in MPa. The two equations shown above are valid only for an elongation > 1.

The quality index value is used to indicate the level of the quality of castings which are susceptible to improvement through factors such as adequate control of impurity elements, casting defects, modification, solution heat treatment and solidification conditions. Yield strength depends on hardening elements such as Mg and Cu and also on the age hardening process. Figure 2.7 shows the quality index chart proposed by Drouzy et al. [70, 71] generated using Equations 2.2 and 2.3, which provides information for each point located on the plotted chart and which is useful in evaluating the appropriate

metallurgical conditions to achieve the desired alloy quality. Each point on the chart provides tensile strength (UTS), elongation to fracture (Ef), yield strength (YS), and quality index (Q) values corresponding to specific heat treatment and alloying conditions.
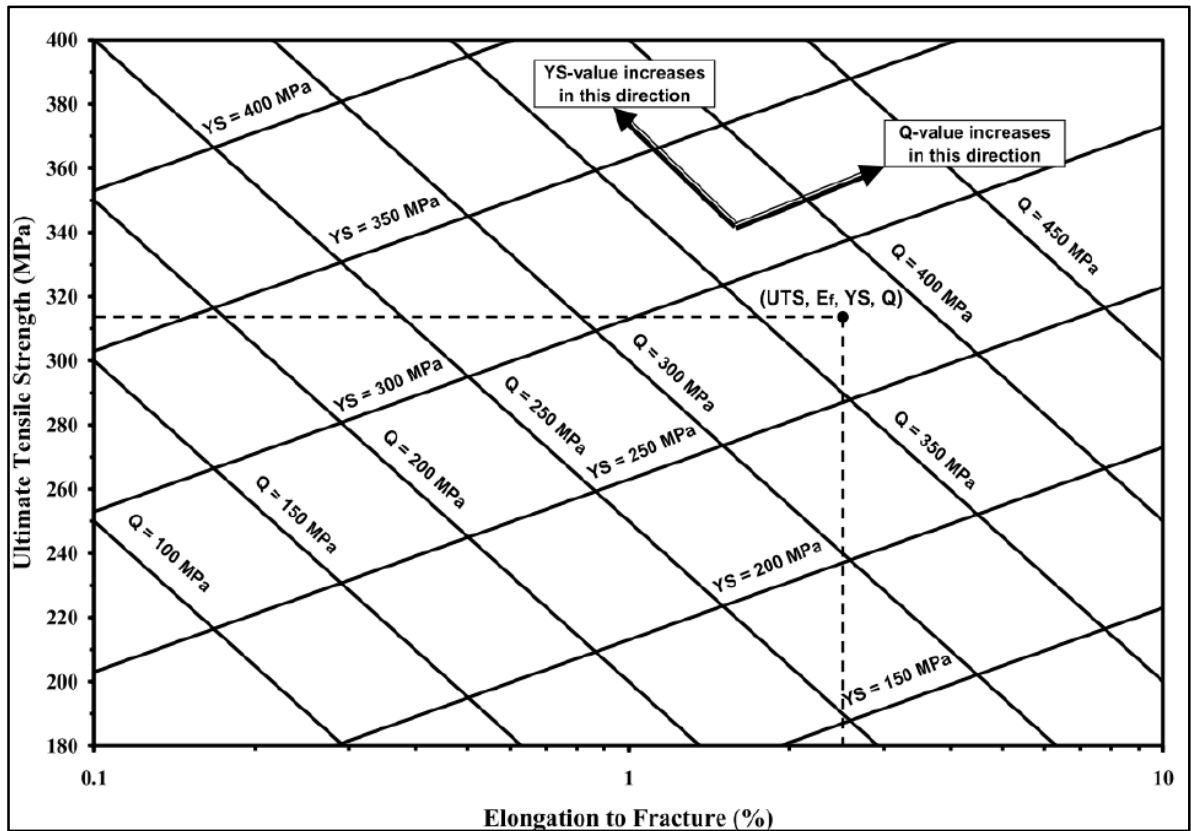


**Figure 2-7: Quality chart proposed by Drouzy et al. generated using Eqns. 2.2and 2.3 [70, 71].**

Cáceres developed a more general framework for casting quality, given by the following equations, which may be used for all alloys [69, 70].

$$\sigma = K\varepsilon^n \qquad\qquad 2.3$$

where $\sigma$ is the true flow stress, $K$ is the strength coefficient of the material, $\varepsilon$ is the true plastic strain, and $n$ is the strain-hardening exponent, defined by

$$n = (\varepsilon/\sigma)(d\sigma/d\varepsilon) \qquad\qquad 2.4$$

The true stress $\sigma$ and the engineering stress $P$ are related by the equation

$$\sigma A_F = PA_0 \qquad\qquad 2.5$$

where $A_0$ and $A_F$ are the cross sectional areas in the initial and strained conditions, respectively. Since the volume is assumed to be constant during deformation, the following equation may be obtained:

$$\frac{A_0}{A_F} = e^{\varepsilon_t} \qquad\qquad 2.6$$

where $\varepsilon_t$ is the total true strain which has elastic and plastic components. Combining Equations 2.3, 2.5, and 2.6 gives

$$P = K\varepsilon^n e^{-\varepsilon_t} \sim KS^n e^{-s} \qquad\qquad 2.7$$

where $S$ is the engineering plastic strain. In Equation 2.7, the sign $\sim$ indicates that the elastic strain component as well as the difference between the engineering and true strain have been disregarded. The latter is a reasonable assumption for casting alloys due to their limited ductility.

Cáceres further simplified his work on quality index, by identifying the material quality through $Q$- and $q$-values as shown in Figure 2.8, using Equations 2.8 and 2.9:

$$\sigma = k[\ln(1 + E)]^n \, e^{-\ln(1+E)} \sim KE^n e^{-E} \qquad\qquad 2.8$$

$$\sigma = KE^{E/q} e^{-E} \qquad\qquad 2.9$$

where $\sigma$, $E$ are the engineering stress and strain, respectively, and $K = 511$ MPa. The values

of $n$ and $K$ may be calculated from the log-log plot of true stress versus true strain [15, 72].
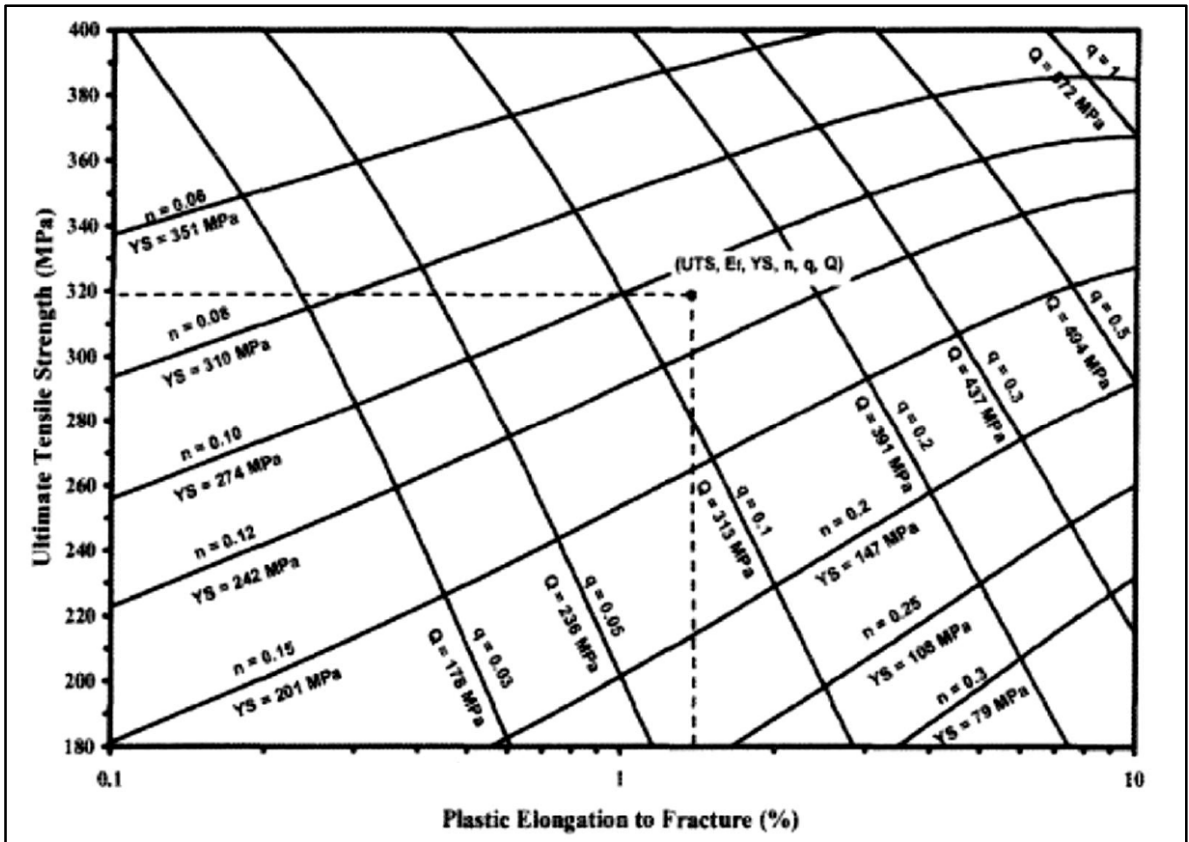


**Figure 2-8: Quality chart proposed by Cáceres, generated using Equations 2.8 and 2.9 [72, 73].**

The quality chart proposed by Cáceres may be explained as follows: the line q = 1 represents the maximum quality, while those with q <1 represents lesser quality values. Each point located on the chart provides the corresponding tensile strength (*UTS*), elongation to fracture (*Ef*), yield strength (*YS*), relative quality index (*q*) and quality index (*Q*) values. The quality chart proposed by Cáceres thus provides a good method for the prediction and selection of the most appropriate metallurgical conditions to be used for a specified aluminum casting alloy and the intended application [72, 73].

# CHAPTER THREE

# EXPERIMENTAL PROCEDURES

# CHAPTER 3

# EXPERIMENTAL PROCEDURES

## 3.1    INTRODUCTION

This chapter provides details of the alloys that were prepared for this study, the melting, casting and heat treatment procedures that were followed, preparation of samples and the techniques used for microstructural investigation, and the mechanical testing procedures used to determine the tensile properties.

The composition of the as-received alloy 220 used to prepare the alloys investigated in this study is shown in Table 3.1. The alloy was grain refined using Al-5%Ti-1%B master alloy to achieve a Ti level of 0.15 wt%. Other alloys were prepared from this grain-refined alloy, considered as the base alloy, by adding Sr, Ni, Zr, V, Cr and La to the 220 alloy melt, individually or in different combinations, to produce six alloy compositions. These alloys were coded 220B0 (base alloy), 220B1, 220B2, 220D0, 220D1 and 220D2. Table 3.2 shows the details of the additions made in each case. The first three alloys 220B0, 220B1 and 220B2 were classified as alloys with low Si content (coded B-series), while the remaining three alloys 220D0, 220D1 and 220D2 were classified as alloys with high Si content (coded D-series). Eighty five test bars were cast from each of the alloys prepared, using the low pressure die casting technique. All of the alloys were mechanically tested in order to acquire an understanding of the effects of these additives on the mechanical properties.

**Table 3-1: Chemical composition of the as-received 220 base alloy.**

| Element (wt %) | | | | | |
|---|---|---|---|---|---|
| **Si** | **Fe** | **Cu** | **Mn** | **Mg** | **Al** |
| 1.2 | 0.4 | 2.4 | 0.6 | 0.4 | Bal. |

**Table 3-2: List of Al-2%Cu based 220 alloys prepared for this study.**

| Alloy Code | Additions (wt%) | No. of Tensile test bars prepared |
|---|---|---|
| 220B0 | Al-2.4% Cu + 1.2% Si + 0.4% Mg + 0.4% Fe + 0.6% Mn + 0.15% Ti | 85 |
| 220B1 | Alloy 220 B0 + 0.15% Zr + 0.2% V + 0.3% Ni | 85 |
| 220B2 | Alloy 220 B0 + 0.15% Zr + 0.2% V+ 1% Ni + 0.015% Sr + 0.2% La + 0.2% Cr | 85 |
| 220D0 | Al-2.4% Cu + 8% Si + 0.4% Mg + 0.4% Fe + 0.6% Mn + 0.15% Ti | 85 |
| 220D1 | Alloy 220D0 + 0.15% Zr + 0.2% V + 0.3% Ni | 85 |
| 220D2 | Alloy 220D0 + 0.15%Zr + 0.2% V+ 1% Ni + 0.015% Sr + 0.2% La + 0.2% Cr | 85 |

40

**3.2    MATERIALS AND CASTING PROCEDURES FOR PREPARATION OF ALLOYS**

The 220 alloy was received in the form of ingots having the composition shown in Table 3.1. The ingots were cut into small pieces, cleaned, dried and then melted in a ~150 kg-capacity SiC crucible, using an electrical resistance furnace as shown in Figure 3.1(a). The melting temperature was held at $730 \pm 5$ °C. All alloy melts prepared were grain refined using Al-5%Ti-1%B using master alloy. Additions of Ni, Zr, V, Cr, La and Sr were carried out using Al-20%Ni, Al-20%Zr, Al-15%V, Al-20%Cr, Al-15%La and Al-10%Sr master alloys, respectively.

The molten metal was degassed for 15-20 min using pure dry argon injected into the melt by means of a rotary graphite impeller rotating at ~130 rpm, as shown in Figure 3.1(b). This was done to minimize the hydrogen level of the melt, and to eliminate inclusions and oxides via flotation. Following this, the melt was carefully skimmed to remove oxide layers and dross from the surface.

The melt was poured into an ASTM B-108 permanent mold preheated at 450°C (to drive out moisture) for preparing test bars for tensile testing, as shown in Figure 3.2. Each casting provides two test bars, with a gauge length of 70 mm and a cross-sectional diameter of 12.7 mm, as shown in Figure 3.3.
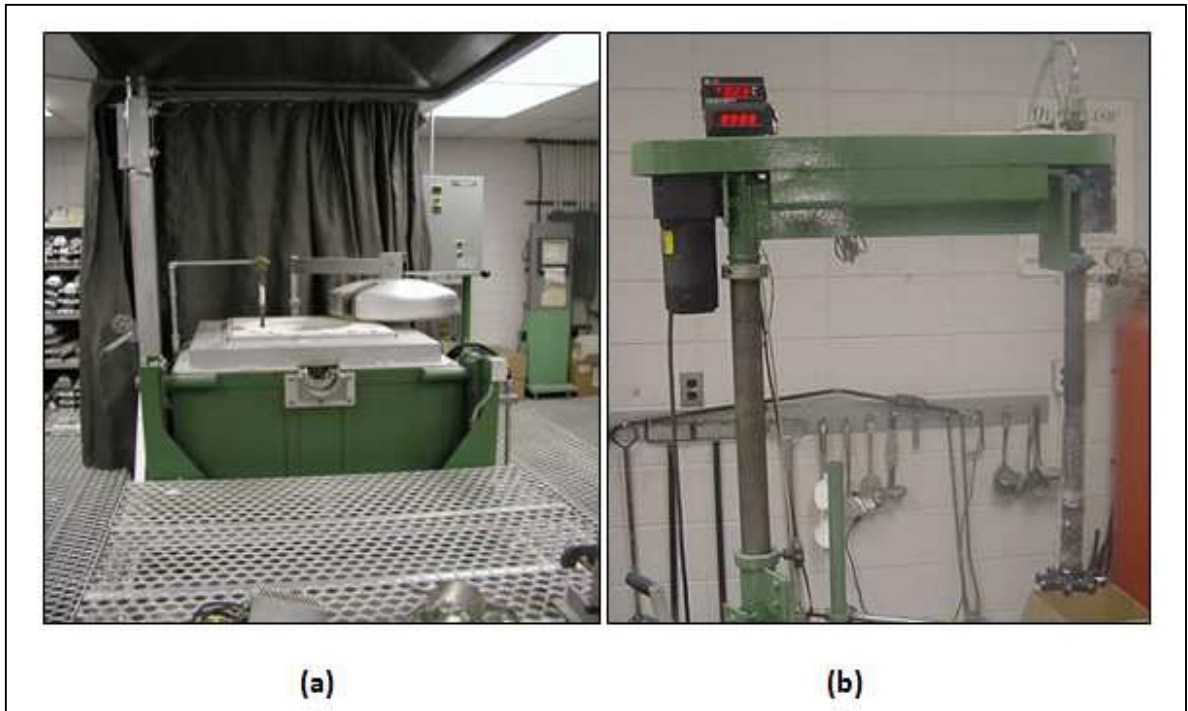
**Figure 3-1: Electrical resistance furnace, (b) Graphite degassing impeller.**



**Figure 3-2: ASTM B-108 permanent mold used for casting tensile test bars.**
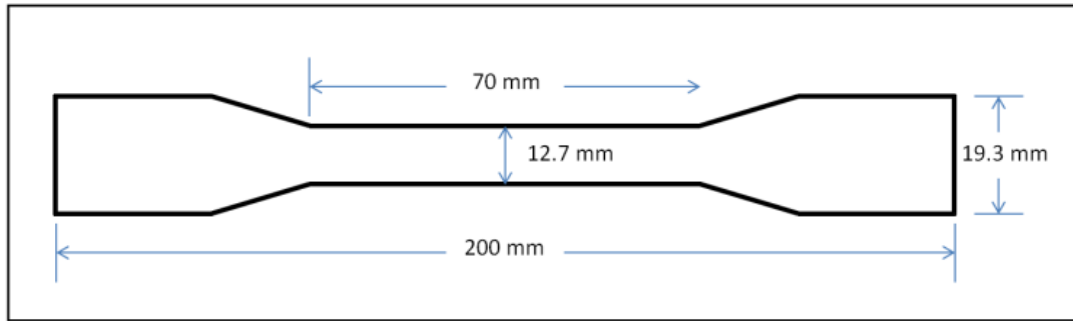
**Figure 3-3: Dimensions of the tensile test bar (in mm).**

Three samplings for chemical analysis were also taken simultaneously at the time of the casting. This was done at the beginning, in the middle, and at the end of the casting process to ascertain the exact chemical composition of each alloy. Master alloys were added just before degassing to ensure homogeneous mixing of the additives together with the degassing.

Table 3.3 lists the actual chemical composition of the various alloys studied and their respective codes, as obtained from the samplings for chemical analysis taken from the corresponding melts prepared for this study. The alloying additions made in each case are highlighted in bold.

**Table 3-3: Chemical composition of the alloys used in this work (wt%).**

| Alloy | Composition (wt%) | | | | | | | | | | | |
|---|---|---|---|---|---|---|---|---|---|---|---|---|
| | Cu | Si | Mg | Fe | Mn | Ti | Zr | V | Ni | Sr | La | Cr |
| Low Si Series | | | | | | | | | | | | |
| **B0** | 2.40 | 1.20 | 0.40 | 0.40 | 0.60 | **0.15** | 0.00 | 0.00 | 0.00 | 0.00 | 0.00 | 0.00 |
| **B1** | 2.40 | 1.20 | 0.40 | 0.40 | 0.60 | 0.15 | **0.15** | **0.20** | **0.30** | 0.00 | 0.00 | 0.00 |
| **B2** | 2.40 | 1.20 | 0.40 | 0.40 | **0.80** | **0.45** | 0.15 | 0.20 | **1.00** | **0.015** | **0.20** | **0.20** |
| High Si Series | | | | | | | | | | | | |
| **D0** | 2.40 | **8.00** | 0.40 | 0.40 | 0.60 | **0.15** | 0.00 | 0.00 | 0.00 | 0.00 | 0.00 | 0.00 |
| **D1** | 2.40 | 8.00 | 0.40 | 0.40 | 0.60 | 0.15 | **0.15** | **0.20** | **0.30** | 0.00 | 0.00 | 0.00 |
| **D2** | 2.40 | 8.00 | 0.40 | 0.40 | **0.80** | **0.45** | 0.15 | 0.20 | **1.00** | **0.02** | **0.20** | **0.20** |

## 3.3    HEAT TREATMENT

In order to enhance the tensile properties, the as-cast test bars were subjected to different heat treatment tempers, namely T5, T6, T62, and T7 treatments which consisted of (a) a single-stage solution heat treatment at 495°C for 5h for T6 and T7 tempers, and a multi-stage solution treatment comprising 495°C/5h + 515°C/2h + 530°C/2h for the T62 temper, followed by (b) quenching in warm water (60-70°C), and then (c) artificial aging at 180°C for 8h for T5, T6 and T62 tempers, and at 240°C for 4h in the case of the T7 temper. Five test bars were used for each heat treatment condition. The Blue M forced air furnace shown in Figure 3.4 was used for carrying out both the solution and aging treatments.



**Figure 3-4: Blue M furnace used for heat treatment.**

## 3.4    MICROSTRUCTURE CHARACTERIZATION

In this study, the microstructure was examined using optical microscopy. Figure 3.5 shows the optical microscope-Clemex image analyzer system that was employed for this purpose.

Selected samples for metallographic investigations were sectioned, mounted, and then ground, and polished to the required finish using standard polishing procedures. Figure 3.6 shows the typical locations in different castings from where these samples were sectioned. As shown in Figure 3.6(a) for the graphite mold castings, 2.5cm x 2.5cm samples were cut at 10 mm height from the bottom, while in the case of the tensile test bars, samples were taken from the gauge length at two different locations; the first was sectioned parallel to the cross section area of the tensile-tested bar, 10 mm below the fracture surface, as shown in Figure 3.6(b) (sample #1); the second was sectioned longitudinally to examine the sample area below the fracture surface, (sample #2). Each sectioned sample was mounted in bakelite, and subjected to grinding, using consecutively finer grit size waterproof SiC papers (grit sizes 320, 400, 600, 800 and 1200). The samples were then polished using polycrystalline diamond suspension (6μm, 3 μm, for 3 min each), followed by colloidal silica suspension (0.06 μm) to obtain a mirror-like finish of the sample surface. The mounting of the samples in bakelite was carried out using a Struers LaboPress-3 machine, while the grinding and polishing procedures were carried out using a TegraForce-5 machine, as shown in Figure 3.7.

**Figure 3-5: Optical microscope-Clemex image analyzer system**
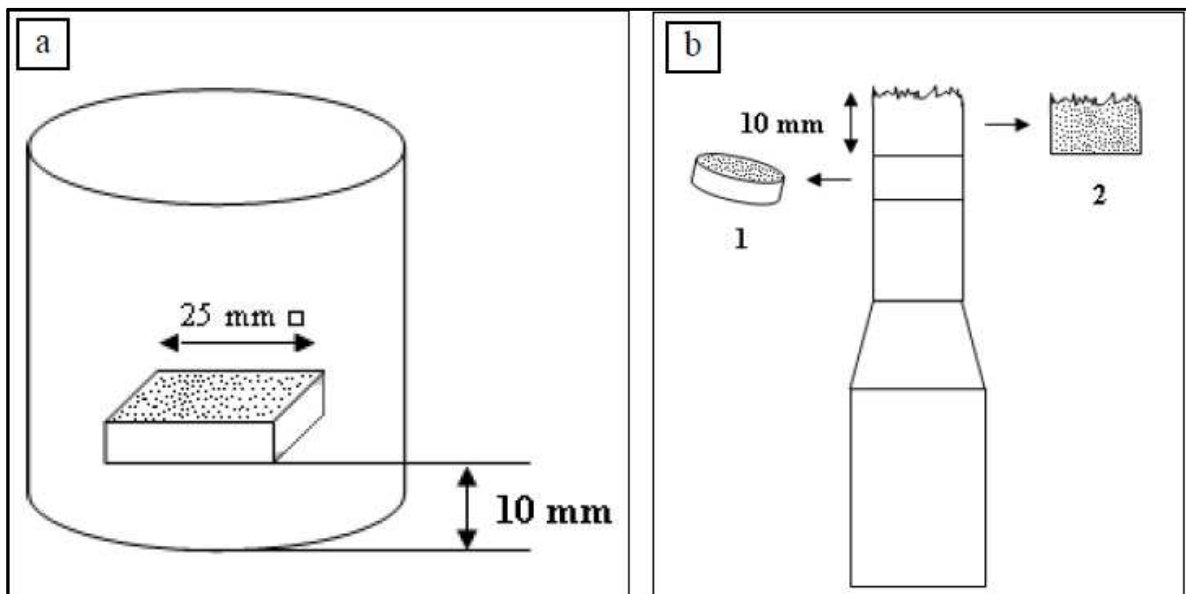


**Figure 3-6: Locations of metallography samples sectioned from (a) graphite mold castings, (b) tensile tested bars.**

**Figure 3-7: (L) Struers LaboPress-3 and (R) TegraForce-5 machines used for mounting and polishing samples for metallography.**

## 3.5    THERMAL ANALYSIS

In order to obtain the cooling curves and to identify the main reactions and corresponding temperatures occurring during the solidification of 220 alloys, thermal analysis of the alloy melt compositions was carried out. Ingots of the as-received commercial 220 alloy were cut into smaller pieces, cleaned, and then dried to prepare the required alloys. The melting process was carried out in a cylindrical graphite crucible of 2-kg capacity, using an electrical resistance furnace. The melting temperature was maintained at 780°C, while the alloys were grain-refined using Al-5%Ti-1%B using master alloy. Additions of Ni, Zr, V, Cr, La and Sr were carried out using Al-20%Ni, Al-20%Zr,

Al-15%V, Al-20%Cr, Al-15%La and Al-10%Sr master alloys, respectively, as was the case with the casting of the tensile test samples. For the purpose of determining the reactions taking place during solidification, part of the molten metal was also poured into an 800 g capacity graphite mold preheated to 650°C so as to obtain near-equilibrium solidification conditions at a cooling rate of (0.35°C/s). A high sensitivity Type-K (chromel-alumel) thermocouple, insulated using a double-holed ceramic tube, was attached to the centre of the graphite mold. The temperature-time data was collected using a high speed data acquisition system linked to a computer system that recorded the data every 0.1 second, as shown in Figure 3.8 and Figure 3.9.

From this data, the cooling curves and the corresponding first derivative curves for a number of selected alloys were plotted so as to identify the main reactions occurring during solidification with the corresponding temperatures; the various phases which constituted the microstructure of each alloy were expected to be revealed as well.
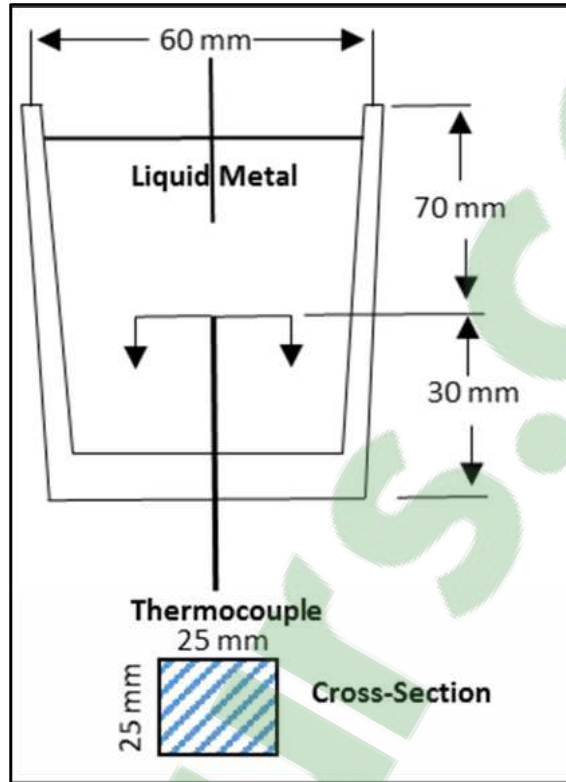
**Figure 3-8: Schematic drawing showing the graphite mold used for thermal analysis**



**Figure 3-9: thermal analysis set-ups**

## 3.6    TENSILE TESTING

Tensile testing of the test bars corresponding to the various alloys/heat treatment conditions investigated was carried out at ambient and at high temperature for the purposes of this study. The description of the samples prepared for these tests has been provided in Section 3.2. Tests were carried out for all as-cast and heat-treated test bars, using five test bars for each alloy composition/condition studied for both room and high temperature tests. Testing was carried out at a strain rate of 4 x $10^{-4}$ $s^{-1}$, using an MTS Servohydraulic Mechanical Testing machine for the ambient temperature tests, and an Instron Universal Mechanical Testing machine for high temperature testing.

### 3.6.1    TENSILE TESTING AT AMBIENT TEMPERATURE

For the ambient temperature testing, the samples were tested using an MTS Servohydraulic Mechanical Testing machine as shown in Figure 3.10. An extensometer or strain gage was used to measure the extent of deformation in the samples. Yield strength (YS) at 0.2% offset strain, ultimate tensile strength (UTS), and percent elongation (%El), were obtained from the data acquisition system of the machine. The room temperature tests covered a total of 210 test bars as follows: 7 conditions x 5 bars/alloy x 6 alloys = 210 bars (tests).

**Figure 3-10: MTS Mechanical Testing machine used for ambient temperature testing**.

### 3.6.2 TENSILE TESTING AT HIGH TEMPERATURE

For testing at high temperature, the samples were tested using an Instron Universal Mechanical Testing machine as shown in Figure 3.11. In this case, the samples were mounted in the testing chamber which was preset to the required testing temperature of 250°C. After mounting, the sample was maintained for 60 min at the testing temperature before starting the test. A data acquisition system attached to the machine provided the tensile data, namely, the ultimate tensile strength (UTS), the yield strength at 0.2% offset strain (YS), and the percent elongation (%El), calculated over the 25.4 mm gauge length of the test bar. The average UTS, YS and %El values obtained from each set of five tests were considered as representing the tensile properties of that alloy/condition. The tests at high

temperature were carried out in two stages: in the first case, the test bars being tested were stabilized for 1 hour at 250°C; a total of 150 bars were tested, covering a total of 5 conditions x 5 bars/alloy x 6 alloys. In the second case, the bars were stabilized for 200 hours at 250°C, also covering a total of 150 bars (5 conditions x 5 bars/alloy x 6 alloys), giving a total of 300 bars used for this part of the study.



**Figure 3-11: Instron Universal Mechanical Testing machine with chamber for high temperature testing.**

# CHAPTER FOUR

# MICROSTRUCTURE CHARACTERIZATION

# AND POROSITY FORMATION

# CHAPTER 4

# MICROSTRUCTURE CHARACTERIZATION AND POROSITY FORMATION

## 4.1 INTRODUCTION

This chapter is divided into two main parts. The first part presents and discusses the results describing the effect of different alloying/transition element additions, individually or in combination, on the microstructure and solidification sequence of Aluminum-Copper 220 type alloys. These effects were studied using the thermal analysis technique which provides close-to-equilibrium slow cooling rate conditions. The low solidification rate (0.35°C/s) achieved by the thermal analysis set-up provides ease of detection and analysis of the phases which are formed in the respective alloys. The second part of this chapter presents the porosity formation observed in these same alloys. The alloy samples investigated in this part include the as-cast and solution heat-treated conditions, covering both one and multi-step solution heat treatments.

## 4.2 THERMAL ANALYSIS

### 4.2.1 BASE ALLOY B0

The base 220 alloy (B0) contains around 2.4% Cu, 1.2% Si, 0.4% Mg, 0.4% Fe, 0.6%Mn and 0.15% Ti. Thus it may be classified as an Al-Cu base alloy. Based on this composition, the main phases expected for this alloy will be restricted to Cu-rich intermetallic phases as well as Fe-rich intermetallic phases. In order to determine the main intermetallic phases and their formation reactions in the base alloy, thermal analysis of the

base alloy melt was carried out under low solidification rate conditions (~0.3°C/s). Based on the temperature-time data obtained, the cooling curve and its first derivative were plotted, as shown in Figure 4.1. The numbers on the first derivative curve correspond to the same reaction numbers as those listed in Table 4.1.

**Table 4-1: Proposed main reactions occurring during solidification of Alloy B0**

| Reaction | Suggested Temperature Range (°C) | Suggested Precipitated Phase |
|---|---|---|
| 1 | 640°C | Formation of α-Al dendritic network |
| 2 | 620°C | Precipitation of α-Al$_{15}$(Fe,Mn)$_3$Si$_2$ |
| 3 | 495°C | Precipitation of θ-Al$_2$Cu and Q-Al$_5$Mg$_8$Si$_6$Cu$_2$ |

As may be seen from Figure 4.1, Alloy B0 starts to solidify at 640°C (Reaction #1) through the development of the α-Al dendritic network, followed by the precipitation of α-iron Al$_{15}$(Fe,Mn)$_3$Si$_2$ at 620°C (Reaction #2), and then Al$_2$Cu and Al$_5$Mg$_8$Si$_6$Cu$_2$ precipitate simultaneously as the final reaction at 495°C (Reaction #3). Figure 4.2 shows the possible morphologies of these intermetallic phases; the α-iron Al$_{15}$(Fe,Mn)$_3$Si$_2$ phase appears in compacted Chinese script form which is gray in color, while the Al$_2$Cu phase may appear either in eutectic form (Al + Al$_2$Cu) or as block-like particles which appear to have a pinkish color when viewed under the optical microscope. The Q-phase, Al$_5$Mg$_8$Si$_6$Cu$_2$, appears in the form of small particles which are dark gray in color, and growing out of the Al$_2$Cu phase. The absence of free Si in the microstructure implies that the Si content of the alloy was consumed in the formation of the Q-Al$_5$Mg$_8$Cu$_2$Si$_6$ and α-iron phases.
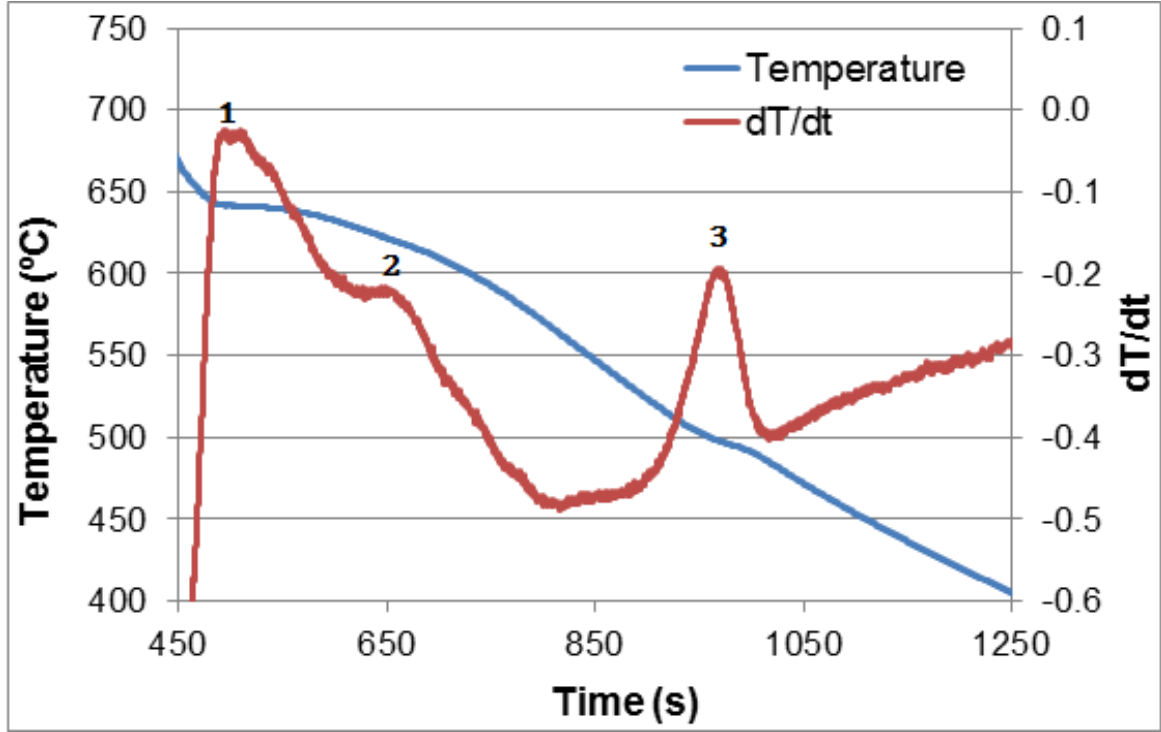
**Figure 4-1: Cooling curve and first derivative obtained from the thermal analysis of base alloy B0.**
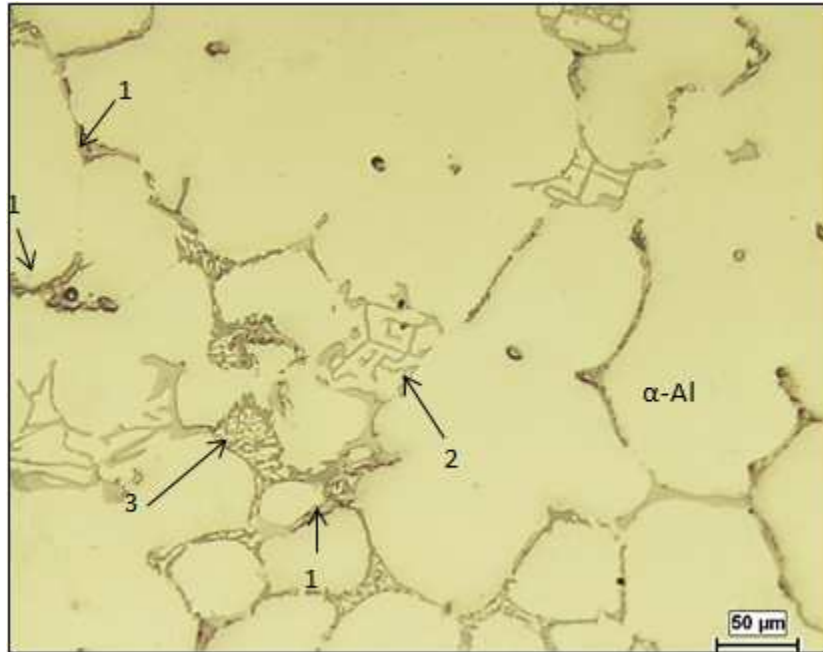
**Figure 4-2: Optical micrograph showing the various phases formed in the base alloy B0: 1- θ-CuAl$_2$; 2- α-Al$_{15}$(Fe,Mn)$_3$Si$_2$,  3- Q-AlCuMgSi..**

### 4.2.2   ALLOY B1

The cooling curve for Alloy B1 (B0 + 0.15wt% Zr + 0.20wt% V + 0.3wt% Ni) obtained from the temperature-time data and its first derivate plot are shown in Figure 4.3. The numbers on the first derivative curve correspond to the reaction numbers listed in Table 4.2. Apart from the α-Al dendrites and the eutectic Al$_2$Cu particles observed in the interdendritic regions, other phases may also be observed, as depicted in the optical micrograph of Alloy B1 shown in Figure 4.4. It is interesting to note that the eutectic Al$_2$Cu particles in Figure 4.4 appear similar to those seen in Figure 4.2 for the base alloy B0. The β-Fe phase is mostly associated with an alloy Fe content of more than 0.1 wt% [10]. Increasing the Fe content to more than 0.1 wt% will increase the quantity and size of the β-

phase platelets in the microstructure, which is not favorable to the mechanical properties [74, 75]. At more than 0.1 wt% Fe, however, most of the β-phase will precipitate at a higher temperature; such β-phase platelets are characterized by their large size in the microstructure, as seen in Figure 4.4.

**Table 4-2: Proposed main reactions occurring during solidification of alloy B1.**

| Reaction | Suggested Temperature Range (°C) | Suggested Precipitated Phase |
|:---:|:---:|:---:|
| **1** | 640°C | Formation of α-Al dendritic network |
| **2** | 620°C | Precipitation of α-Al$_{15}$(Fe, Mn)$_3$Si$_2$ |
| **3** | 495°C | Precipitation of θ-Al$_2$Cu and Q-Al$_5$Mg$_8$Si$_6$Cu$_2$ |
| **4, 5** | 570°C-530°C | Zr and V- rich phases |

**Figure 4-3: Cooling curve and first derivative obtained from the thermal analysis of Alloy B1.**
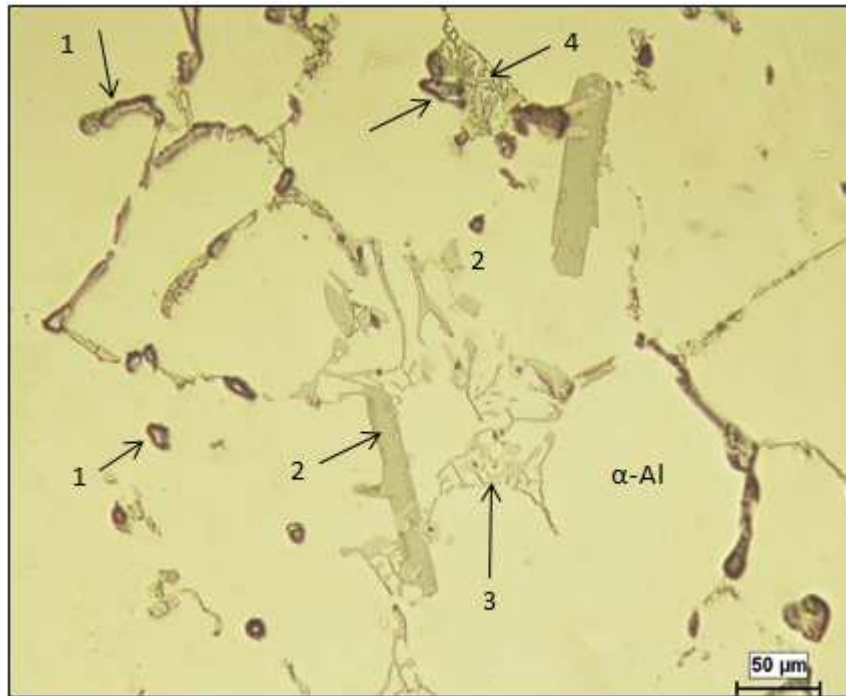
**Figure 4-4: Optical micrograph showing the phases formed in Alloy B1: 1- CuAl$_2$; 2- Zr-V-rich phase; 3- α-Al$_{15}$(Fe,Mn)$_3$Si$_2$;  4- Q-AlCuMgSi;**

### 4.2.3   ALLOY B2

The cooling curve of Alloy B2 (B0 + 0.80% Mn + 0.20% La + 0.20% Cr) was obtained from its temperature-time data and is shown along with its first derivate plot in Figure 4.5. The reactions taking place during solidification for this alloy are listed in Table 4.3. Similarities between the solidification curves of Alloys B1 and B2 are noted. Apart from the α-Al dendrites and the eutectic Al$_2$Cu particles observed in the interdendritic regions, other phases observed in the optical micrograph include the α-iron α-Al$_{15}$(Fe,Mn)$_3$Si$_2$ script phase, the Q-AlCuMgSi phase, Mg$_2$Si phase in black script form, and the AlSiTiZrV phase, as shown in Figure 4.6. Neutralization of the harmful effects of iron through the promotion of the less harmful α-Fe Chinese-script phase rather than the

brittle needle-like β-Fe phase is sought with the goal of improving strength, ductility and other properties [12, 13].

In the alloys containing nickel, the $Al_3CuNi$ phase is observed situated adjacent to the $Al_2Cu$ phase and both phases are located at the limits of the dendritic α-Al phase; this observation is in agreement with the fact that the reactions noted in the thermal analysis curves, namely Reactions #4 and #5, are contiguous to one another [76].

**Table 4-3: Proposed main reactions occurring during solidification of Alloy B2.**

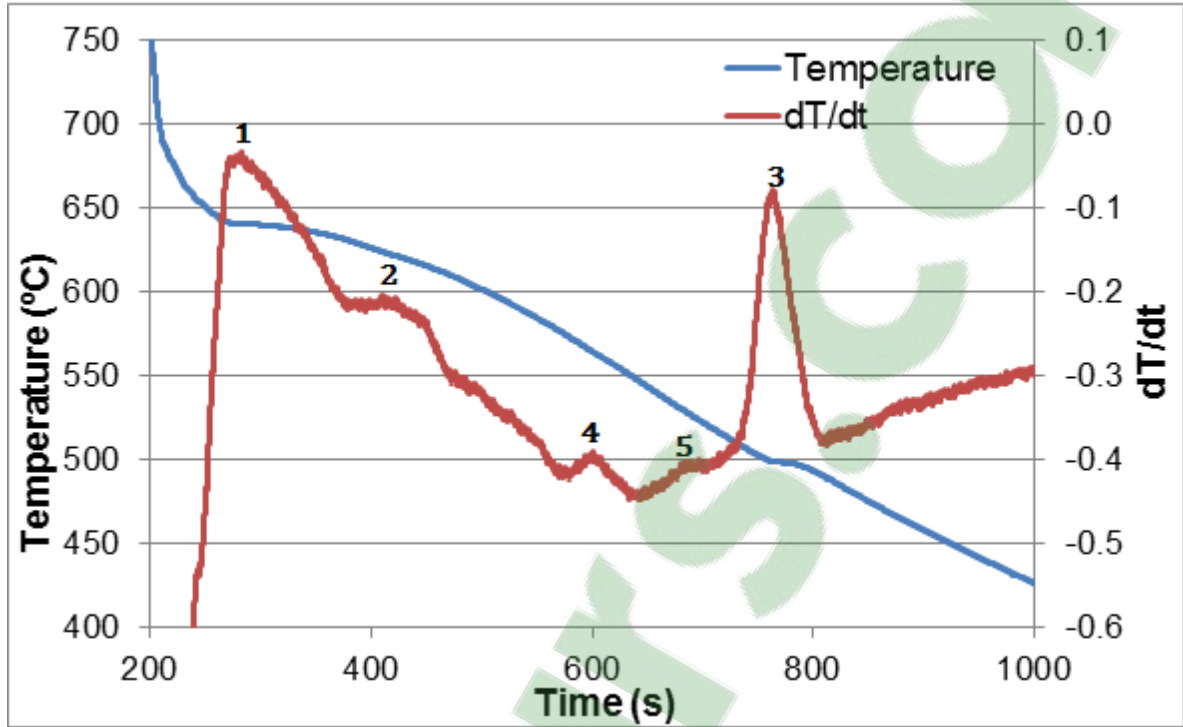| Reaction | Suggested Temperature Range (°C) | Suggested Precipitated Phase |
|:---:|:---:|:---:|
| **1** | 639°C | Formation of α-Al dendritic network |
| **2** | 615°C | Precipitation of $α-Al_{15}(Fe,Mn)_3Si_2$ |
| **3** | 497°C | Precipitation of $θ-Al_2Cu$ and $Q-Al_5Mg_8Si_6Cu_2$ |
| **4, 5** | 570°C-530°C | Zr- and V-rich phases |
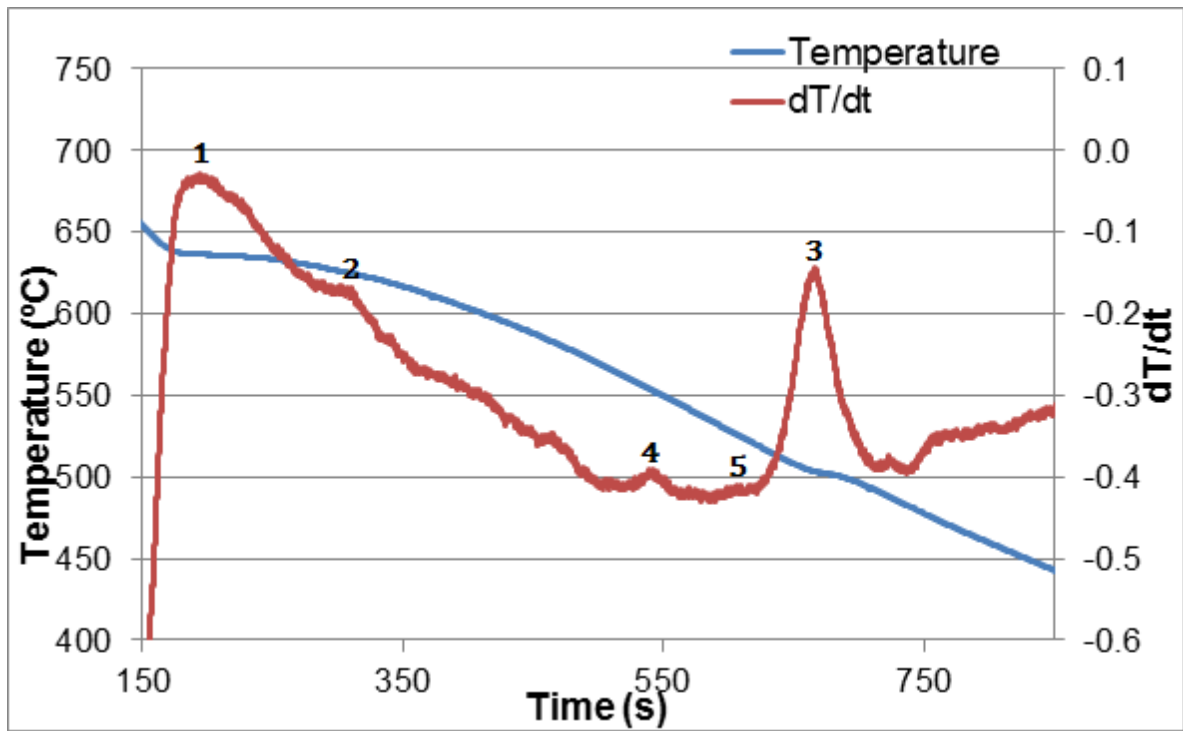
**Figure 4-5: Cooling curve and first derivative obtained from the thermal analysis of Alloy B2.**
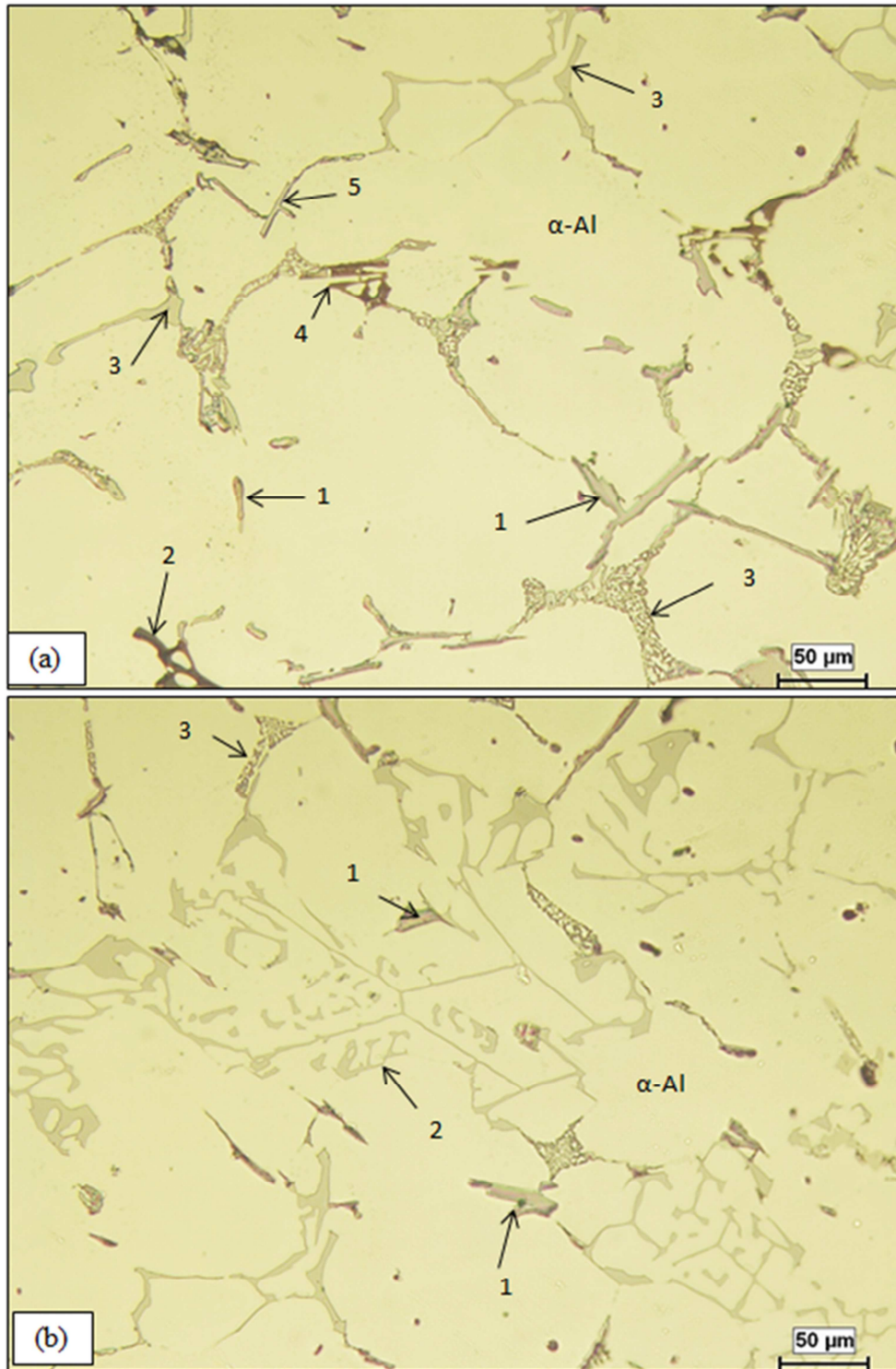
**Figure 4-6: Optical micrographs showing the phase formed in Alloy B2: (a) 1- CuAl$_2$; 2- α-Al$_{15}$(Fe,Mn)$_3$Si$_2$; 3- Q-AlCuMgSi; 4- Mg$_2$Si; 5- AlSiTiZrV.**

### 4.2.4 ALLOY D0

The cooling curve of alloy D0 contains around 2.4% Cu, 8% Si, 0.4% Mg, 0.4% Fe, 0.6%Mn, 0.15% Ti; as the Si content is 8 wt.%, which led to the difference in Reaction # 2, compared to the B0-based alloys, with the precipitation of the eutectic Al-Si phase in addition to the α-iron phase. Based on the thermal analysis data obtained, the cooling and first derivative curves were drawn, as shown in Figure 4.7 for the base alloy D0. The numbers on the first derivative curve correspond to the same reaction numbers listed in Table 4.4. The alloy D0 starts to solidify at 600°C (Reaction #1) through the development of the dendritic network followed by the precipitation of eutectic Si and α-iron $Al_{15}(Fe,Mn,Cu)_3Si_2$ at 570°C (Reaction #2) and then $Al_2Cu$ and $Al_5Mg_8Si_6Cu_2$ precipitate simultaneously as a final reaction at 510°C (Reaction #3). Apart from the α-Al dendrites and the eutectic Si particles observed in the interdendritic regions, other phases may also be observed in the optical micrograph image of the alloy D0 as shown in Figure 4.8. The Si particles appear in their acicular, non- modified form without the addition of Sr.

Table 4-4: Proposed main reactions occurring during solidification of alloy D0.

| Reaction | Suggested Temperature Range (°C) | Suggested Precipitated Phase |
|----------|----------------------------------|------------------------------|
| 1 | 600°C | Formation of α-Al dendritic network |
| 2 | 570°C | Eutectic reaction(eutectic Si + α-Fe) |
| 3 | 510°C | Precipitation of θ-$Al_2Cu$ and Q-$Al_5Mg_8Si_6Cu_2$ |

**Figure 4-7: Cooling curve and first derivative obtained from the thermal analysis of alloy D0.**
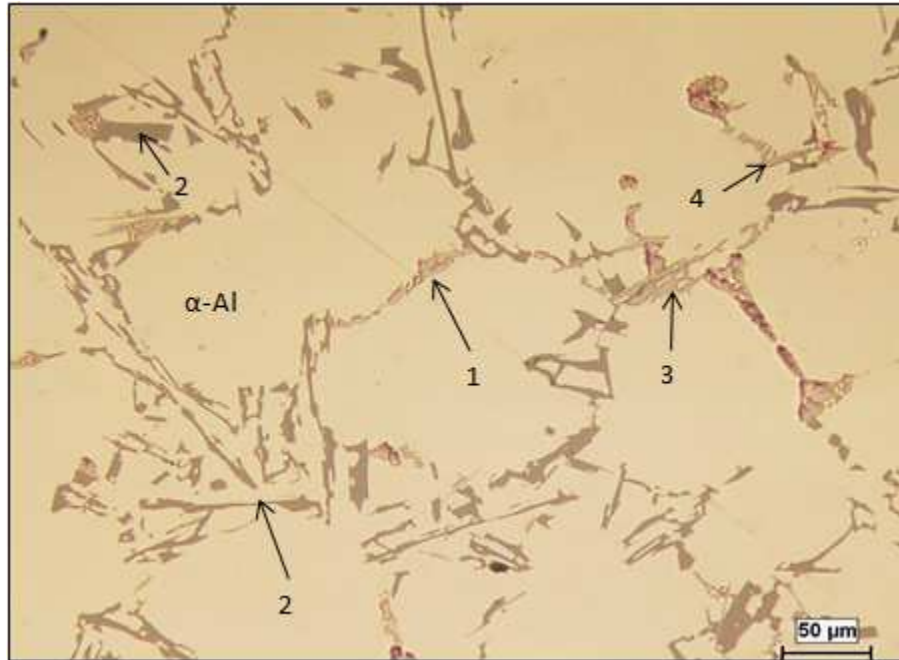
**Figure 4-8: Optical micrograph showing the phases formed in Alloy D0: 1- CuAl$_2$; 2- eutectic Si; 3-AlSiMgCu; 4- AlSiMnFe.**

### 4.2.5 ALLOY D1

The cooling curve and the first derivate plot for Alloy D1 (comprising D0 + 0.15 wt% Zr + 0.2 wt% V + 0.3 wt% Ni) are shown in Figure 4.9, obtained from the temperature-time data for the alloy. The reactions observed during the solidification of Alloy D1 are listed in Table 4.5. Apart from the α-Al dendrites and the eutectic Si particles observed in the interdendritic regions, other phases may also be observed, as shown in the optical micrographs presented in Figure 4.10. The Q-Al$_5$Mg$_8$Si$_6$Cu$_2$ phase appears in the form of small particles growing out of the Al$_2$Cu phase.

**Table 4-5: Proposed main reactions occurring during solidification of Alloy D1.**

| Reaction | Suggested Temperature Range (°C) | Suggested Precipitated Phase |
|---|---|---|
| 1 | 600°C | Formation of α-Al dendritic network |
| 2 | 570°C | Al-Si eutectic reaction + α-Fe |
| 3 | 510°C | Precipitation of $\theta$-$Al_2Cu$ and Q-$Al_5Mg_8Si_6Cu_2$ |
| 4 | 538°C-528°C | Zr- and V- rich phases |
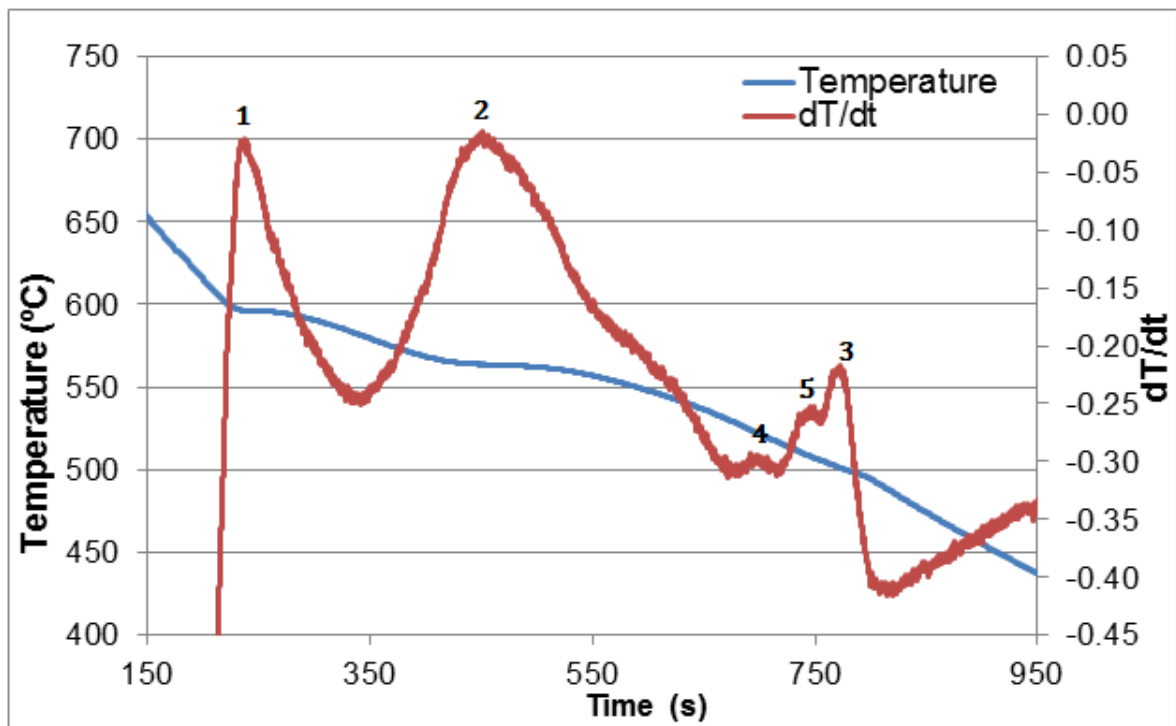


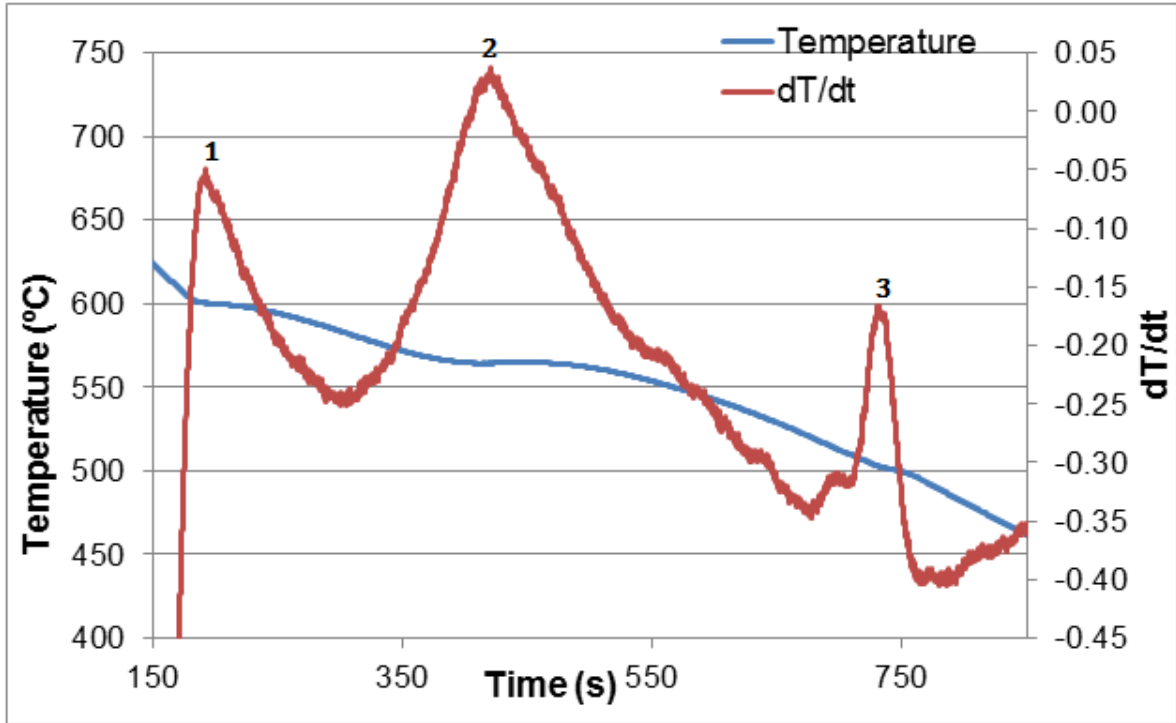**Figure 4-9: Cooling curve and first derivative obtained from the thermal analysis of Alloy D1.**

**Figure 4-10: Optical micrographs showing the phases formed in Alloy D1: 1- CuAl$_2$; 2-eutectic Si; 3-sludge; 4- AlNiCu; 5- AlSiMnFe.**

### 4.2.6  ALLOY D2

The cooling curve of Alloy D2 (D0 + 0.80% Mn + 0.20% La + 0.20% Cr) obtained from its time-temperature data and its first derivate plot are shown in Figure 4.11. The numbers on the first derivative curve correspond to the reaction numbers listed in Table 4.6. The peak corresponding to the reaction for $Al_2Cu$ phase formation was decreased due to the consumption of Cu in the formation of $Al_3CuNi$ intermetallic phase. Apart from the α-Al dendrites and the eutectic Si particles observed in the interdendritic regions, other phases may also be observed, as seen from the optical micrographs of alloy D2 displayed in Figure 4.12.

Although Alloy D2 was modified with 0.02 wt% Sr, the eutectic silicon phase appears to be only partially modified. This partial modification of the eutectic silicon structure may be attributed to the slow cooling rate obtained in the thermal analysis experiments. The variation of the eutectic Si morphology from coarse brittle flakes to a finer fibrous form can be attributed to Sr addition that leads to an enhancement in the tensile properties, in particular, the ductility of the alloy [48]. The higher Mn:Fe ratio and/or the presence of chromium lead to the formation of another version of the α-Fe phase, $\alpha\text{-}Al_{15}(Fe,Mn,Cr)_3Si_2$, termed sludge. In this alloy an $\alpha\text{-}Al_{15}(Fe,Mn,Cr)_3Si_2$ phase was observed, displaying a star-like morphology, and located within the α-Al dendrites, as shown in Figure 4.12. The sludge particles are usually observed in the interdendritic regions. This phenomenon of iron intermetallic precipitation within the α-Al dendrites proves very useful in the case of such Al-Si die-casting alloys as 380 alloy, containing 9 wt% Si, where the proportion of α-Al dendrites is relatively higher [77]. These sludge

particles are extremely hard and thus have a detrimental effect on the mechanical properties and machinability. The formation of these particles may be controlled by calculating the sludge factor given by the following formula,

$$\text{Sludge Factor (S.F.)} = 1 \times \text{wt\% Fe} + 2 \times \text{wt\% Mn} + 3 \times \text{wt\% Cr}$$

which correlates the %Fe, %Mn, and %Cr levels in the alloy [66, 67].

The critical sludge factor beyond which sludge is formed equals 1.8, if a casting temperature of 650°C or more is maintained. However, for holding temperatures lower than this value, a critical sludge factor of 1.4 is recommended, since sludge formation is a temperature dependent process in combination with the Fe, Mn, and Cr concentrations.

**Table 4-6: Proposed main reactions occurring during solidification of Alloy D2.**

| Reaction | Suggested Temperature Range (°C) | Suggested Precipitated Phase |
|:---:|:---:|:---:|
| **1** | 600°C | Formation of α-Al dendritic network |
| **2** | 570°C | Al-Si eutectic reaction + α-Fe |
| **3** | 510°C | Precipitation of θ-$Al_2Cu$ and Q-$Al_5Mg_8Si_6Cu_2$ |
| **4, 5** | 538°C-528°C | Zr- and V-rich phases |

**Figure 4-11: Cooling curve and first derivative obtained from the thermal analysis of Alloy D2.**

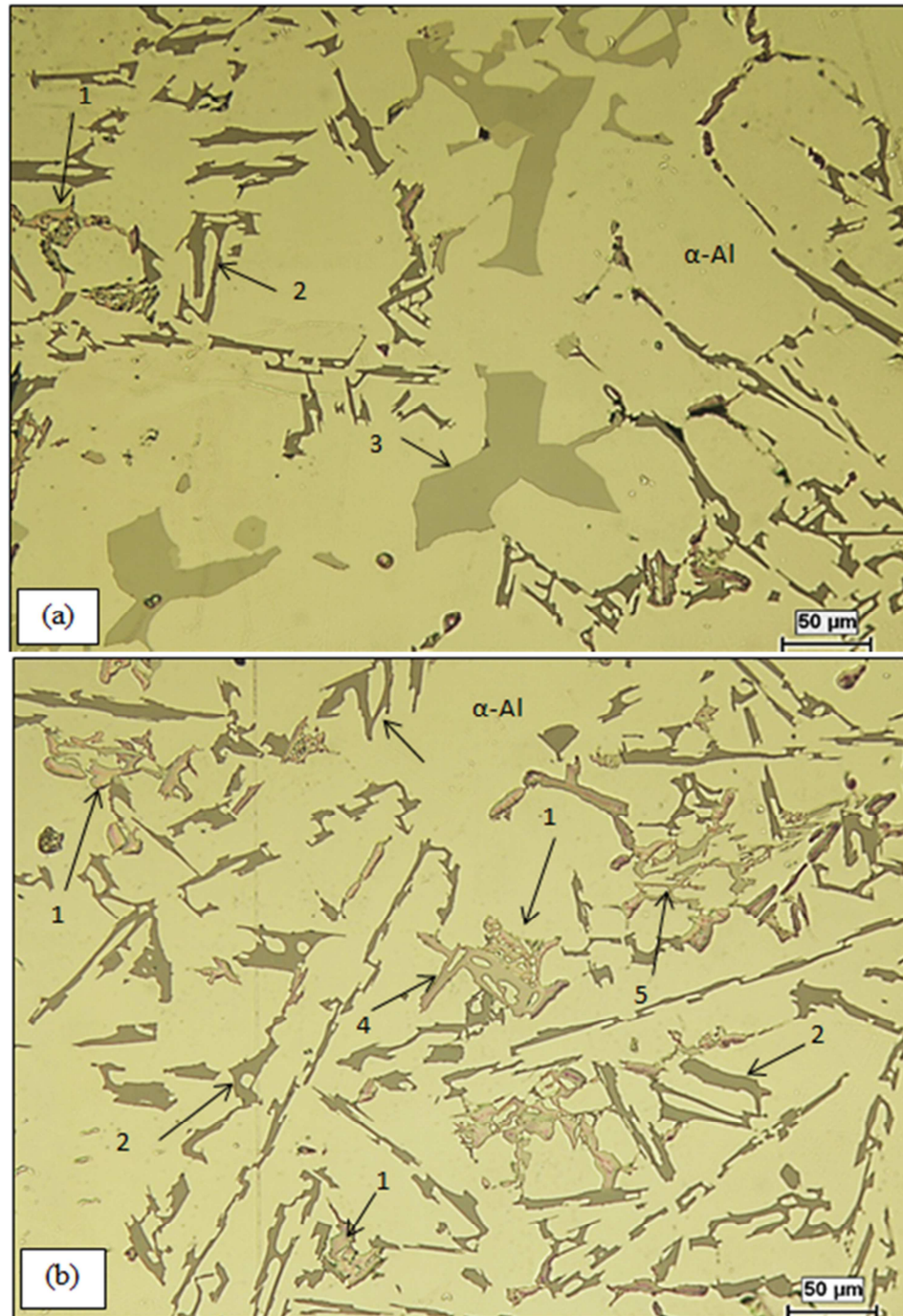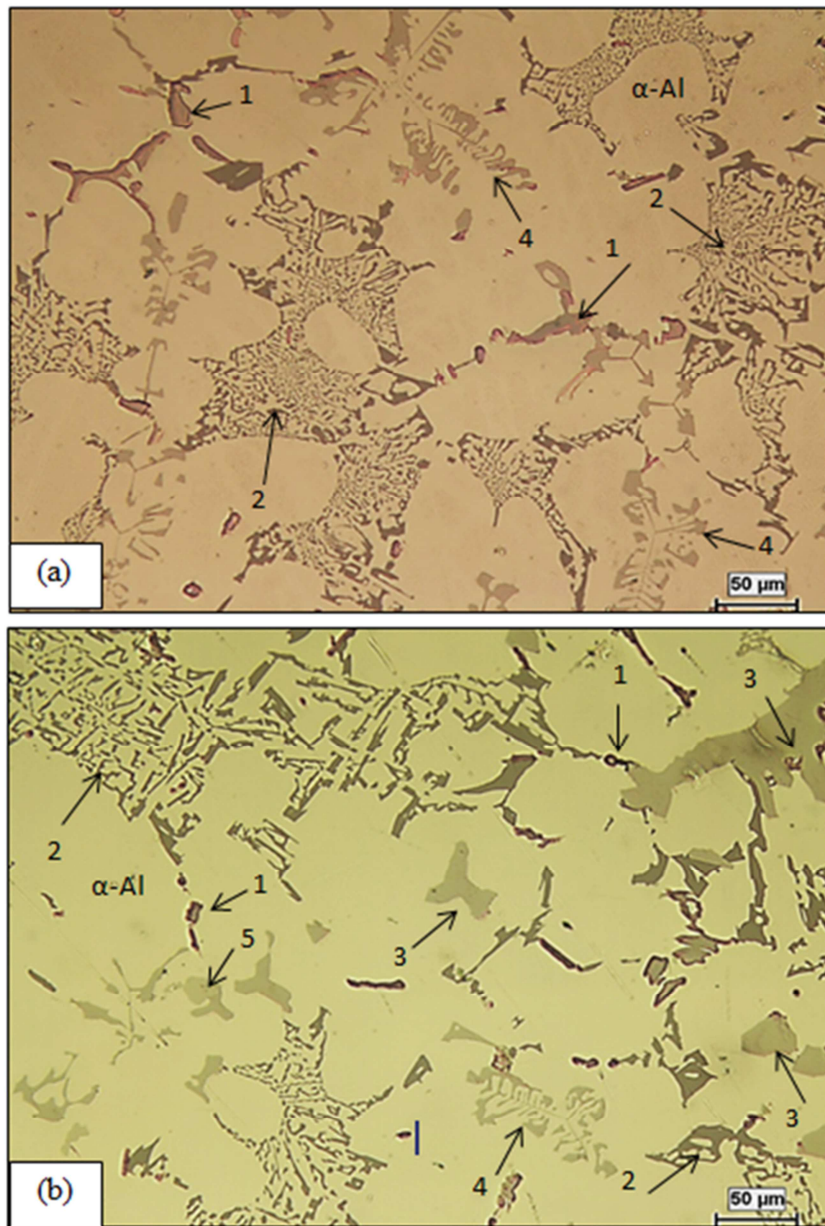**Figure 4-12: Optical micrographs showing the phases formed in Alloy D2: 1- CuAl$_2$; 2- eutectic Si; 3-AlFeMnCrSiVNi; 4- AlSiCuNiLa; 5- AlNiSiZrCuFe.**

## 4.3    POROSITY FORMATION DUE TO INCIPIENT MELTING

A main consequence of incipient melting in Al-Si-Cu alloys is the formation of a structureless form of the $Al_2Cu$ phase and related porosity on quenching. As reported by De la Sablonnière and Samuel [106], the $Al_2Cu$ intermetallic may melt at 525°C, so that when the temperature of the multi-step solution heat treatment reaches 530°C, or when local heating occurs at any point in the sample, it is expected that the $Al_2Cu$ phase will melt, causing the formation of porosity, leading, in turn, to a deterioration in the mechanical properties.

Control of the solution treatment process is very critical because, if the solution heat treatment temperature exceeds the melting point, there is localized melting at the grain boundaries and the mechanical properties are reduced. In this study, all alloy melts were degassed to minimize the hydrogen level before casting. The as-cast alloys were heat treated using one step and multi-step solution treatments. The multi-step solution heat treatment was carried out at three different  temperatures consecutively, for different solution times, viz., 5 hrs at 495°C, followed by 2 hrs at 515°C, and then 2 hrs at 530°C. Thus, as the only variable factor in this case is the temperature, any big changes in the amount of porosity observed could be reasonably assumed to be mainly due to the melting of the copper phase resulting from the changes in the temperature variable.

Porosity measurements were therefore carried out to monitor the incipient melting that resulted in the alloys studied, corresponding to the various solution heat treatments. The parameter measured was the average area percent porosity (percentage porosity over a

constant sample surface area) that was quantified using an optical microscope-Clemex Vision PE 4.0 image analysis system, where the samples were examined at 200x magnification. The details of these measurements are listed in Table 4.7.

As may be seen from Table 4.7, the as-cast samples for all alloys show minimum porosity, whereas after solution heat treatment, the porosity values increase. In general, compared to the one-step or SHT 1 solution treatment, the multi-step or SHT 2 solution treatment leads to somewhat higher porosity values.

Table 4-7: Percentage porosity values observed in B and D alloys

| Alloy Code | Condition | Area (%) | | Alloy Code | Condition | Area (%) | |
|---|---|---|---|---|---|---|---|
| | | Mean | SD | | | Mean | SD |
| B0 | As Cast | 0.42 | 0.21 | D0 | As Cast | 0.04 | 0.02 |
| | SHT 1 | 1.25 | 0.44 | | SHT 1 | 0.14 | 0.30 |
| | SHT 2 | 1.43 | 0.55 | | SHT 2 | 0.26 | 0.31 |
| B1 | As Cast | 0.25 | 0.28 | D1 | As Cast | 0.13 | 0.08 |
| | SHT 1 | 1.13 | 0.78 | | SHT 1 | 0.20 | 0.31 |
| | SHT 2 | 0.98 | 0.58 | | SHT 2 | 0.30 | 0.20 |
| B2 | As Cast | 0.32 | 0.27 | D2 | As Cast | 0.10 | 0.10 |
| | SHT 1 | 0.56 | 0.22 | | SHT 1 | 0.25 | 0.38 |
| | SHT 2 | 0.17 | 0.14 | | SHT 2 | 0.39 | 0.40 |

The microstructures of the alloys studied were also examined at 500x magnification in certain cases to highlight some of the interesting features observed with respect to the incipient melting-related porosity observed in the different samples, as well as the effect of the progress of solution heat treatment on the micro-constituents themselves. Examples of the microstructures of the B0, B1, B2 and D0, D1 and D2 alloys listed in Table 4.7 are shown below.

Figure 4.13 depicts the microstructures observed for the 220 base alloy B0 in the as-cast, and solution heat-treated SHT-1 and SHT-2 conditions, where instances of incipient melting may be observed in each case. In Figure 4.13(c), the extended duration of the multi-step solution treatment refines the constituents present in the interdendritic regions. At high magnification, the onset and progress of melting of the copper phase can be clearly seen.

In the case of Alloy B1, the as-cast sample shown in Figure 4.14(a) reveals a very slight presence of incipient melting along the grain boundaries where the copper phase precipitated (see arrows), whereas a larger amount of incipient melting is observed after SHT 1treatment, as may be noted near the top left corner of Figure 4.14(b). The circled area in the higher magnification micrograph of Figure 4.14(c) shows an interesting example of the beginning of incipient melting of the copper phase. The two small arrows point to the spheroidization of the eutectic silicon particles observed in the microstructure with the progress of solution treatment. Figure 4.14(d), also taken at 500x magnification, gives an idea of the extent to which the other constituents in the microstructure have become refined

with the extended duration of the SHT 2 treatment. Evidence of incipient melting is also observed.
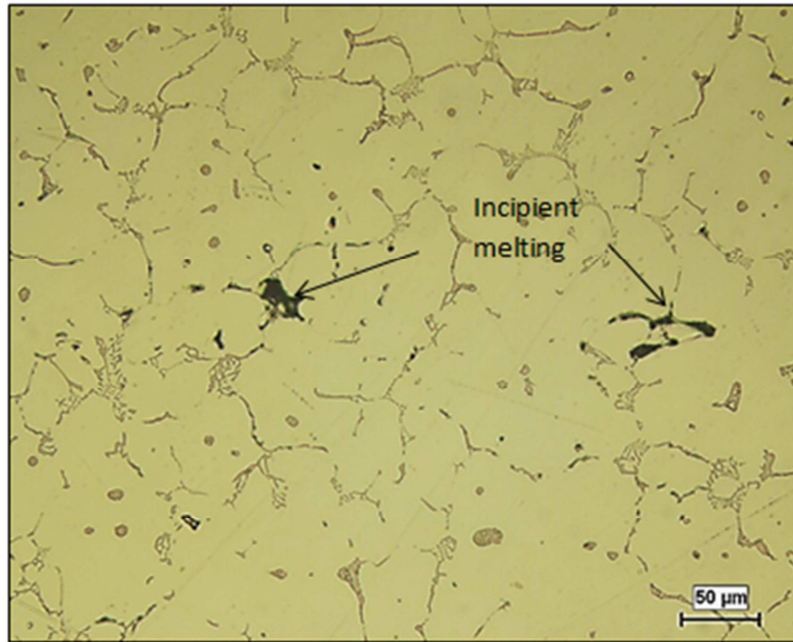

(a) B0-As-Cast
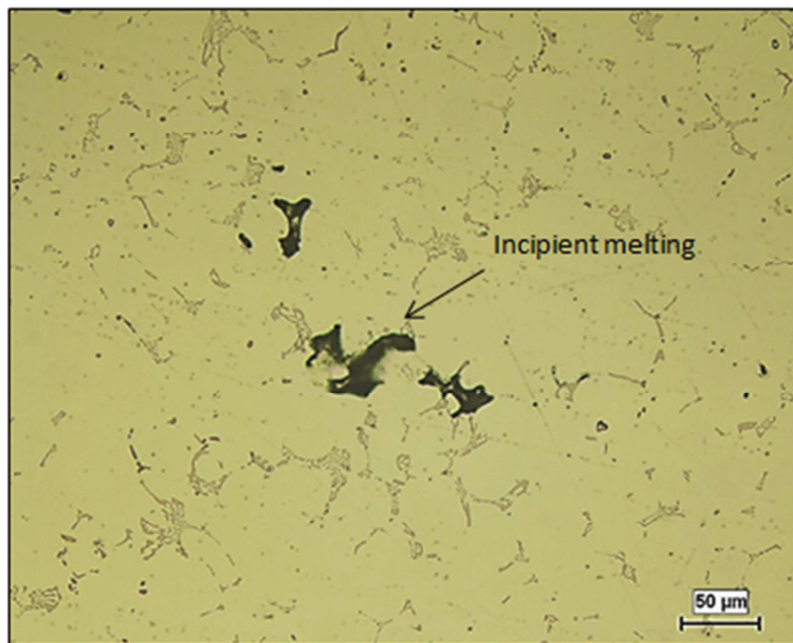

(b) B0-SHT-1
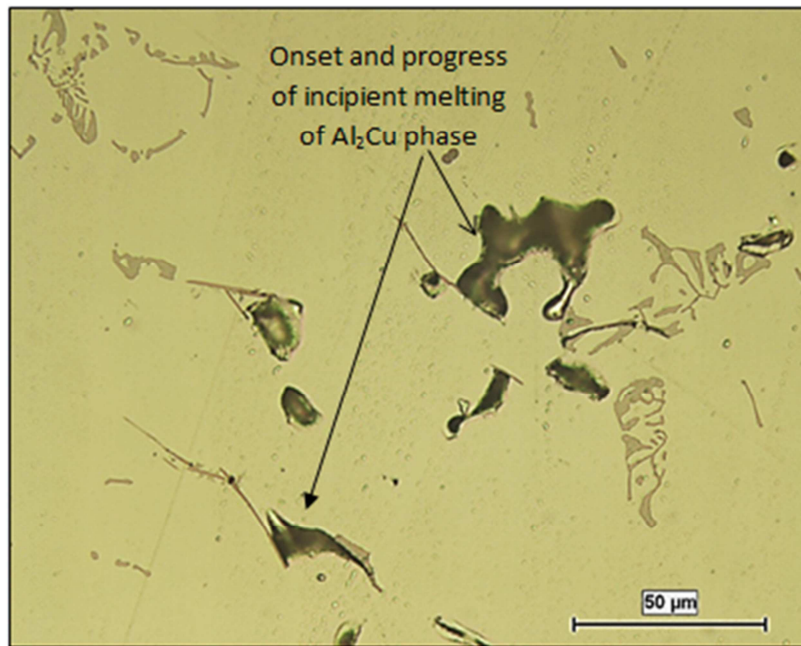
(c) B0-SHT-2

**Figure 4-13: Examples of incipient melting observed in B0 alloy samples in the: (a) As-cast, (b) SHT-1, and (c) SHT-2 conditions.**
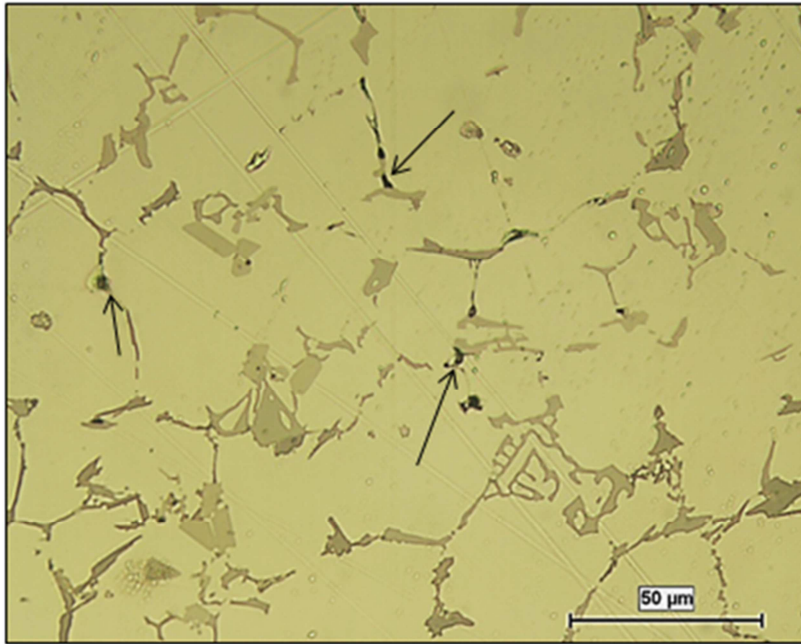
(a) B1-As-Cast 500X
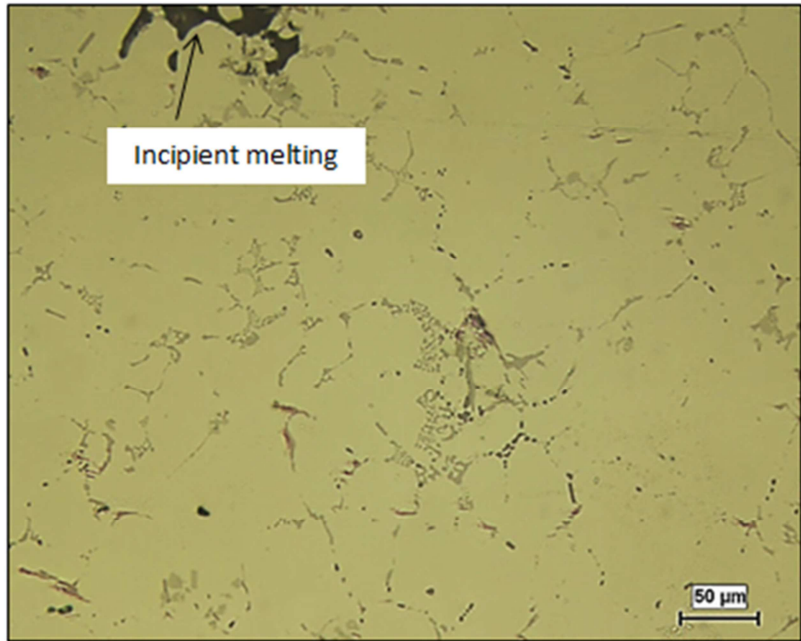


Incipient melting

(b) B1-SHT-1

(c) B1-SHT-1 500X
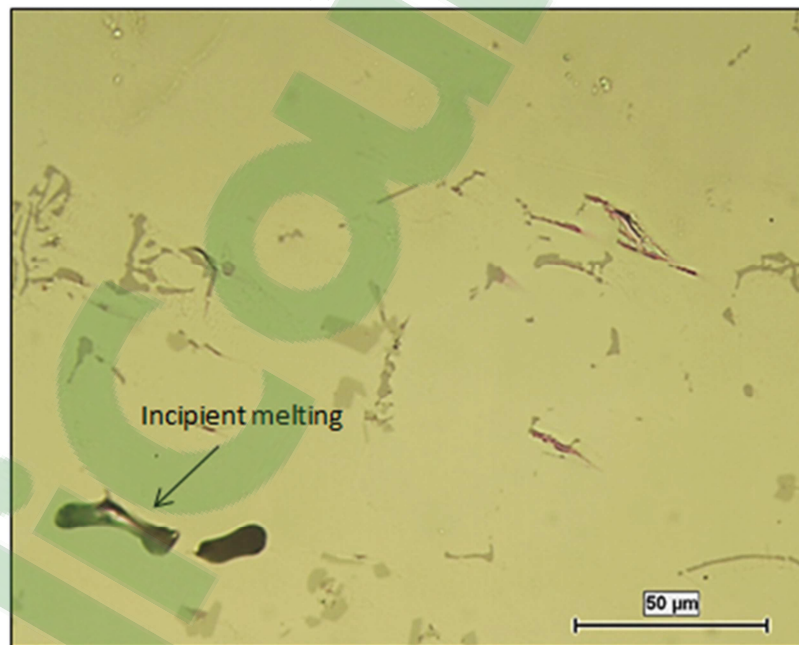


Incipient melting

(d) B1-SHT-2 500X

**Figure 4-14: Examples of incipient melting observed in B1 alloy samples in the: (a) As-cast, (b, c) SHT-1, and (d) SHT-2 conditions.**

Figure 4.15 shows examples of the incipient melting observed in the as-cast and solution heat treated samples of Alloy B2. In the as-cast case, Figure 4.15(a), the melting appears to occur at the α-Al grain boundaries where the copper phase precipitates. In this case, the melting would be attributed to the localized heating occurring at these points. Figure 4.15(b) shows both the onset and occurrence of incipient melting at the locations within the circled areas, by the droplet like nature of the copper phase (onset) and the darkened areas associated with these drops where the incipient melting has already occurred so that it appears as porosity in the microstructure. Figure 4.15(c) shows a clearer view of this at 500x magnification in the SHT-2 treated sample.

Examples of the incipient melting observed in the D alloys, namely, D0, D1 and D2 alloys are shown in Figures 4.16 through 4.18. Compared to the B alloys, the D alloys containing a higher Si content show much smaller porosity/incipient melting in the as-cast condition, as well as eutectic Si regions dispersed in the matrix as is seen in Figure 4.16(a) which shows almost no porosity.

(a) B2-As-Cast



(b) B2-SHT-1
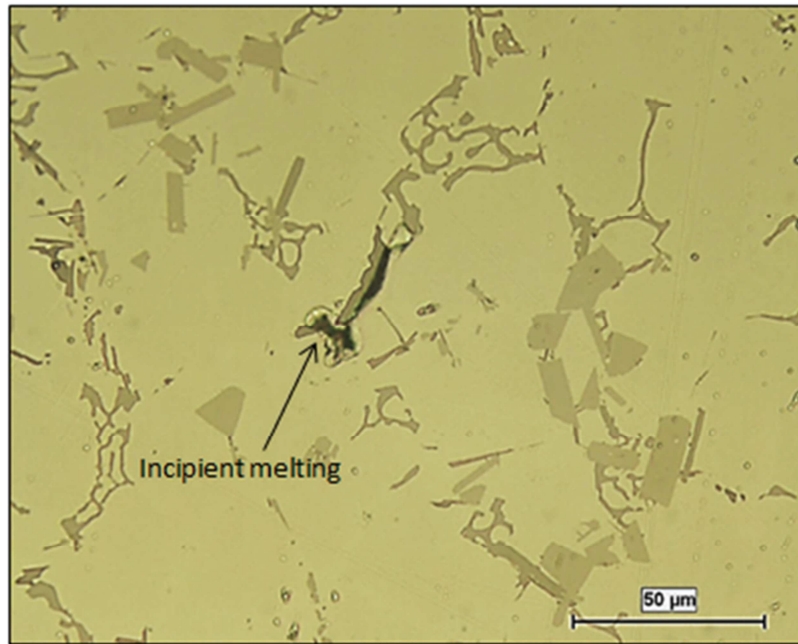
(c) B2-SHT-2 500X

**Figure 4-15: Examples of incipient melting observed in B2 alloy samples in the: (a) As- cast, (b) SHT-1, and (c) SHT-2 conditions.**

The higher magnification micrograph of Figure 4.16(b) shows the different phases existing in the D0 alloy, among them the pinkish particles of the copper phase, eutectic Si regions dispersed throughout the matrix, and other intermetallic phases (arrowed). With the application of solution heat treatment, incipient melting starts to occur, as seen in Figures 4.16(c) through 4.16(e). It is also interesting to note the progress of Si particle necking, fragmentation and spheroidization during the SHT-1 treatment of the alloy, followed by coarsening of the spheroidized Si particles during the extended duration of the multi-step SHT-2 solution treatment, Figure 4.16(e). Figure 4.17 shows examples of incipient melting (circled or arrowed) observed in D1 alloy samples Figures 4.17 (b) and (c). The black circled in (b) reveals the presence of fine Si particles indicating the dissolution of the $Al_2Cu$

phase. Examples of incipient melting observed in D2 alloy samples are shown in Figure 4.18 when the samples were solution heat treated in SHT conditions 1 and 2. The black arrow in (c) displays the presence of oxide film trapped in the casting during pouring the liquid metal.
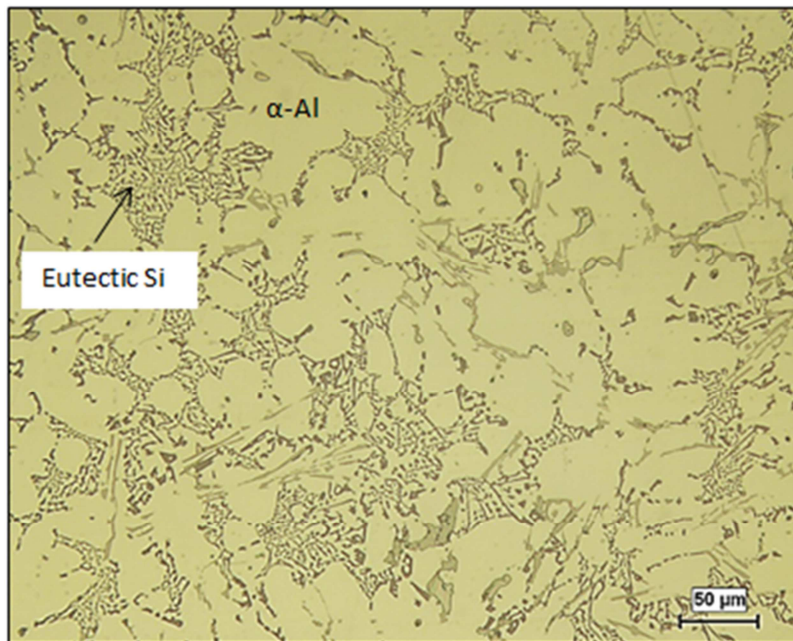


(a) D0-As-Cast
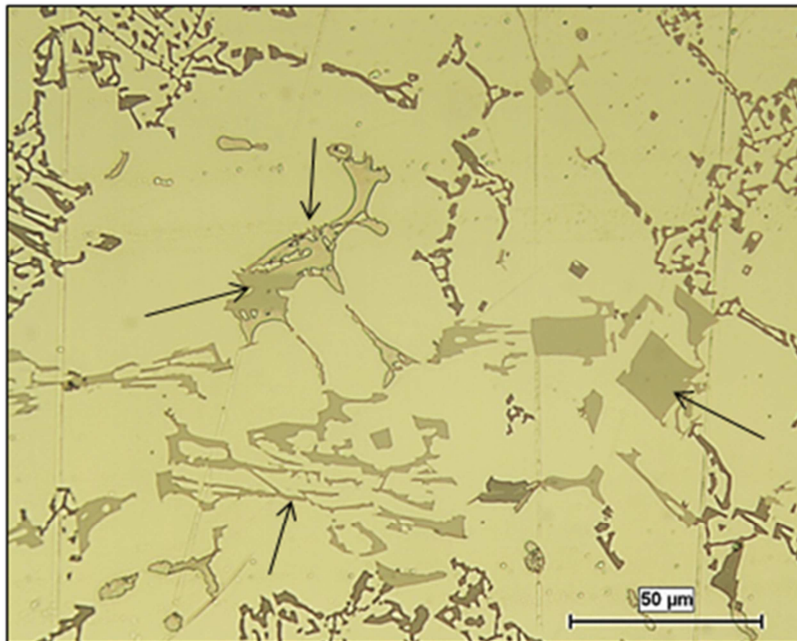
(b) D0-As-Cast 500X
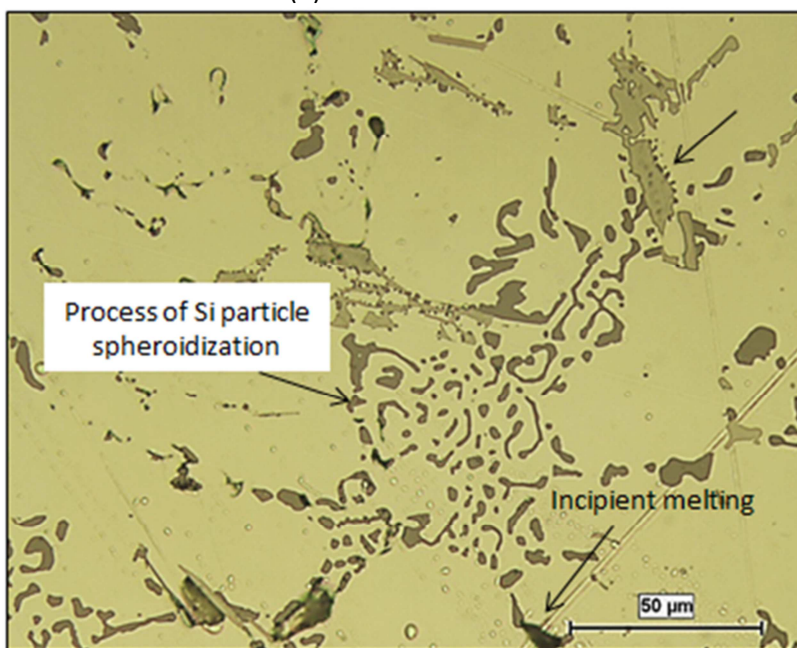


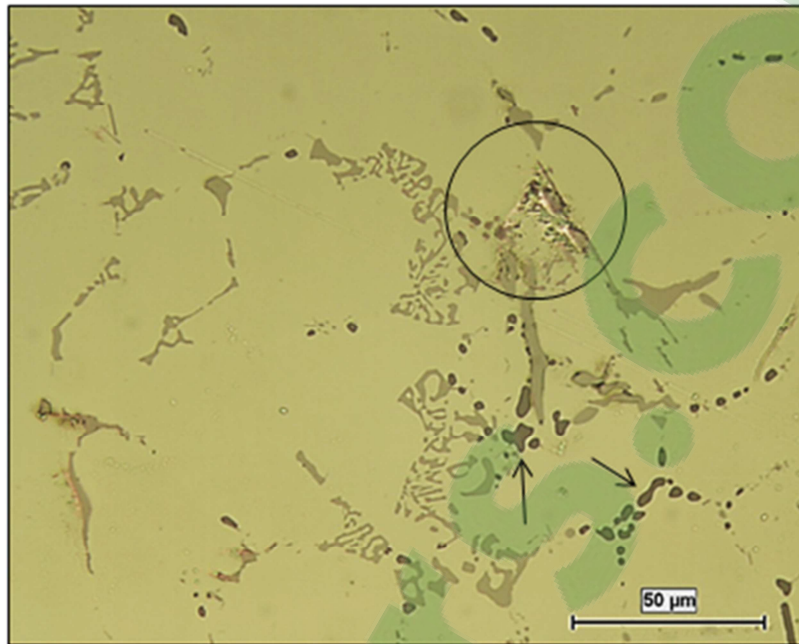(c) D0-SHT-1 500X
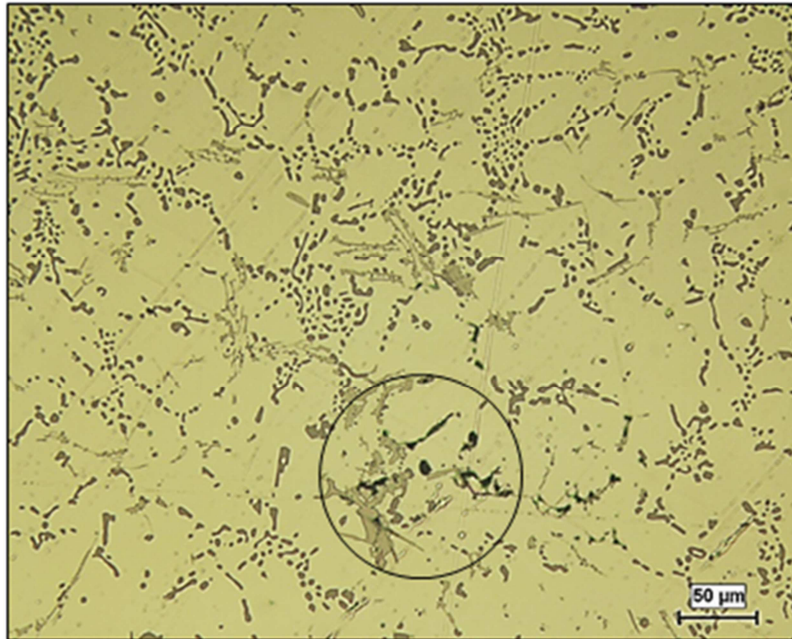
(d) D0-SHT-2
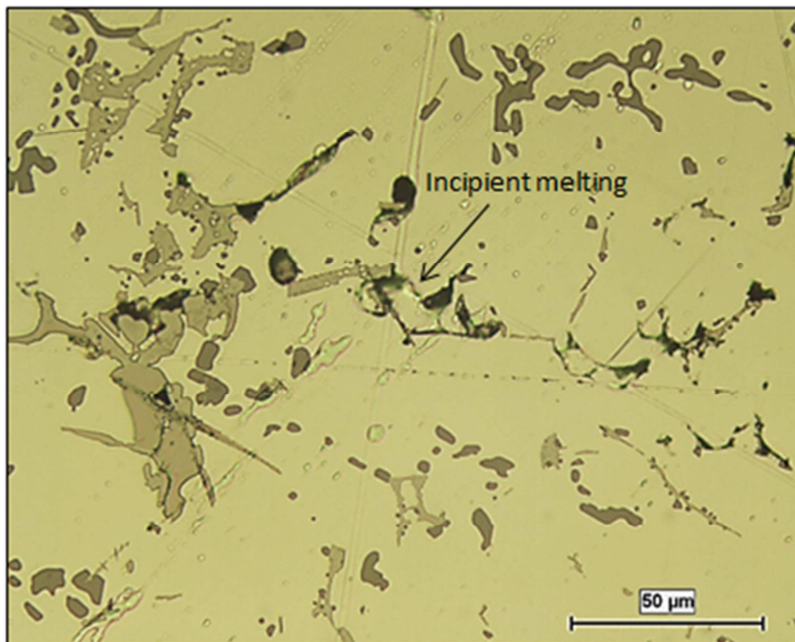


(e) D0-SHT-2 500X

**Figure 4-16: Examples of incipient melting observed in D0 alloy samples in the: (a, b) As-cast, (c) SHT-1, and (d, e) SHT-2 conditions.**
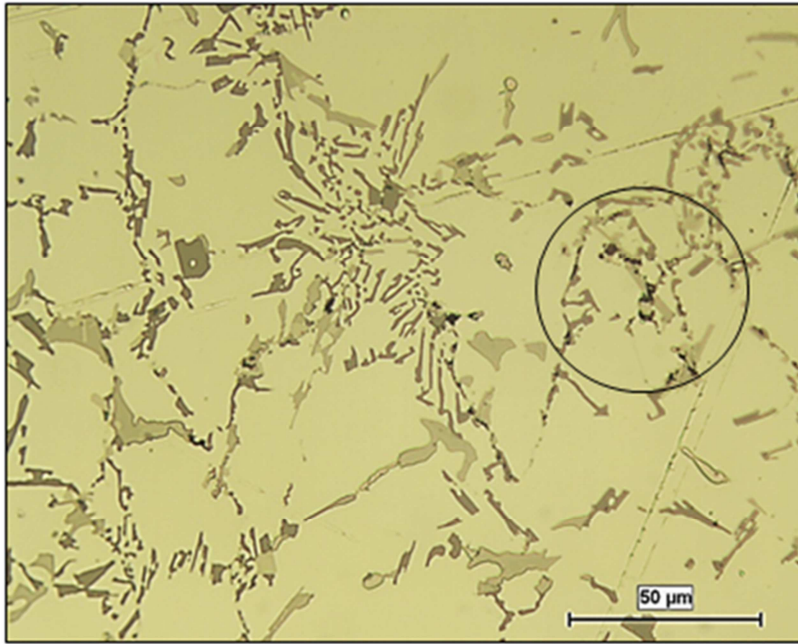
(a) D1-As-Cast 500X
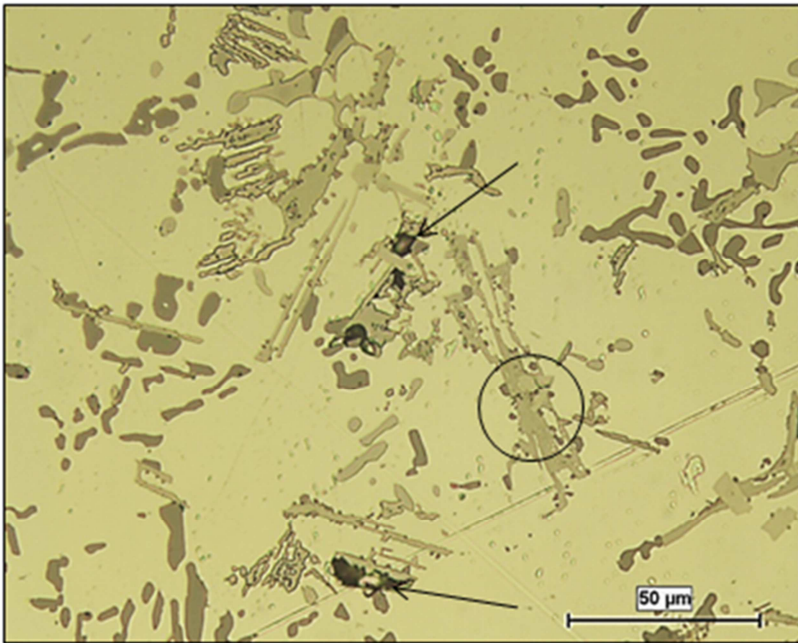


(b) D1-SHT-1 500X
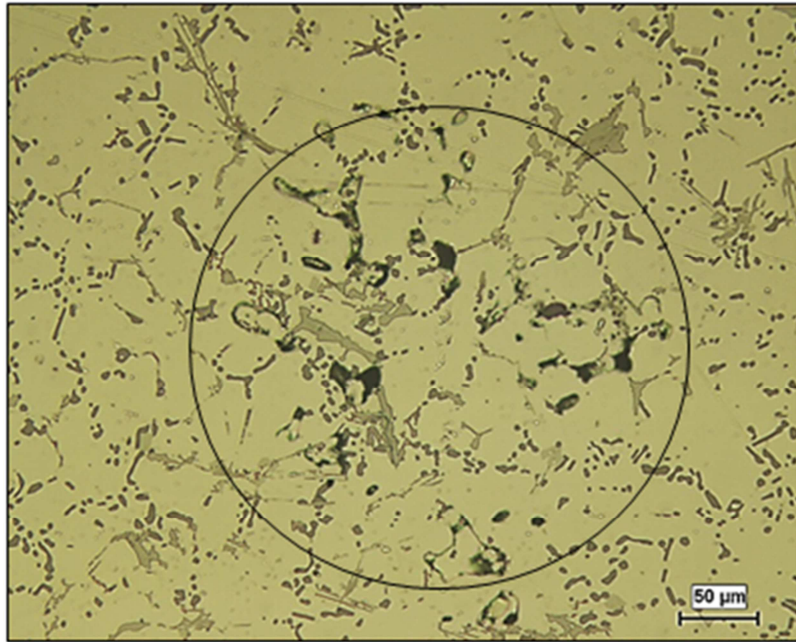
(c) D1-SHT-2

**Figure 4-17: Examples of incipient melting (circled or arrowed) observed in D1 alloy samples in the: (a) As-cast, (b) SHT-1, and (c) SHT-2 conditions.**
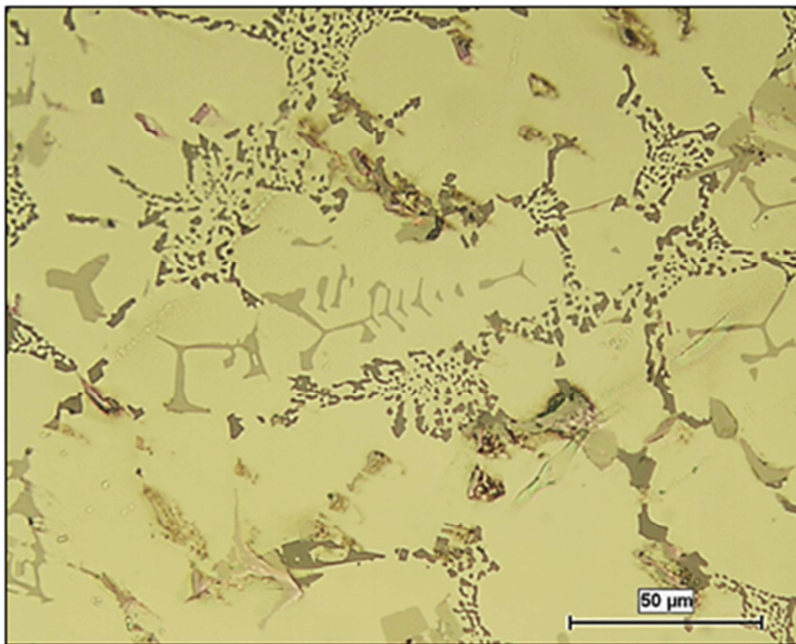


(a) D2-As-Cast 500X
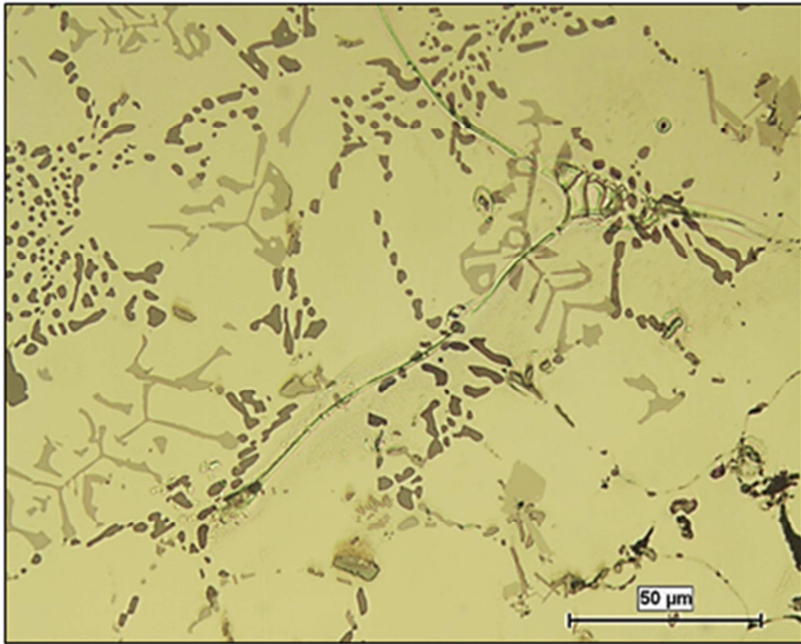
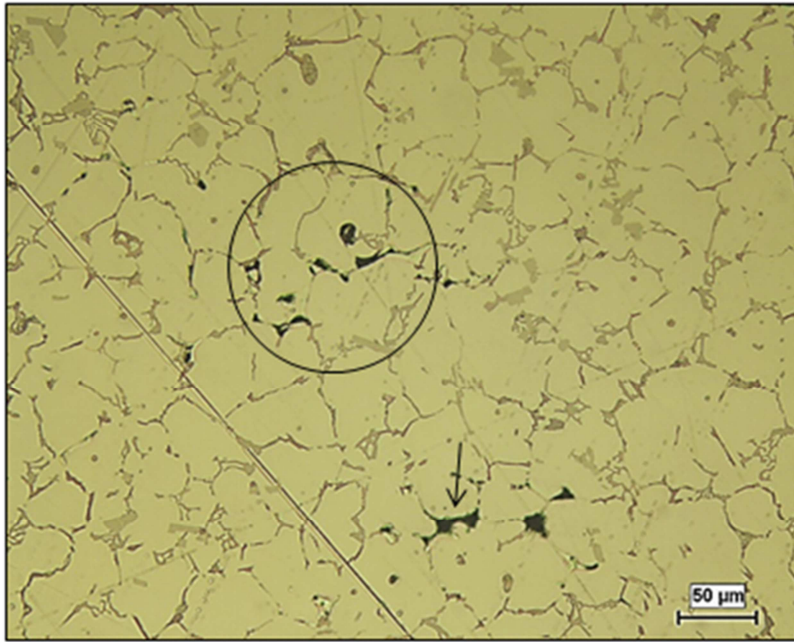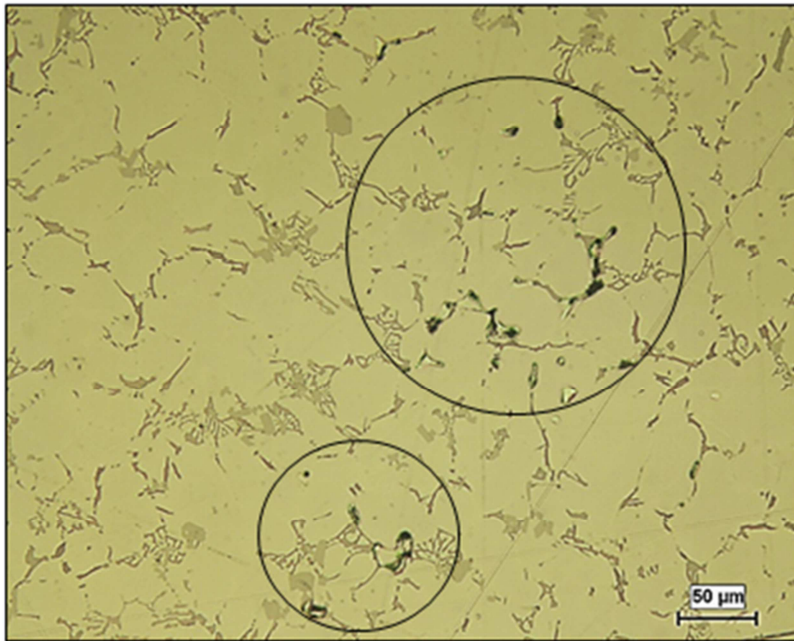(b) D2-SHT1 500X
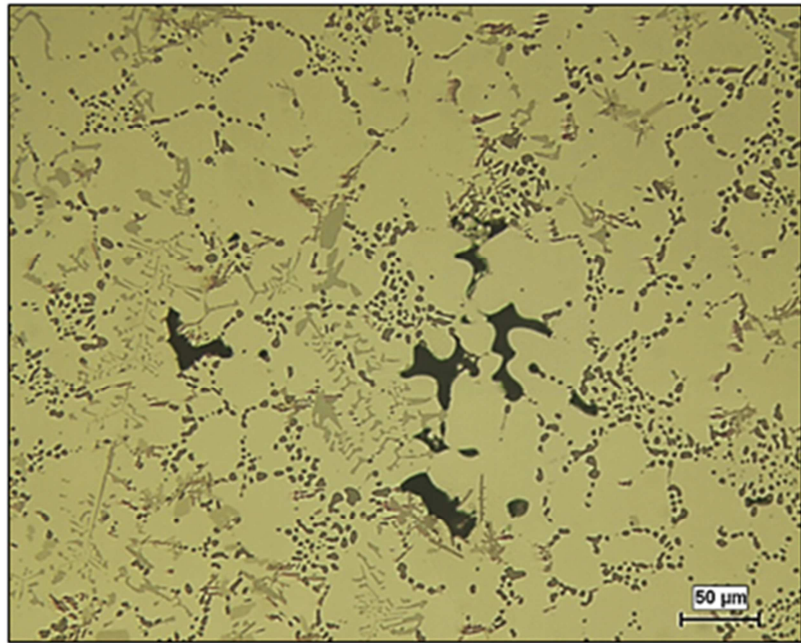


(c) D2-SHT-2
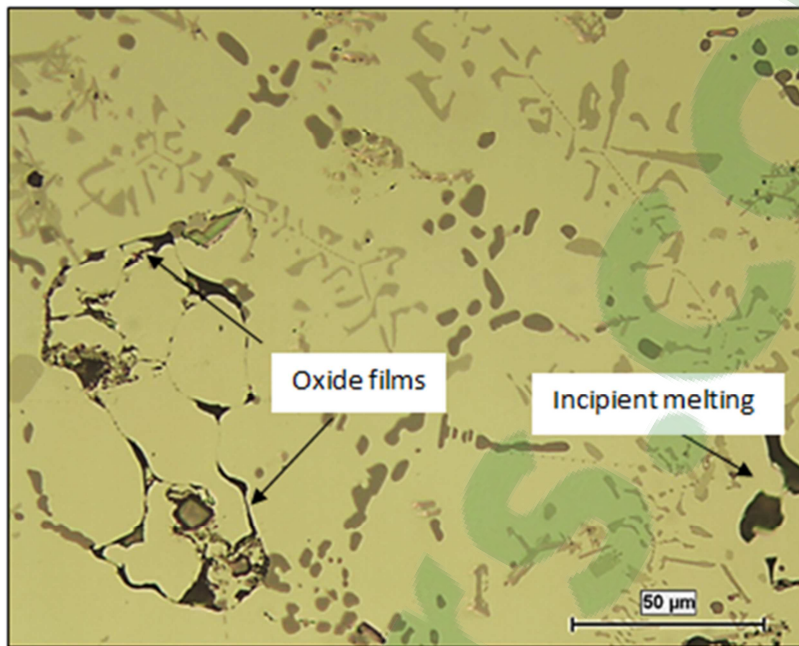
(d) D2-SHT-2 500X

**Figure 4-18: Examples of incipient melting observed in D2 alloy samples in the: (a) As-cast, (b) SHT-1, and (c) and (d) SHT-2 conditions.**

# CHAPTER FIVE

# Ambient and High temperature Tensile Testing

# CHAPTER 5

## Ambient and High temperature Tensile Testing

### 5.1    INTRODUCTION

This chapter will focus on the tensile properties of the alloys which were prepared for this study with the intention of identifying the effects of the additives and heat treatment regimes on the tensile properties of the base alloy B0, namely, the 220 alloy. The quality index technique will be applied here as a means to correlate the ultimate tensile strength (UTS) and yield strength (YS), as well as the percentage elongation (%El) values, and to evaluate the quality of the alloys corresponding to the additives introduced, as was described previously in Chapter 2. Plots of ΔP will also be presented, with P representing Property (*i.e*., UTS, YS and %El) and ΔP representing the difference in property value obtained for a specific alloy composition/heat treatment condition, taking the B0 alloy as the base line. This approach helps to better visualize the effects and interactions of the various additions used and the different heat treatment conditions applied.

The tensile properties of a casting are initially determined by the microstructure obtained upon solidification (as-cast condition), and may be improved thereafter by subjecting the casting to a suitable heat treatment process and following the evolution of the microstructure in order to optimize the heat treatment conditions. An examination of the microstructure allows for the determination of the constituent phases present in the solidified structure, as well as the phases and precipitates that form following heat treatment. The alloy properties may then be analyzed in terms of the corresponding

microstructures. As mentioned previously in Chapter 3, five test bars were used per alloy/condition in the tensile tests carried out for selected alloys/conditions. The tensile test data are provided in the form of graphs in the sections that follow. For the sake of simplicity, only selected data have been highlighted in this chapter.

All tensile testing was carried out at a strain rate of 4 x $10^{-4}$ $s^{-1}$. For ambient temperature testing, an MTS Servohydraulic Mechanical Testing machine was used, whereas the high temperature tensile testing was carried out using an Instron Universal Mechanical Testing machine. Figure 5.1 shows the YS, UTS, and %El values obtained at ambient temperature for the different alloys/conditions. The X-axis represents the alloys and the respective heat treatment conditions. The primary Y-axis represents the strength values (UTS and YS), while the secondary Y-axis represents the percentage elongation value obtained for each alloy/condition studied. From Figure 5.1, it will be observed that the strength values for the as-cast alloy samples exhibit tensile strength values of 265-230 MPa, giving a difference of about 10-35 MPa between the base alloy B0 (UTS 332.8 MPa) and the remaining alloys, namely B1 (322 MPa), B2(265.7 MPa), D0 (291.3 MPa), D1 (293.5 MPa) and D2 (285.8 MPa). The solution heat treatment temperature of 495°C in combination with the aging temperature/time (180°C/8h) increases the alloy strength (UTS and YS) while the ductility values show noticeable reduction compared to the values obtained in the as-cast condition.

After T6 and T62 treatments, the strength values increase significantly, reaching peak strength in each case. The yield strength follows the same trend, exhibiting somewhat lower values compared to UTS. Alloy B1 shows the maximum increase in tensile properties

with UTS of 401.55 MPa, followed by a UTS value of 380.55 MPa for alloy B0. On the other hand, B2 and D2 alloys display strength values that are lower than those exhibited by the base alloy in the as-cast and other heat-treated conditions, as seen in Figure 5.1.

**Figure 5-1: Average values of ultimate tensile strength (UTS), yield strength (YS), and percentage elongation to fracture (%El) obtained from 220 alloys (B0 to D2) in the as-cast, T5, T6, T62 and T7 heat-treated conditions (at ambient temperature).**

For the high temperature tests, all tests were carried out at 250°C, using two stabilization times of 1 hour and 200 hours at testing temperature, prior to testing. Samples were tested in the as-cast and various heat-treated conditions to determine the effect of the additions and heat treatment conditions on the high temperature mechanical performance of the 220 alloys. Figures 5.2 and Figure 5.3 show respectively the tensile properties obtained from B0, B1, B2, and the D0, D1and D2 alloys with respect to the various heat treatment conditions, following stabilization times of 1 hr and 200 hrs at the 250°C testing temperature. Compared to the as-cast case, heat treatment obviously affects the tensile performance of the alloys. As may be observed from Figure 5.2, in case of one hour stabilization, the strength of the alloy increases with the T6 and T62 heat treatment conditions, but remains the same after T5 heat treatment.

On the other hand, all alloys display tensile strength values that are higher than those exhibited by the base alloy B0 in the T7-tempered condition, with a noticeable improvement in performance of the D series alloys compared to the B series alloys. Moreover, the D2 alloy shows unchanged UTS and improved YS values in the T7-treated condition compared to the corresponding strength values in its as-cast condition; this behavior is opposite to the general trend followed by the other alloys (B0 through D1) which show a noticeable decrease in their strength values in the T7-treated condition in comparison to their as-cast values in each case.

The yield strength follows the same trend, exhibiting somewhat lower values compared to UTS. In keeping with the tensile strength values, the lowest ductility values

are observed for the T62-tempered alloys, while all T7-tempered alloys show maximum ductility.

After 200 hours stabilization at 250°C, Figure 5.3 shows that the alloy strength increases after the T5 heat treatment but decreases in the T6 and T62 conditions. The yield strength values follow the same trend as the UTS. In keeping with these trends in strength values, the highest ductility values are observed in the T6 and T62 conditions while the T5-treated alloys exhibit the lowest ductility values, with the D1 and D2 alloys showing the same ductility as in the as-cast condition.

The ambient temperature and high temperature tensile test results are elaborated upon and discussed in Sections 5.2 and 5.3.
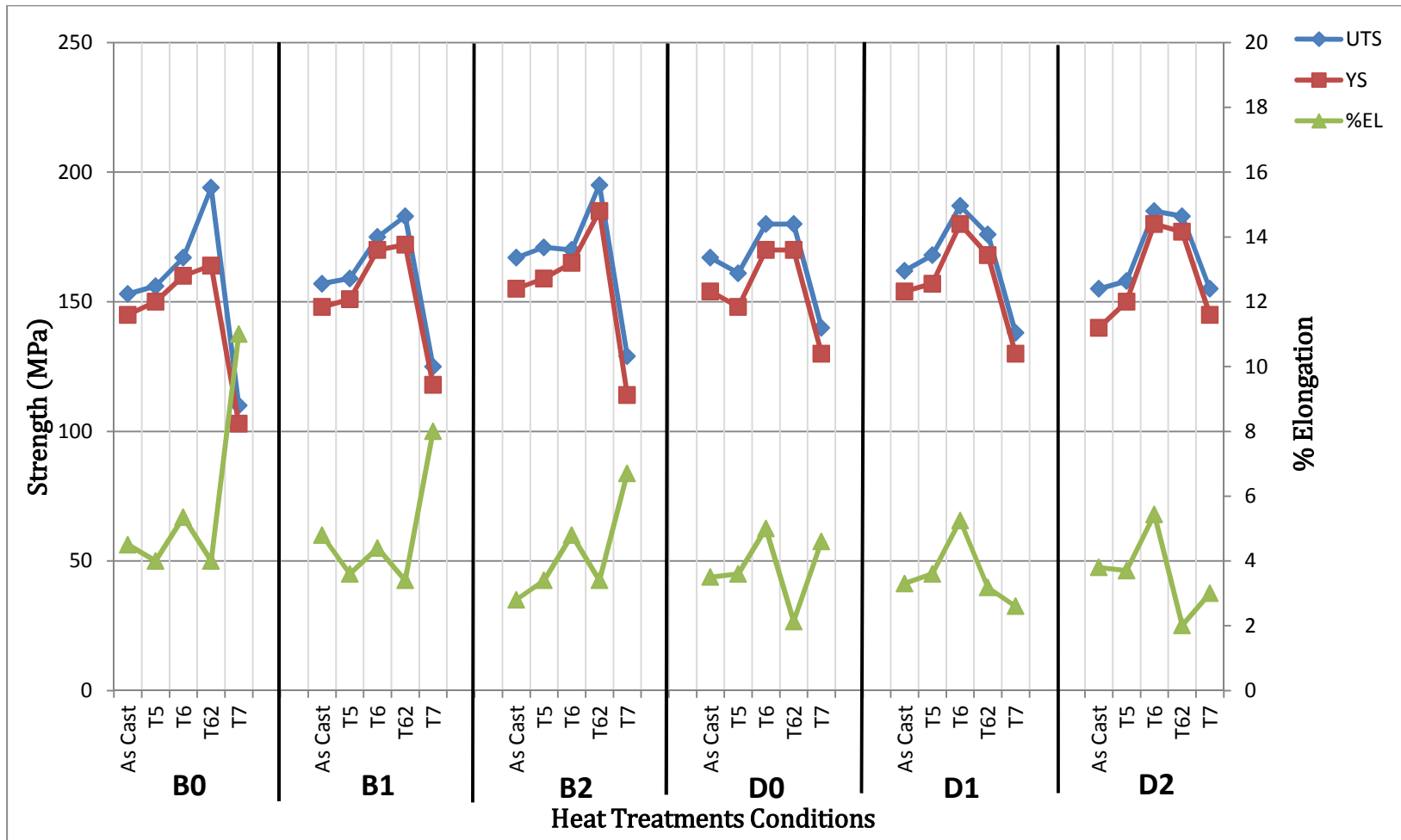
**Figure 5-2: Average values of ultimate tensile strength (UTS), yield strength (YS), and percentage elongation to fracture (%El) obtained from 220 alloys (B0 to D2) in the as-cast, T5, T6, T62 and T7 heat-treated conditions (after stabilization at 250°C/1hr).**
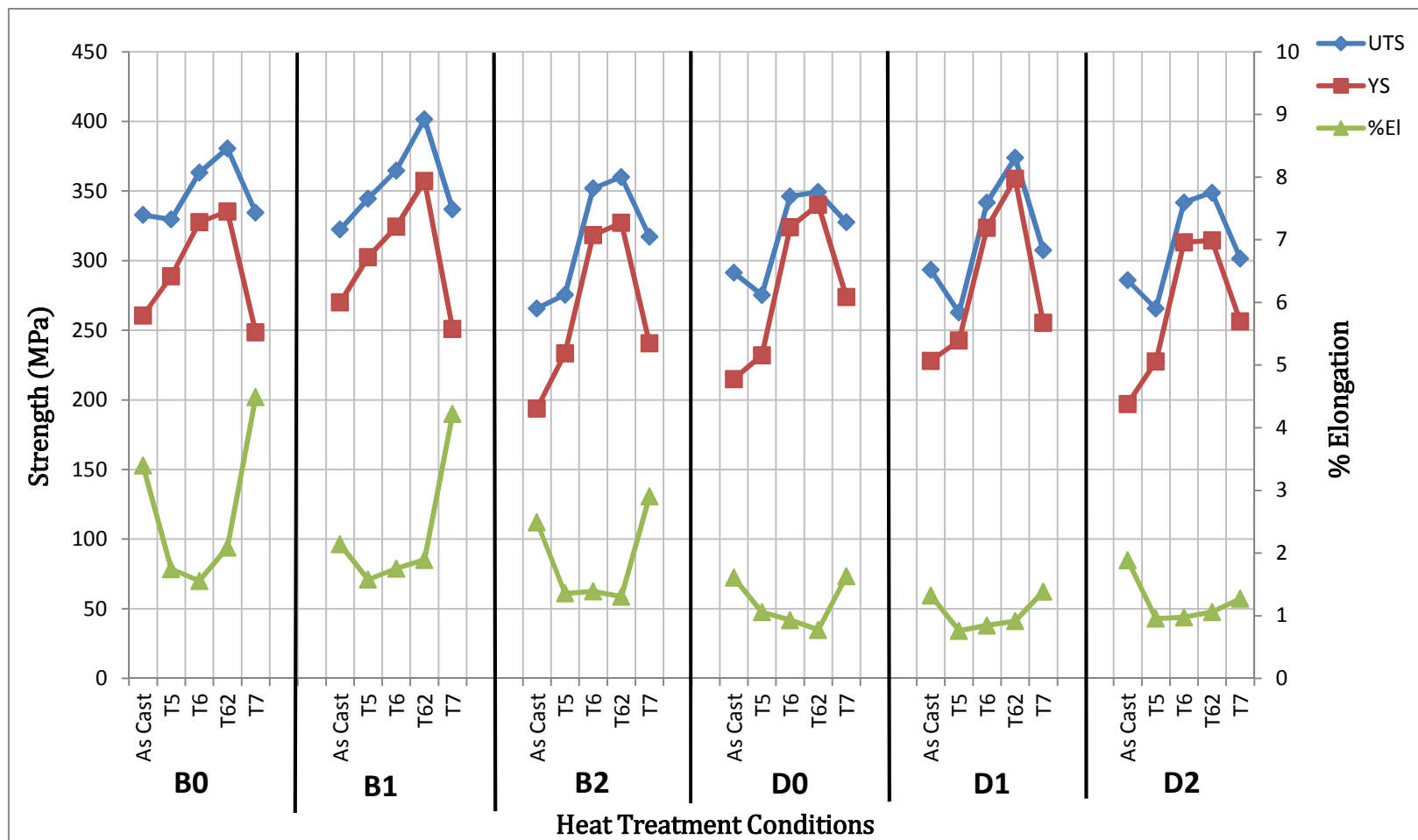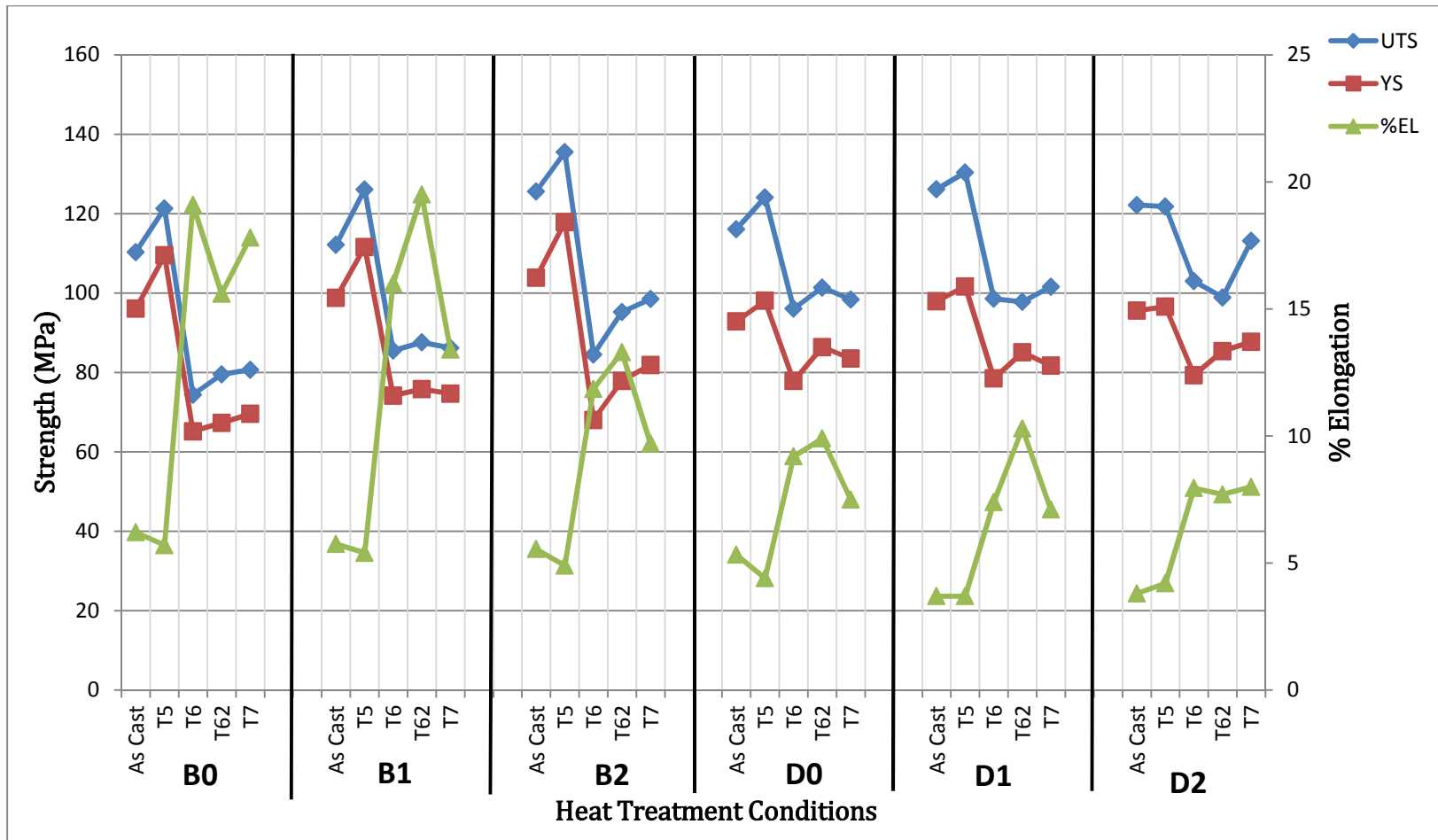
Figure 5-3: Average values of ultimate tensile strength (UTS), yield strength (YS), and percentage elongation to fracture (%El) obtained from 220 alloys (B0 to D2) in the as-cast, T5, T6, T62 and T7 heat-treated conditions (after stabilization at 250°C/200hr)

## 5.2 EVALUATION OF AMBIENT TEMPERATURE TENSILE PROPERTIES

### 5.2.1 AS-CAST AND SOLUTION HEAT-TREATED CONDITIONS

The ultimate tensile strength values for all alloys tested in the as-cast and as-solutionized conditions are displayed in Figure 5.4. The tensile strength values lie in the range of 265 MPa to 333 MPa in the as-cast condition, between 320 MPa and 389 MPa after the one-stage solution heat treatment (SHT-1), and from 337 MPa to 396 MPa after the multi-stage solution heat treatment (SHT-2). The observed increase in tensile strength may be attributed to the dissolution of the Cu-rich intermetallic phase particles, mainly the $Al_2Cu$ phase during solution treatment, so that solid solution hardening is the process mainly responsible for the observed increase in strength. In the as-cast condition, the microstructure of the alloys investigated may contain mainly coarse particles of the solidified intermetallic phases such as $Al_2Cu$, $Al_5Mg_8Cu_2Si_6$, $Al_{15}(Mn,Fe,Cu)_3Si_2$, and acicular eutectic Si. These particles have a deleterious effect on the ultimate tensile strength and ductility of the alloy because of their sharp edges which act as crack initiators. During tensile testing, the cracking phenomenon is usually instigated by the cracking of these intermetallics followed by crack propagation, ending up with complete fracture of the sample; this sequence is easier in the as-cast condition as the intermetallics are coarse. When solution heat treatment is applied, these intermetallics break down and dissolve by losing their elements which then diffuse in the matrix, producing a supersaturated solid solution; this solid solution strengthens the matrix by increasing the resistance to dislocation movement during deformation in the process of tensile testing [19, 84].

Figure 5.5 depicts the yield strength results for the as-cast and as-solutionized conditions. From this figure, it will be noted that the yield strength of the base alloy increases from 260 MPa in the as-cast condition to 277 MPa after single-stage and multi-stage solutionizing treatments. This increase in the yield strength can also be attributed to the hindering of the dislocation movement within the supersaturated solid solution, as mentioned above; any mechanism which resists the mobility of dislocations in an alloy will increase its yield (and tensile) strength.

The highest yield strength is exhibited by alloy B1 (B0+Zr+V+Ni), where the as-cast yield strength increases from 270 MPa to 279 MPa after the multi-stage solution treatment SHT-2, which may be attributed to the addition of Zr and Ni. The addition of transition elements such as Zr and Ni to aluminum alloys can form dispersoid precipitates, such as $Al_3Zr$ and $Al_3Ni$, throughout the α-Al matrix, producing an intensified hardening effect [11, 85]. These dispersoids may form when passing through their temperature formation range, during the cooling of the solidified alloy from the melting temperature to room temperature. The low yield strength exhibited by alloy B2 may be attributed to the interaction between Sr and Ti which has been reported to cause mutual 'poisoning' of the beneficial effects of the two elements [86]. In general, upon solution heat treatment, the YS values of all alloys increase, in a manner similar to that shown in Figure 5.4 for the UTS results. The same strengthening mechanisms apply in this case, with solid solution strengthening acting as the operating mechanism.

As will be seen from Figure 5.6, the percent elongation of the alloys in the as-cast condition is improved with solution heat treatment. For example, ductility values of the

base alloy B0, and alloys B2 and B1 alloy respectively increase from 3.4, 2.5 and 2.1% in the as-cast condition to 6.4, 4 and 4.8% after undergoing the multi-stage solution heat treatment SHT-2. During solidification, the alloying elements tend to segregate as localized clusters producing intermetallic particles in coarse shapes. As mentioned above, the solution heat treatment dissolves and refines the brittle intermetallic particles such as $Al_2Cu$ and $Al_5Mg_8Cu_2Si_6$ existing in the as-cast alloy. The dissolution of the Cu-rich intermetallic phases, as well as refining of the α-Fe intermetallic phase due to the presence of Sr, such that it is more evenly distributed in the matrix, are the reasons for the increase in elongation observed. It is worth mentioning the deleterious effect that an increase in Si content has on the alloy ductility, as one can easily note the variation in percent elongation values between the B-series alloys (low Si content, high %El) and the D-series alloys (high Si content, low %El).
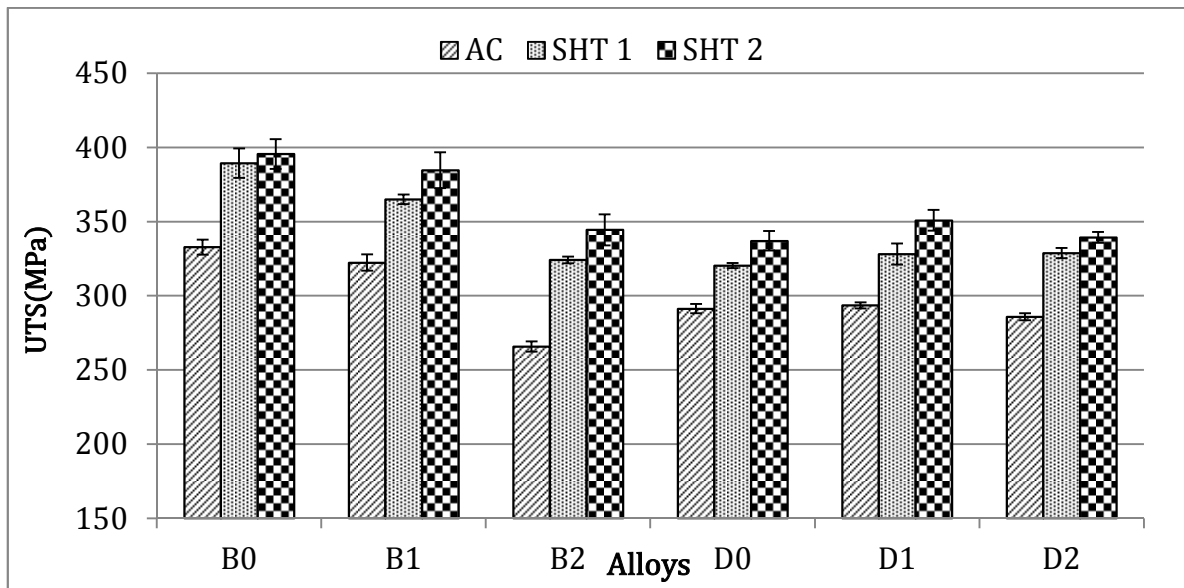
**Figure 5-4: Ultimate tensile strength of the 220 alloys investigated in the as-cast and solutionized conditions at ambient temperature.**
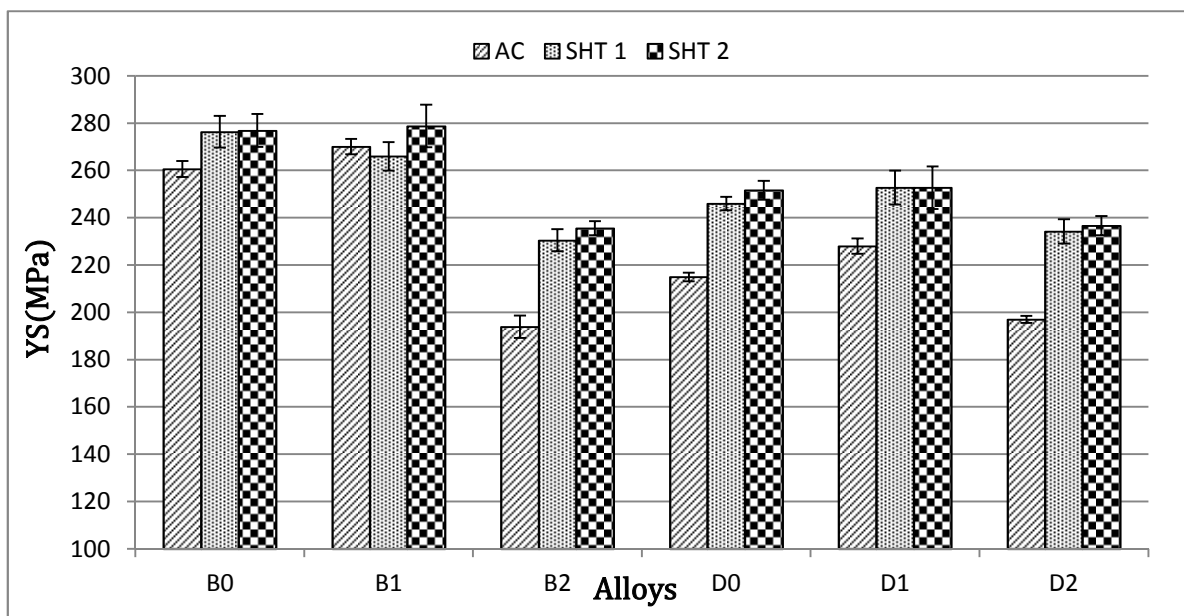


**Figure 5-5: Yield strength of the 220 alloys investigated in the as-cast and solutionized conditions at ambient temperature.**
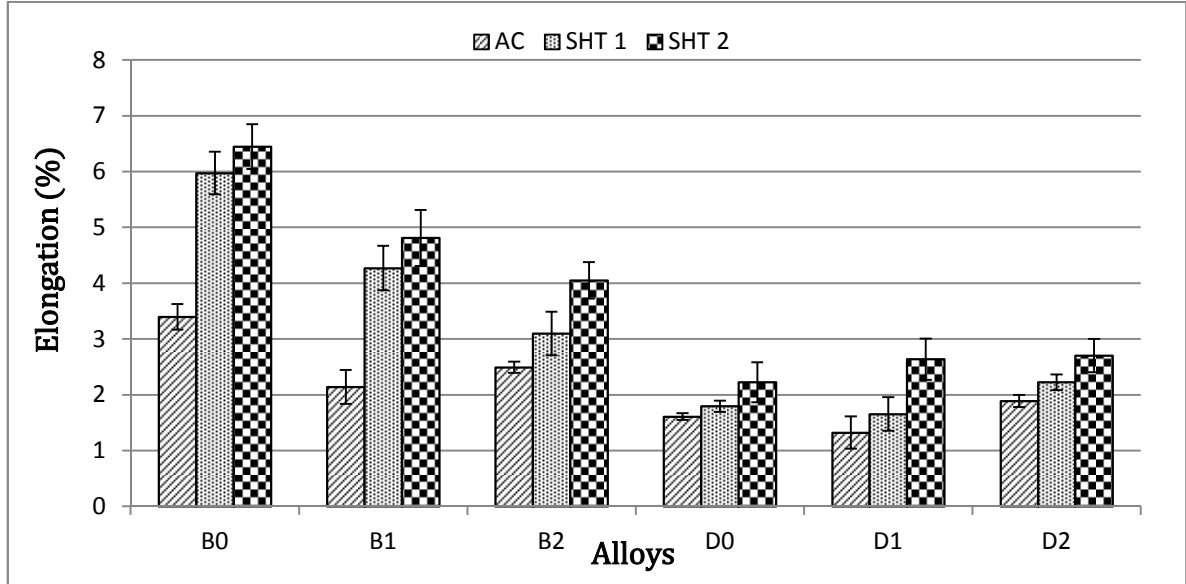
**Figure 5-6: Percentage elongation (%El) of the 220 alloys investigated in the as-cast and solutionized conditions at ambient temperature.**

### 5.2.2   AGE-HARDENING CONDITIONS

The purpose of carrying out artificial aging in an alloy is to develop fine precipitates that act as barriers for dislocation movements, resulting in strengthening the alloy; however, the effectiveness of the strengthening behavior may vary depending on the aging parameters (i.e., aging temperature and time).

Figures 5.7 through 5.9 show how the tensile properties of the six alloys studied vary with different heat treatment tempers. In Figure 5.7, the highest improvement is noted for B1 alloy in the T62-tempered condition, which exhibits a UTS-value of ~ 400 MPa. Similarly, in the D-series alloys, the D1 alloy exhibits a UTS-value of ~ 370 MPa. The addition of Zr and Ti produces a refined non-dendritic structure that decreases the probability for porosity formation and increases the amount of dissolved $Al_2Cu$ after

solution heat treatment, and thereby the level of Cu in solid solution of α-Al, which then allows for a larger amount of precipitation hardening to take place upon aging, and therefore improves the alloy strength. Additionally, dispersoid precipitates of $Al_3Zr$ and/or $Al_3(Zr_{1-x}Ti_x)$ may act as nucleation sites for the hardening phases during the aging process, resulting in further improvement in strength [87, 88].

In the T62 temper, the alloy is solutionized through two stages at two different temperatures in order to avoid the incipient melting of the copper phase at the higher solutionizing temperature [27]; this also gives rise to a better homogenization prior to aging, thereby improving the tensile properties, as seen in Figure 5.7. In order to enhance the tensile properties of an aluminum alloy, it is important to obtain a thermally stable microstructure and coarsening-resistant dispersoids. This may be achieved by adding Zr, which has the smallest diffusion flux in aluminum of all the transition metals; the presence of Zr leads to the formation of fine dispersoids that resist coarsening at higher temperatures, which helps to improve/maintain the tensile properties [89, 84,90 ].

With respect to the alloy yield strength, Figure 5.8 reveals that the highest YS values are observed for the B1 and D1 alloys; the YS values of all alloys increase with the application of T6 and T62 tempers, in a manner similar to that shown in Figure 5.7 for the UTS results. It is interesting to note that the B1 and D1 alloys contain Ti and Zr, as was mentioned earlier in the context of the UTS results, which promotes the formation of $Al_3(Zr,Ti)$ precipitates and hence positively affects the alloy tensile properties.

With respect to the alloy ductility, Figure 5.9 shows that the lowest ductility values are also observed in the D-series alloys. In fact, the base alloy B0 shows almost the best

ductility values among all the alloys regardless the aging condition. This may be attributed

to the presence of Zr, Ni and Ti in the other alloys, which may result in the formation of

trialuminide dispersoids that would resist alloy softening in all alloys except the base alloy

B0.



**Figure 5-7: Ultimate tensile strength values of the 220 alloys investigated in the T5, T6, T62 and T7**

**tempered conditions, and tested at ambient temperature.**

**Figure 5-8: Yield strength values of the 220 alloys investigated in the T5, T6, T62 and T7 tempered conditions, and tested at ambient temperature.**



**Figure 5-9: Percentage elongation (%El) values of the 220 alloys investigated in the T5, T6, T62 and T7 tempered conditions, and tested at ambient temperature.**

## 5.3 EVALUATION OF HIGH TEMPERATURE TENSILE PROPERTIES

Tensile tests were performed at 250°C temperature after stabilizing the tensile test bars for times of 1 hour and 200 hours at the testing temperature, in order to determine the effects of the alloying additions on the high temperature mechanical performance of the 220 alloys. It was found that the tensile properties showed a different tendency to those observed at ambient temperature, resulting in improved strength, particularly yield strength, at the high temperature.

### 5.3.1 STAGE I - STABILIZATION AT 250°C FOR 1 HR PRIOR TO TESTING

In general, an improvement in the mechanical properties of Cu- and Mg-containing aluminum alloys is attributed to the formation of age-hardening compounds $Al_2Cu$ and $Mg_2Si$, respectively, which precipitate from the solid solution during aging. The degree of strengthening depends on the copper and magnesium content, and an increase in strength due to higher levels of these elements is always accompanied by a corresponding decrease in ductility.

The application of an aging treatment to these alloys causes an entire range of precipitates to form according to the temperature and time applied. While Cu and Mg are added to improve the ambient and high temperature strength, the development of intermetallic phases including $\theta$-$Al_2Cu$, $\beta$-$Mg_2Si$, $\pi$-$Al_8Mg_3FeSi_6$, $Q$-$Al_5Cu_2Mg_8Si_6$, $\alpha$-$Al_{15}(Mn,Fe)_3Si_2$ and $\beta$-$Al_5FeSi$ in these alloys promotes alloy strengthening, however at the expense of ductility [91, 92].

For this stage of the study, all alloys were tested at 250 °C after stabilization for 1 hour at the testing temperature. Figure 5.10 shows the UTS values obtained for all alloys/conditions under these conditions of testing. The highest UTS value is exhibited by the T62-tempered B2 alloy with ~ 195 MPa; this value is very close to that of the T62-tempered B0 alloy. However, for other heat treatment conditions, alloy B2 is superior to alloy B0. This enhanced behavior of alloy B2 can be clearly attributed to the presence of 1 wt% Ni and 0.15 wt% Zr in the alloy and hence to the existence of trialuminide dispersoids which will resist the coarsening of the strengthening precipitates.

It may also be noted from Figure 5.10 that the D-series alloys exhibit competitive strength values when compared with the B-series alloys, as opposed to the room temperature behavior, with emphasis on the T7 condition. The only difference that exists between the two series of alloys is heir silicon content. Thus, it may be said that the relatively enhanced performance of the D-series alloys at elevated temperature is related to their increased Si content.

Figure 5.11 shows the yield strength values obtained for these alloys, the highest YS value being exhibited by the T62-tempered B2 alloy, with ~ 185 MPa, and a profile that is more or less similar to that shown by the ultimate tensile strength, based on the same reasons proposed earlier.

In regard to the ductility, Figure 5.12 shows that the B0, B1 and B2 alloys (B-series) possess the highest ductility values in T7-tempered condition. Besides the T62 and T7 tempers, the variations in ductility values between B and D-series alloys obtained with

other heat treatment conditions are not high, contrary to what was observed under room temperature testing conditions.
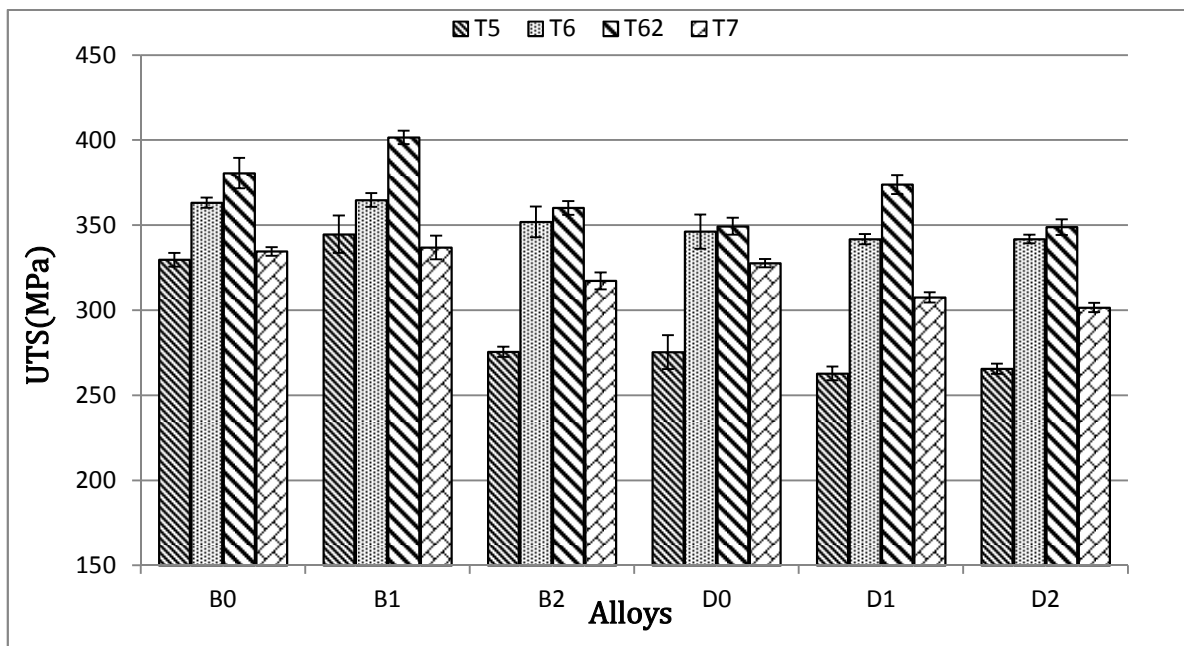


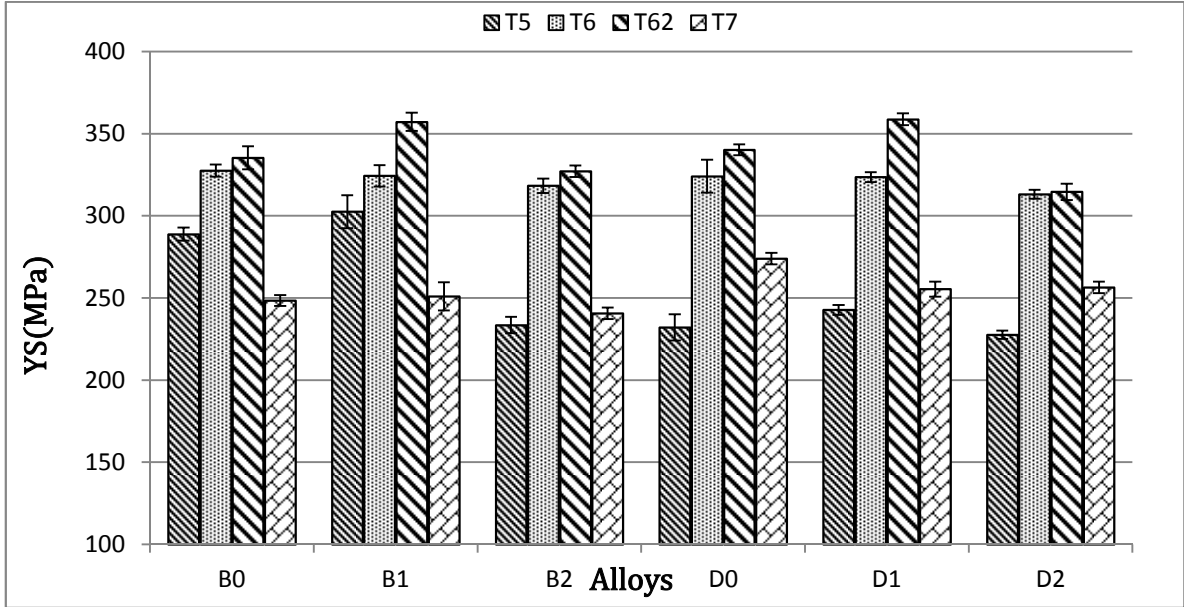**Figure 5-10: Ultimate tensile strength values of the 220 alloys investigated in the as-cast, T5, T6, T62 and T7-tempered conditions, and tested at 250°C temperature following stabilization for 1 hr at testing temperature.**

**Figure 5-11: Yield strength values of the 220 alloys investigated in the as-cast, T5, T6, T62 and T7-tempered conditions, and tested at 250°C temperature following stabilization for 1 hr at testing temperature.**
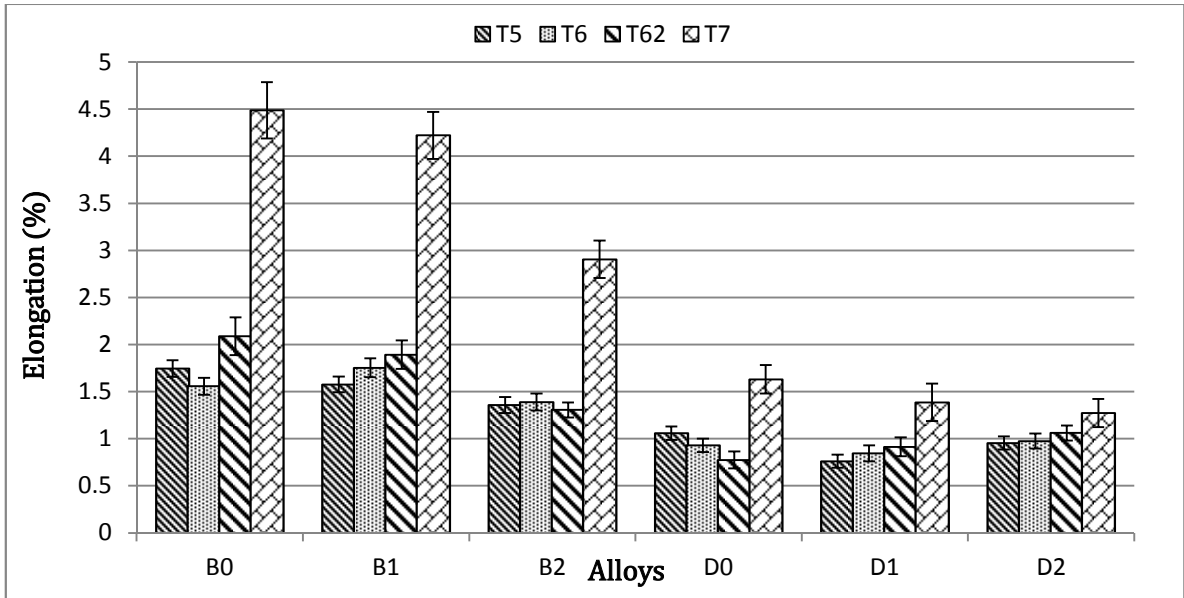
**Figure 5-12: Percentage elongation (%El) values of the 220 alloys investigated in the as-cast, T5, T6, T62 and T7-tempered conditions, and tested at 250°C temperature following stabilization for 1 hr at testing temperature.**

## 5.3.2   STAGE II – STABILIZATION AT 250°C FOR 200 HRS PRIOR TO TESTING

In this stage of the study, the tensile test data was obtained after the test bars were subjected to an extended period of stabilization of 200 hrs at the testing temperature, prior to testing. It may be easily noticed from Figures 5.13 and 5.14, that the UTS and YS values obtained under these conditions are lower than the strength values obtained after one hour stabilization. In relation to these low strength values, the percentage elongation values are noticeably higher, as expected, compared to those obtained after one hour stabilization. As shown in Figure 5.13, the highest UTS value is observed for the T5 heat-treated B2 alloy with ~ 135 MPa followed by D1, B1, D0, D2 and B0 alloys, exhibiting values of ~ 130

MPa, 126 MPa, 124 MPa, 122 MPa, 121MPa, respectively. The as-cast and T5 conditions show the best strength values; these conditions are usually used to prevent precipitate growth while being subjected to high temperature; the two conditions are very similar to a large extent because they both were stabilized at 250 °C for a long time (200 hrs); this is also reflected in their strength values which are very close to each other.

With the other heat treatment conditions (i.e. T6, T62, and T7), the strength is highly affected by the long stabilization process at 250 °C; the reduction in strength values is related to the coarsening of the strengthening precipitates to the extent that the precipitates become completely incoherent with the matrix.

It is also noticeable that the UTS values of the D-series alloys are generally higher than those of the B-series alloys; with alloys B2 and D2 exhibiting the best UTS values in their respective series, due to the presence of 1 wt% Ni and 0.15 wt% Zr. The yield strength values shown in Figure 5.14 follow the same trend as the UTS (Figure 5.13). The highest yield strength value, ~117 MPa, is obtained for the B2 alloy in the T5-treated condition, followed by B1 and B0 alloys with ~112 MPa and 110 MPa, respectively, in a manner similar to that shown in Figure 5.13 for the UTS results.

Generally, the percentage elongation values (Figure 5.15) of the alloys improved by ~42% following stabilization for 200 hrs compared to the values that were achieved after one hour stabilization. The highest %El is achieved by the T62 heat-treated B1 alloy after 200 hrs stabilization with a value of ~19.5%, followed by the T6 heat-treated B0 alloy with ~19%. The base alloy B0 shows almost the best elongation values among all the alloys/conditions studied except for the T62-treated B1 alloy; this behavior emphasizes the

effect of the chemical additions on resisting the softening behaviour of the base alloy B0, which is a result of the long thermal exposure at elevated temperature. The role of the chemical additions is to form more stable intermetallics at higher temperatures as well as precipitate coarsening-resistant dispersoids which are capable of maintaining/improving the strengthening effect when the alloys are exposed to higher temperatures for prolonged periods of time.
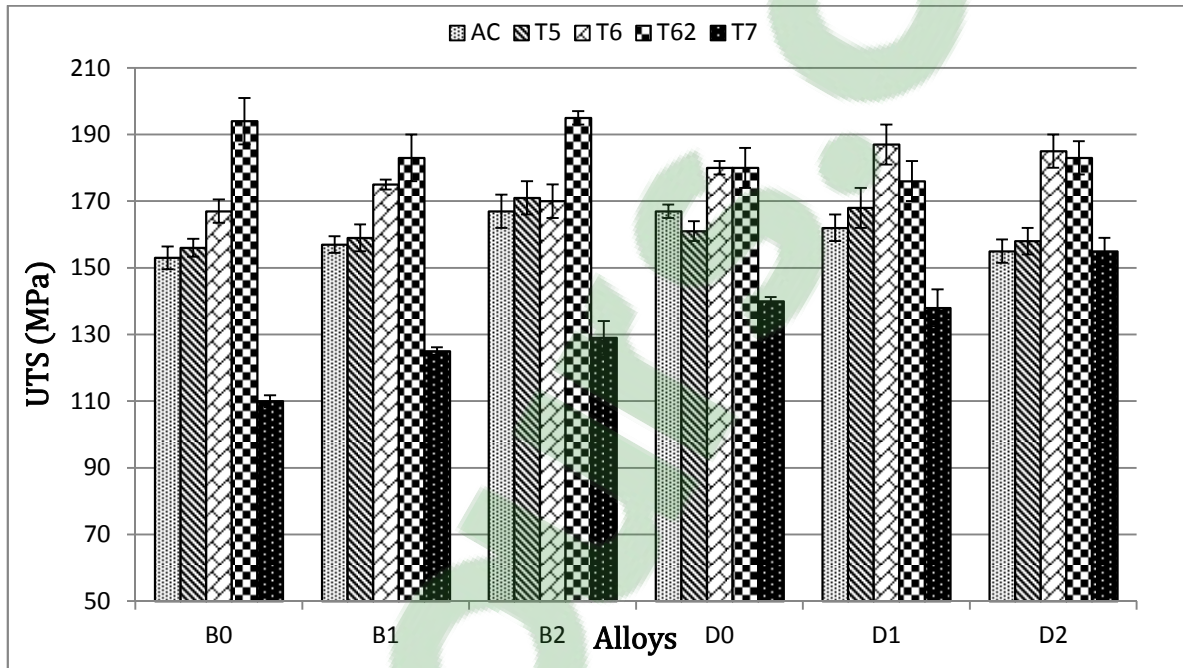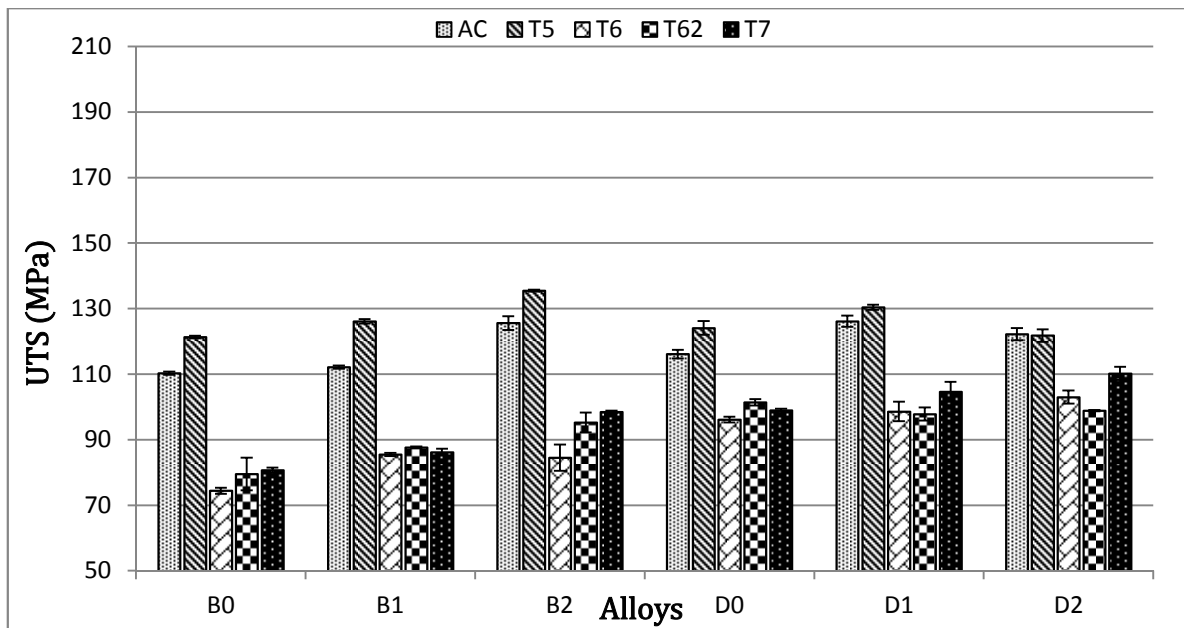


**Figure 5-13: Ultimate tensile strength values of the 220 alloys investigated in the as-cast, T5, T6, T62 and T7-tempered conditions, and tested at 250°C temperature following stabilization for 200 hrs at testing temperature.**
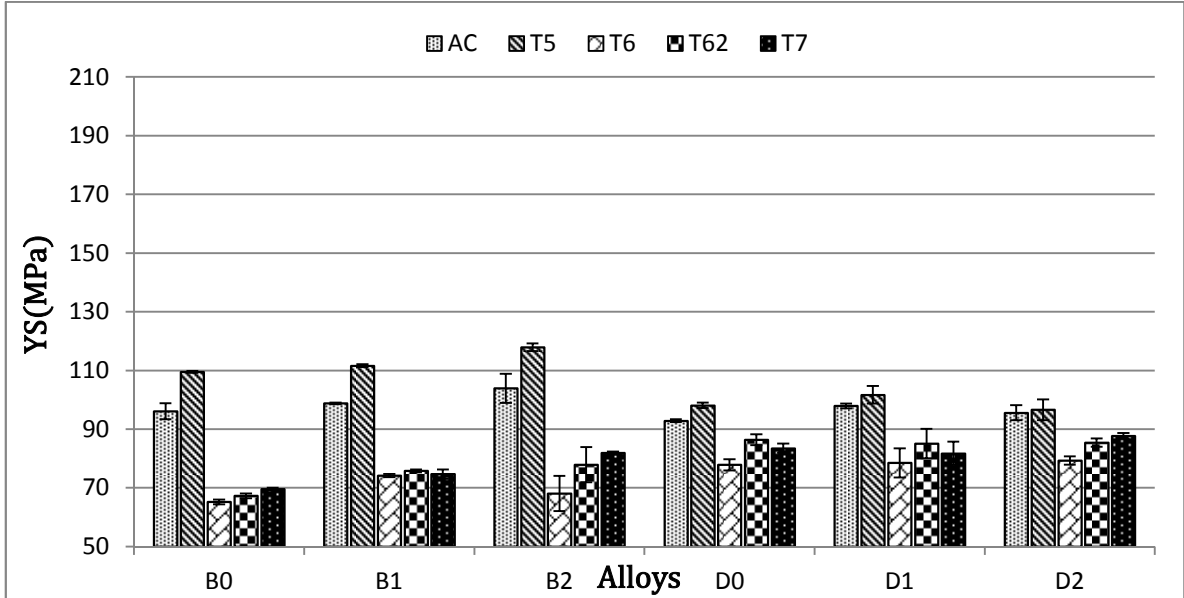
**Figure 5-14: Yield strength of the 220 alloys investigated in the as-cast, T5, T6, T62 and T7-tempered conditions, and tested at 250°C temperature following stabilization for 200 hrs at testing temperature.**
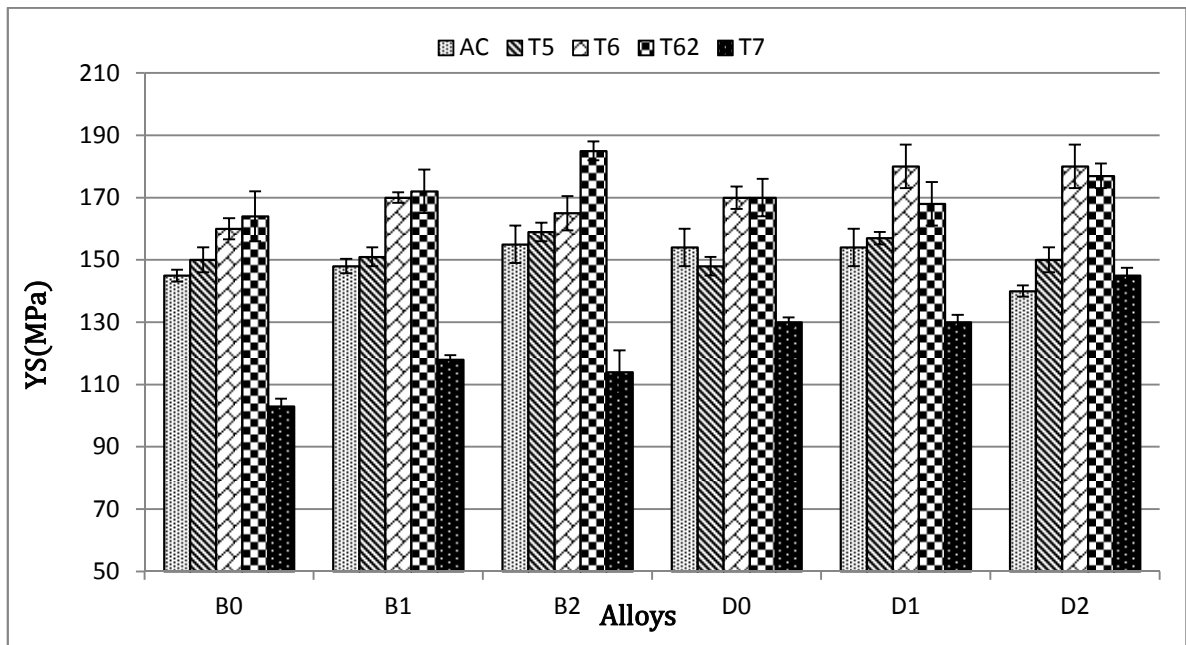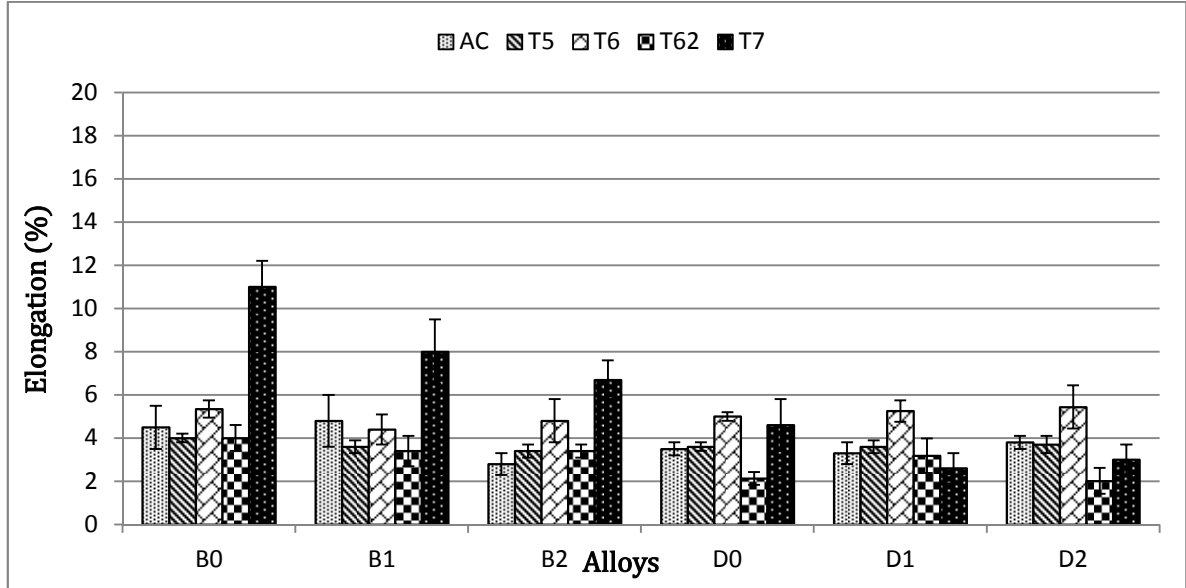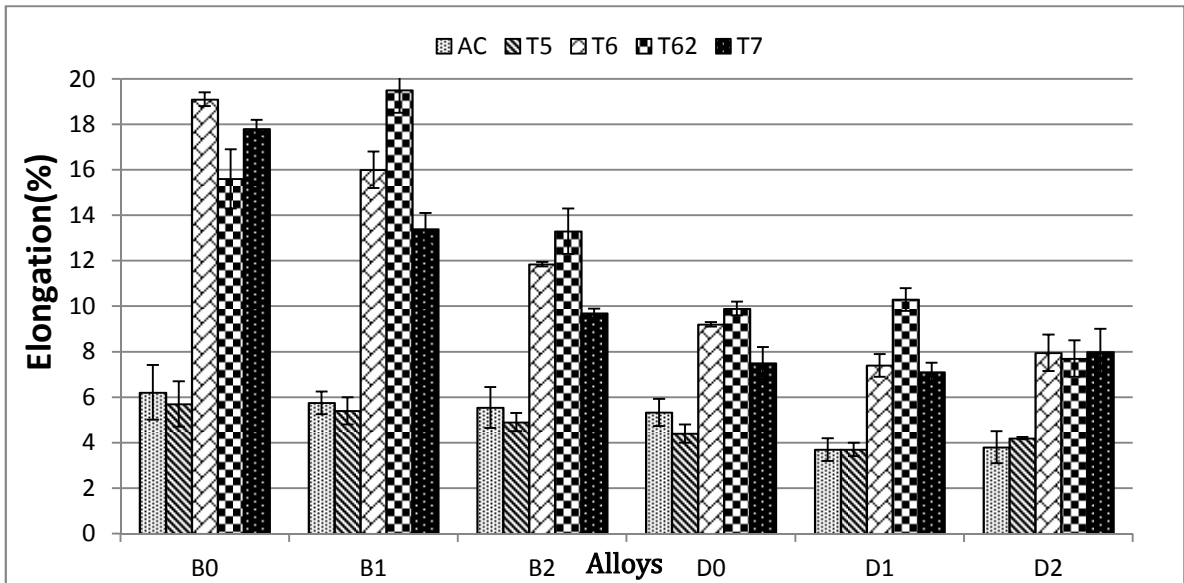


**Figure 5-15: Percentage elongation (%El) values of the 220 alloys investigated in the as cast, T5, T6, T62 and T7-tempered conditions, and tested at 250°C temperature following stabilization for 200 hrs at testing temperature.**

## 5.4 ANALYSIS OF TENSILE PROPERTIES USING THE QUALITY INDEX CONCEPT

As mentioned in Chapter 2, Drouzy *et al.* [93, 94] proposed the concept of the Quality Index Q as a means of better expressing the tensile properties of Al-Si-Mg alloys, in terms of how variations in Mg content and aging conditions affected the alloy "quality" or performance in their study of Al-7%Si-Mg or 356-type alloys, by the use of equations that allowed to plot charts of *iso-Q* versus *iso-YS* lines on a quality index chart such that it was easy to see how the alloy quality was affected by the heat treatment and alloy composition. This concept was later extended to include Al-Si-Cu and Al-Si-Cu-Mg alloys by Cáceres [72, 73] whose model was based on the assumption that the deformation curves of a material may be represented by the Holloman equation, $P = KS^n$ [15]. The methodology and the equations used by both groups of researchers were described in detail in Chapter 2.

In the present study, quality charts were generated for evaluating the influence of metallurgical parameters on the tensile properties. As described in Chapter 2, Equations 1 and 2 were used to generate *iso-Q* lines and *iso-Yield Strength* lines, respectively. The *iso-Q* and *iso-YS* lines in these charts facilitate knowing which additions are beneficial for improving the alloy properties. By increasing the copper content, it is possible to improve the strength of the alloys, although this would result in a reduction in ductility [44, 95, 96]. The strengthening effect obtained by adding copper to an Al-9wt%Si-0.5wt%Mg alloy is based on the formation of Cu- and Cu-Mg-containing precipitates such as $\theta$-Al$_2$Cu, S-Al$_5$Cu$_2$Mg$_8$Si$_6$, Q-Al$_5$Cu$_2$Mg$_8$Si$_6$, and may be further optimized by applying adequate heat

treatment procedures [97, 98, 99]. The quality of these castings will be affected according to the net amount by which the increase in strength is balanced by the reduction in ductility.

The main purpose of solution heat treatment is to maximize dissolution of the hardening elements in solid solution, to convert the acicular eutectic silicon to fragmented and spheroidized particles, as well as cause the fragmentation and dissolution of undissolved phases, namely Fe-intermetallics, and to achieve a homogeneous structure for improving the ductility and the quality of Al-Si cast alloys [44, 100, 101]. These improvements are reflected in the alloy properties and Q values obtained in the solution heat-treated condition compared to the as-cast case, as may be seen from the quality charts displayed in Figures 5.16 through 5.21.

The application of a solutionizing treatment leads to significant improvement in the strength and quality of the castings; it will be clear from Figures 5.16 and 5.17 that, for the two alloy series studied at ambient temperature, solution heat treatment provided a considerable improvement in reducing the compromise between strength and quality, since both parameters were increased after solution heat treatment. As may be seen from these figures, the highest UTS-value and highest quality were obtained after T62 and T7 heat treatments. An improvement in the tensile properties and alloy quality are noted upon solution heat treatment for all alloys, indicating that although the solution heat treatment is mainly responsible in improving the alloy quality, the presence of Ni and Zr in alloy B1 and alloy D1 provide even further improvement, since these alloys show the best $Q$ and UTS values. The aging time and temperature also have an influence on the Q values that

may be related to the precipitation of the Cu- and Mg-containing phases in the metal matrix.

The formation of coherent precipitates is the main source of strengthening and leads to an increase in the strength values of the alloys. The semi-coherent precipitates which may exist in the peak-aging conditions are the needle-like β' ($Mg_2Si$), the plate-shaped θ'' ($Al_2Cu$), and the lathlike S' ($Al_2CuMg$) phases [102]; these precipitates provide an increase in the strength associated with a reduction in ductility. However, upon applying an aging temperature of 240°C (overaging) during T7 heat treatment, the tensile strength, yield strength, and quality index values are reduced in relation to the softening which occurs as a result of the overaging conditions at which the equilibrium (incoherent) precipitates form, leading to the loss of coherency strain between the precipitates and the matrix, and to coarser precipitates having larger inter-particle spacing and thus less density in the metal matrix. The low density of the precipitates in the matrix will result in larger inter-particle spacing that will reduce the resistance to dislocation movements, and hence softening takes place [102].

Figures 5.18 and 5.19 shows the quality index charts for the five selected heat treatment conditions for alloys studied at high temperature after one hour stabilization time at the testing temperature (250°C). In these figures, the highest UTS and Q values were obtained for the T62-tempered B2 alloy and the T6-tempered D2 alloy when aged at 180°C for 8 hrs. It is also noted that the tensile strength and quality index values were reduced in all alloys subjected to the T7-temper compared with other tempers at an aging temperature

of 240°C. This behavior may be ascribed to the fact that the decrease in ductility is more substantial that the slight increase in YS and UTS values observed at low aging temperatures. The aging rate can be accelerated when treating the alloy/casting at a higher temperature, so as to enhance the diffusion of solute atoms and precipitation of secondary phases. The degree of strengthening will depend on the system involved, the volume fraction and size of the second phase particles, as well as on their interactions with the dislocations [103, 104, 105].

Figures 5.20 and 5.21 show the quality index chart for the five selected heat treatment conditions for alloys studied at high temperature, after stabilization for 200 hours at the testing temperature (250°C). In these graphs, the general mechanical behavior for all alloys appears to be similar for the same heat treatment temper. It is observed that alloys B2 and D1 have the highest UTS values after T5 heat treatment when aged at 180°C for 8 hrs. At high temperature testing after stabilization for 200 hrs, all alloys show slight improvement in their UTS values in the T7-tempered condition (aging at 240°C for 4 hrs) compared to the UTS values obtained with T62 and T6 tempers; the highest quality index in the B-series alloys is achieved by the alloy B1 in the T7-tempered condition.

The 220 casting alloys contain three hardening elements, namely, copper, magnesium and silicon. The application of an aging treatment to these alloys causes an entire range of precipitates to form according to the temperature and time applied. The aging behavior observed when applying aging temperature at 180°C is related to the precipitation of the Cu- and Mg-containing phases. The features of these precipitates vary

according to the aging time applied to the casting; in the case of aging at high temperatures, the strength and aging time relation displays a curvilinear form. This specific form of the aging curves is a result of overaging, which occurs upon increasing the aging time for durations longer than the specified peak-aging times with respect to each temperature. The increase in ductility due to overaging of the alloy compensates for the decreased strength in Equation 1, so that the overall quality does not display any significant change within this range of time. Such a decrease in strength and increase in the ductility of the alloy is related to the softening which occurs as a result of the overaging conditions at which the equilibrium precipitates form, leading to the loss of the coherency strain between the precipitates and the matrix. In addition, overaging results in the continuous growth of the large precipitates at the expense of the smaller ones according to the Ostwald ripening phenomenon, ultimately leading to coarser precipitates having large inter-particle spacing and less density in the metal matrix [102].

The quality of these castings, however, will be affected according to the net amount by which the reduction in strength is balanced by the increase in ductility. The fulfilment of the objectives of this research relies strongly on the use of quality index charts as a useful tool for illustrating, in an accessible way, the general behavior of the alloys with respect to tensile properties as the aging temperatures and times increase.

**Figure 5-16: Quality chart showing the tensile properties and the quality indices (Q) of B0, B1 and B2 alloys in the as-cast, T5, T6, T62 and T7-tempered conditions (tested at ambient temperature)**
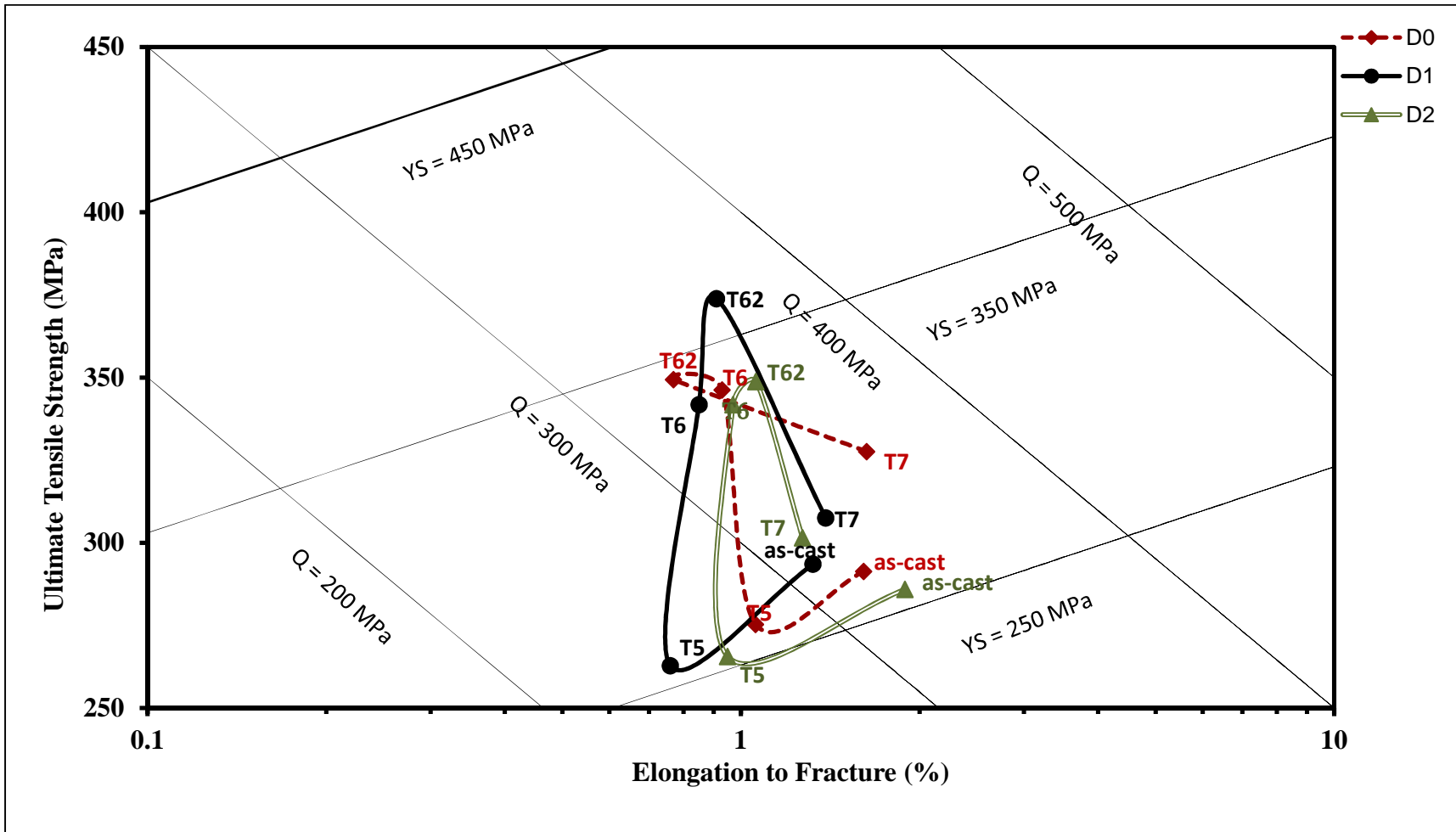
Figure 5-17: Quality chart showing the tensile properties and the quality indices (Q) of D0, D1 and D2 alloys in the as-cast, T5, T6, T62 and T7-tempered conditions (tested at ambient temperature).
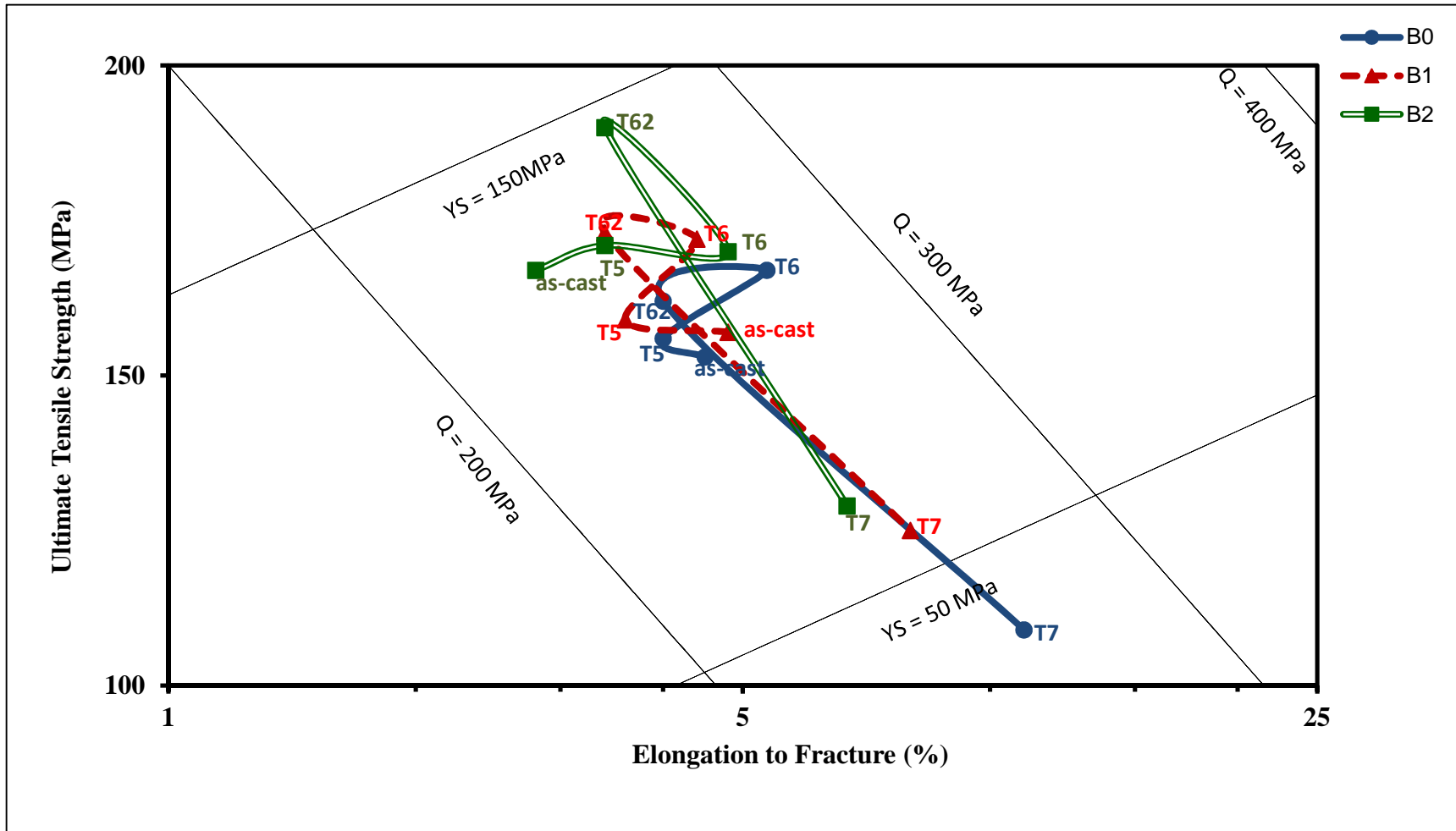
**Figure 5-18: Quality chart showing the tensile properties and the quality indices (Q) of B0, B1 and B2 alloys in the as-cast, T5, T6, T62 and T7-tempered conditions tested at 250 °C after 1 hr stabilization at testing temperature.**
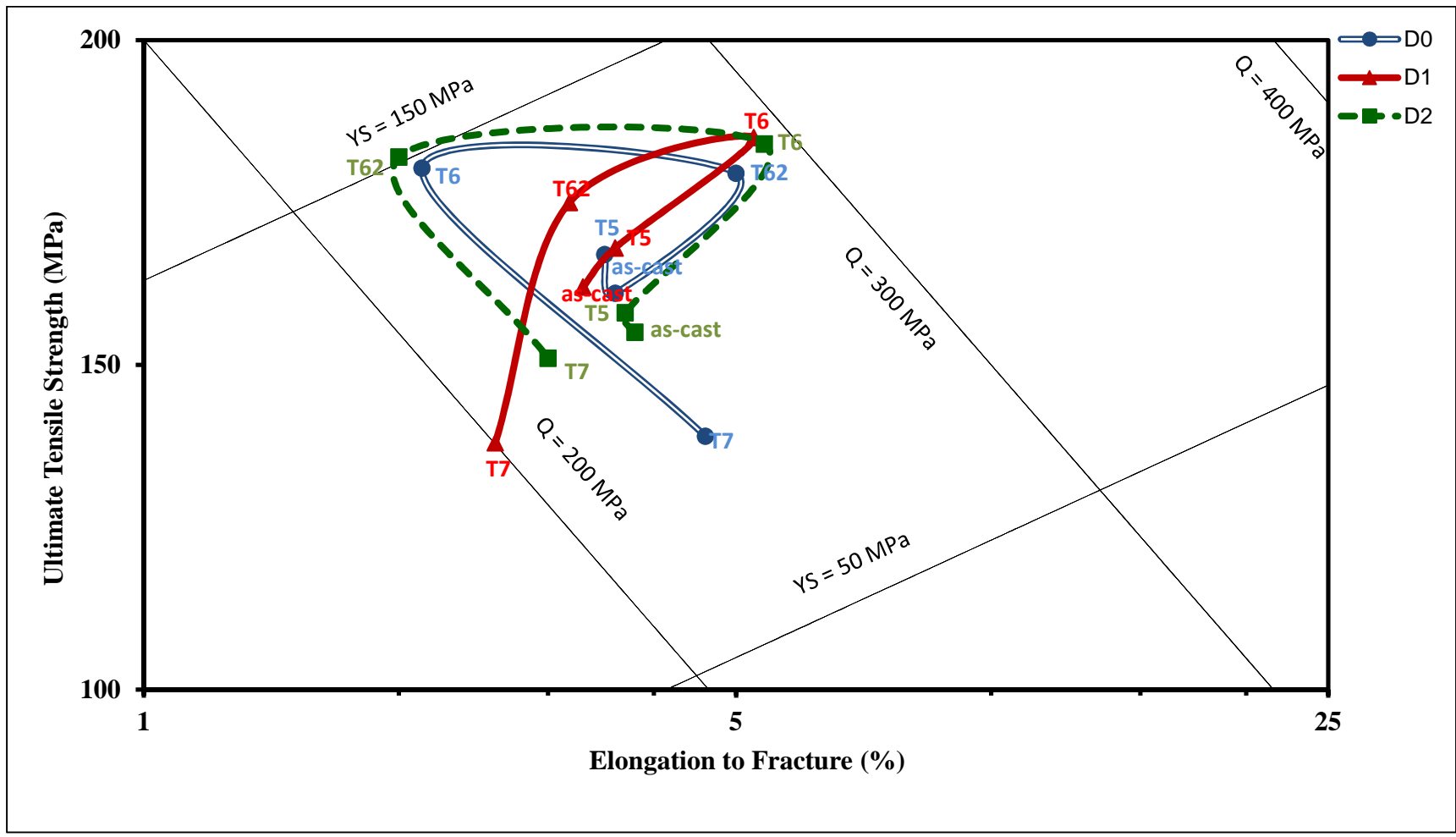
**Figure 5-19: Quality chart showing the tensile properties and the quality indices (Q) of alloys D0, D1 and D2 in the as-cast, T5, T6,      T62 and T7-tempered conditions tested at 250 °C after 1 hr stabilization at testing temperature.**
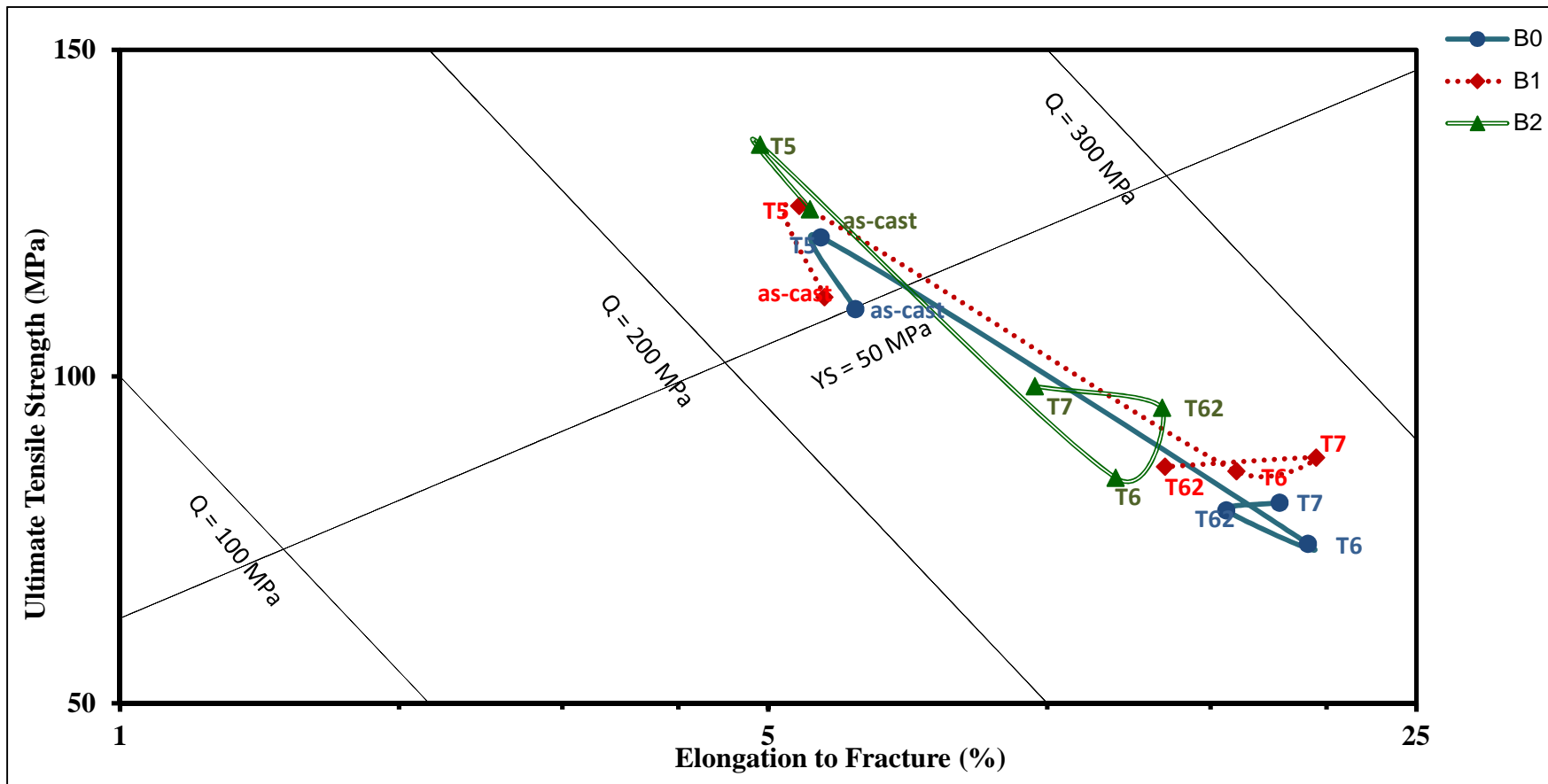
**Figure 5-20: Quality chart showing the tensile properties and the quality indices (Q) of alloys B0, B1 and B2 in the as-cast, T5, T6, T62 and T7-tempered conditions tested at 250 °C after 200 hrs stabilization at testing temperature.**
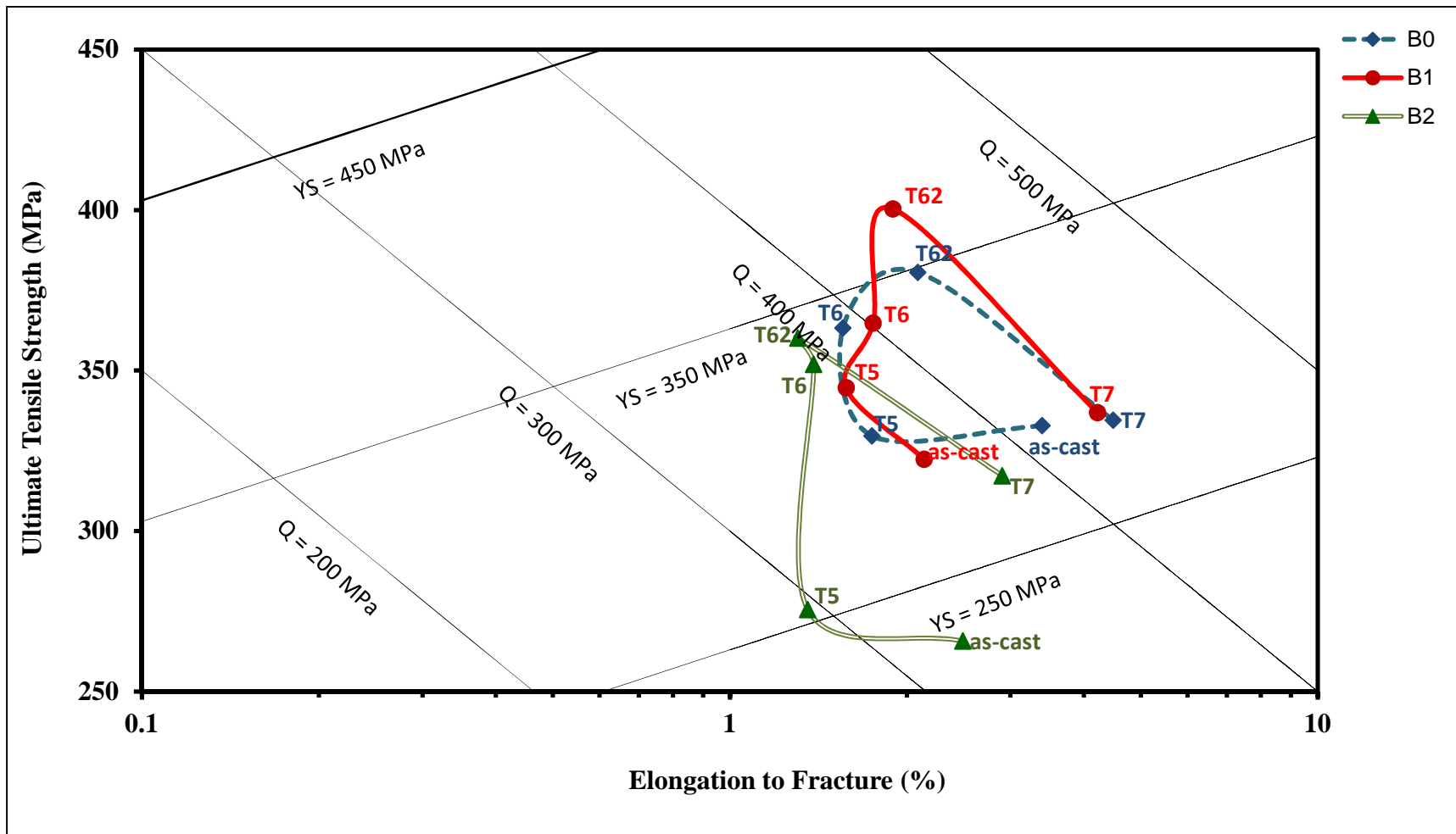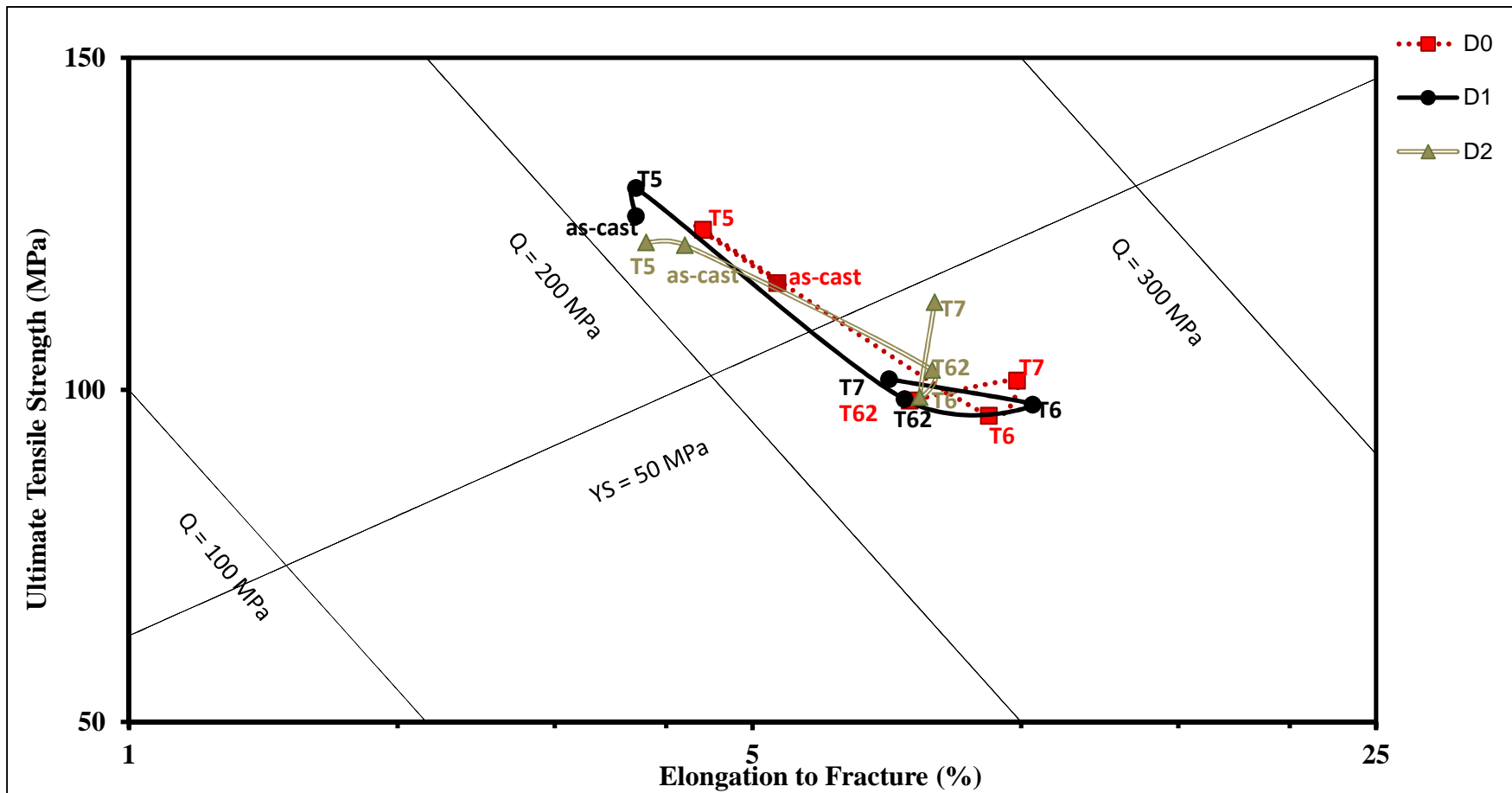
**Figure 5-21: Quality chart showing the tensile properties and the quality indices (Q) of alloys D0, D1 and D2 in the as-cast, T5, T6, T62 and T7-tempered conditions tested at 250 °C after 200 hrs stabilization at testing temperature.**

Color-contour maps are 2D vector plots that display a field of vectors in x, y coordinates where both direction and magnitude are represented. It is a tool that can help to present the tensile test results obtained in a different way, whereby one can observe how the alloy quality and properties vary with the heat treatment conditions, according to the change in color and magnitude of the contour regions. Each contour line represents a specific value of the property being considered. As an example, Figure 5.22 shows the quality index (Q) color-contour maps for all B and D alloys tested at (a) room temperature and at 250°C after (b) one hour, and (c) 200 hours stabilization at 250°C, respectively. Quality index (Q) values were obtained using Equations 1 and 2 (described in Chapter 2), and are plotted as a function of the heat treatment conditions.

As may be seen from Figure 5.22, the tensile performance of the as-cast base alloy B0 is improved after the application of the different heat treatments. With the T5 treatment, the quality of the alloy decreases with the addition of alloying elements to the B0 base alloy. The figure also reveals that alloy B1 shows the best quality index values after T62 heat treatment, i.e., 443 MPa at room temperature, 270 MPa at 1hr/250°C and 280 MPa at 200 hr/250°C, followed by alloy B2 which displays Q values of 429 MPa, 253 MPa and 263 MPa at room temperature, 1 hr/250°C and 200 hrs/250°C, respectively.

(a)
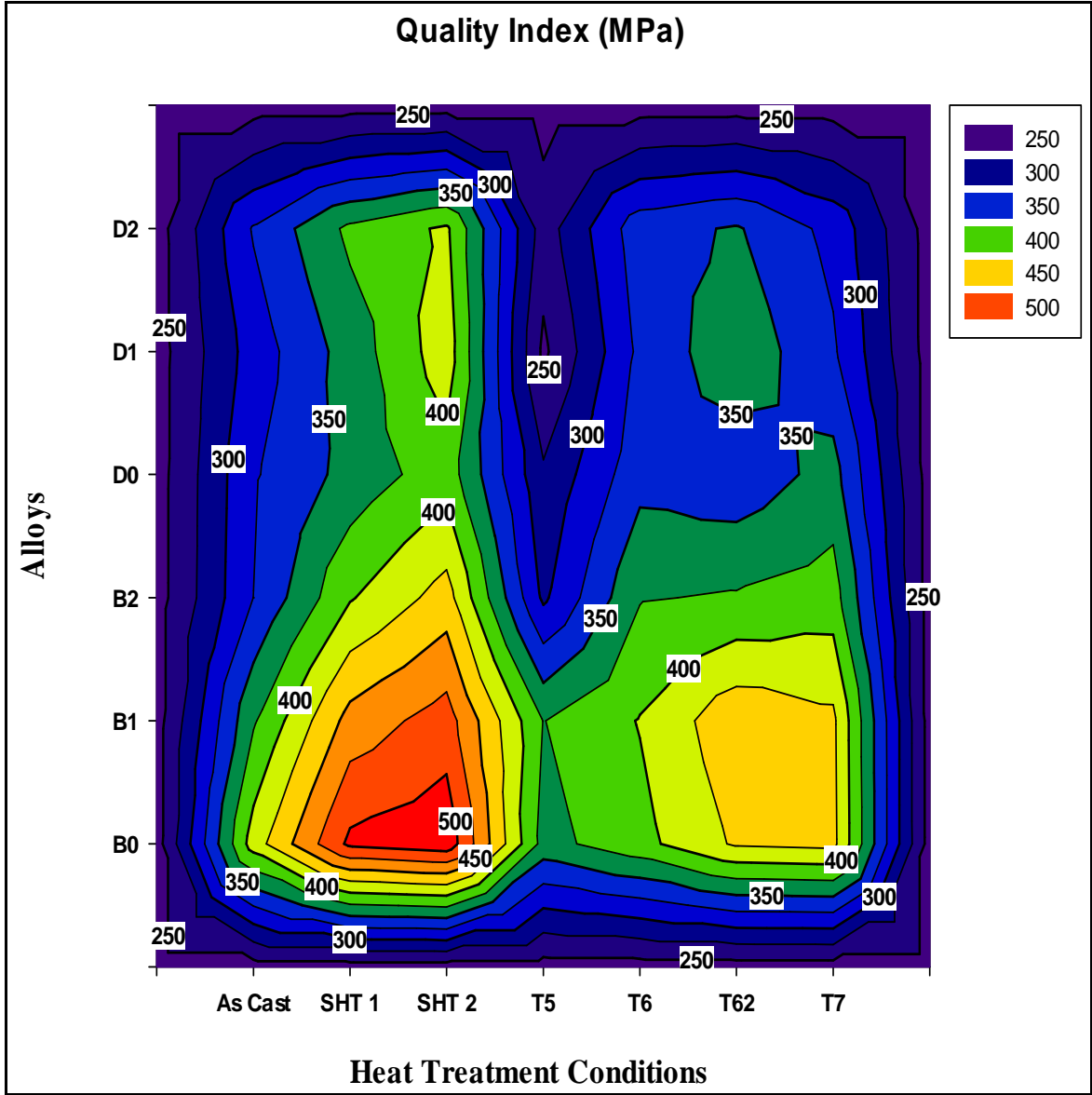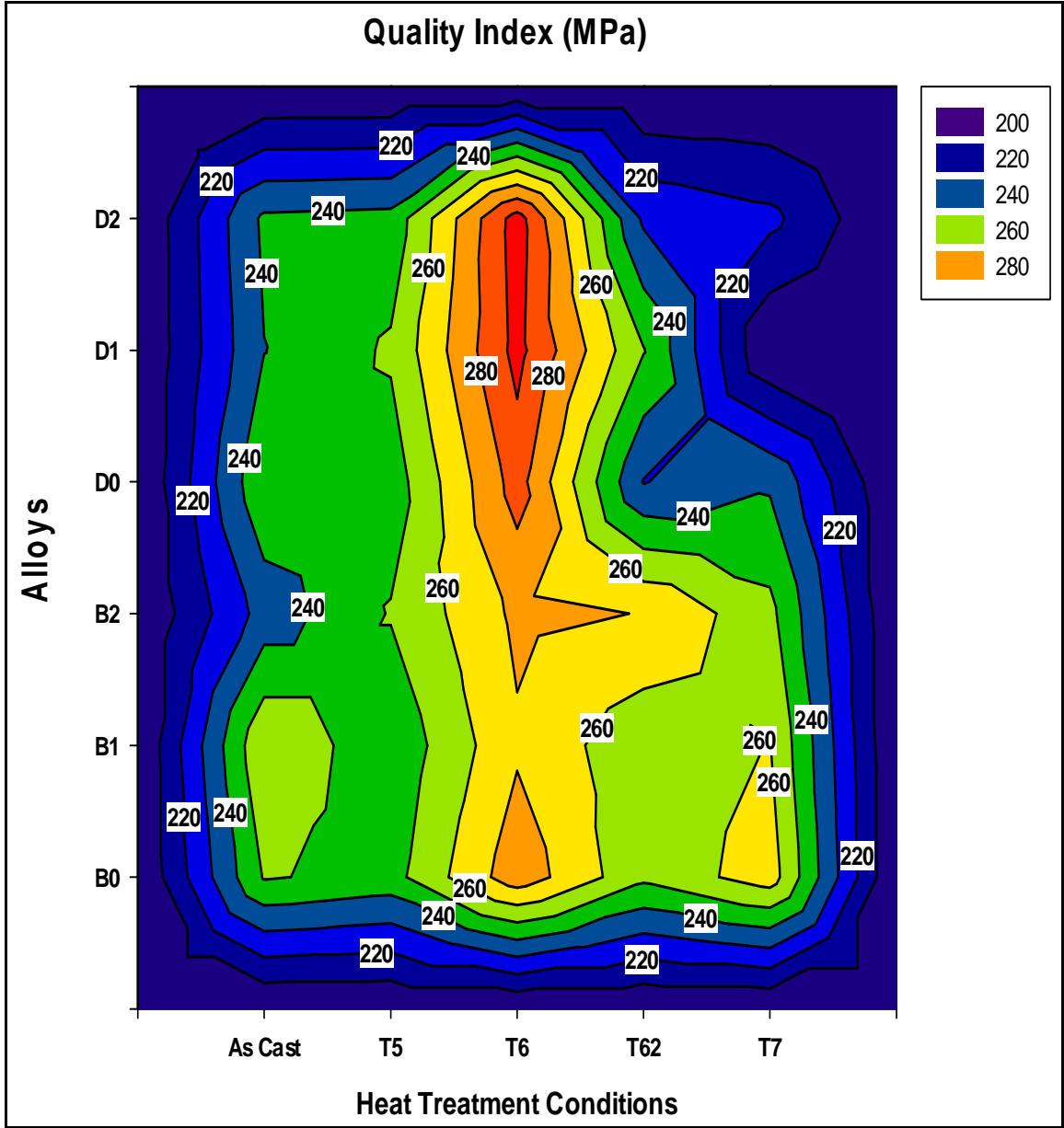
**Quality Index (MPa)**

**(b)**
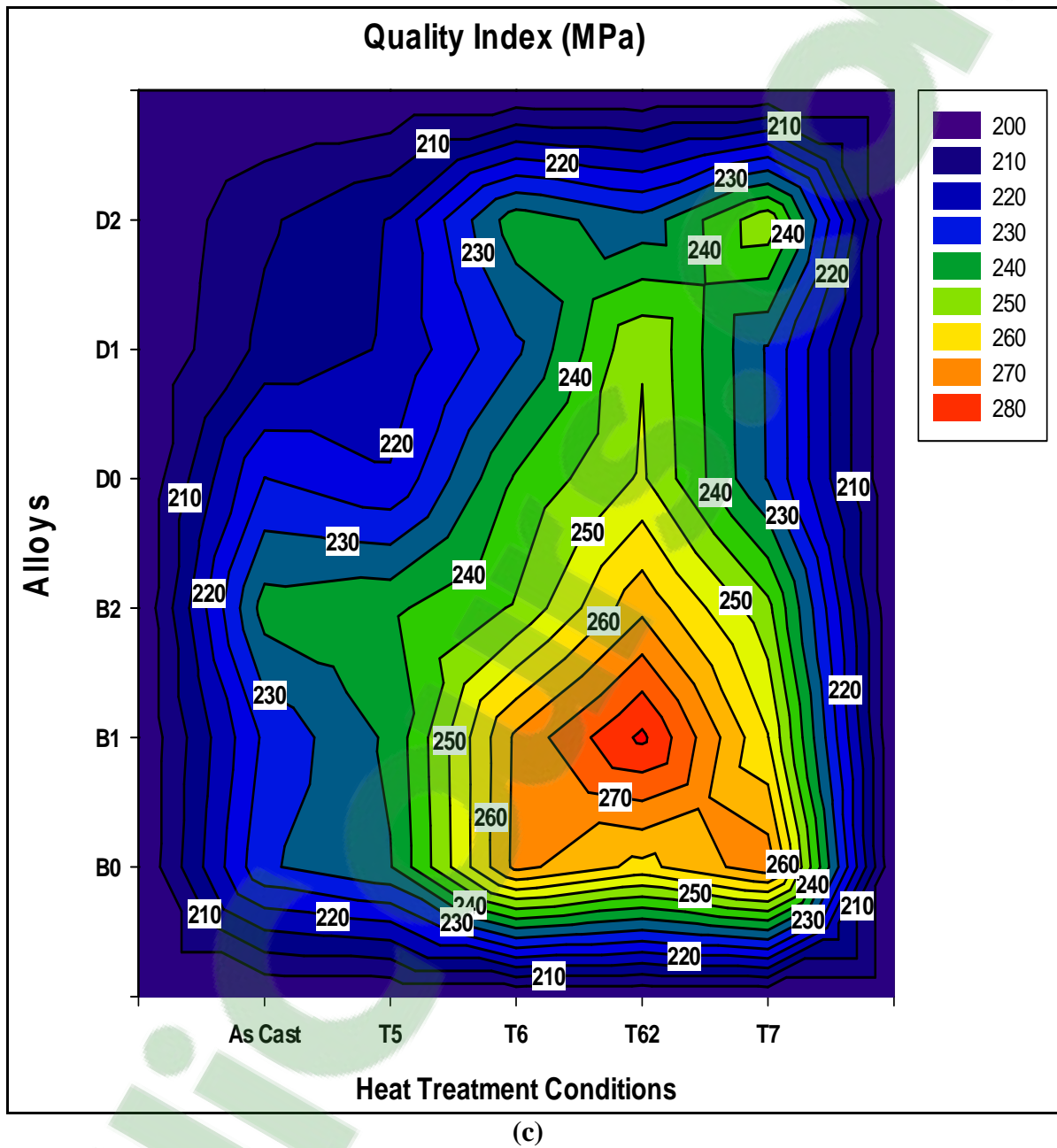
**Figure 5-22: Quality index color contour charts for the 220 alloys studied, comparing the effect of heat treatment condition for tensile tests carried out at (a) room temperature, and at 250 °C after stabilization for (b) 1 hr, and (c) 200 hrs at 250 °C.**

## 5.5    COMPARISON BETWEEN BASE ALLOY AND OTHER ALLOYS

Figures 5.23 (a-c) through 5.25 (a-c) shows plots of $\Delta P$ generated from the UTS, YS and percent elongation values obtained under different heat treatment conditions for the six alloys investigated (B0, B1, B2, D0, D1 and D2), tested at room temperature and at high temperature (250°C) following stabilization for 1 hr and 200 hrs at 250°C, respectively. These $\Delta P$ values were obtained after subtracting the values obtained for the base alloy B0 in each case; the $\Delta P$ values (P = Property) are plotted on the Y-axis, with the X-axis representing the base line for B0 in the as-cast condition. This approach helps to better visualize the effects and interactions of the various additions used and the different heat treatments applied. As will be seen from the figures presented subsequently, such $\Delta P$ plots instantly show how the various 220 alloys stand with respect to the as-cast base (reference) alloy and the different heat treatment conditions.

As Figure 5.23(a) reveals, the T62-tempered B1 alloy provides the highest UTS value overall. Figure 5.23(b) shows that the YS-$\Delta P$ value of D1-T62 is higher than those of the other alloys and that alloys B1 and D1 exhibit almost the same values in the T6-treated condition. As expected, the %El-$\Delta P$ values in Figure 23(c) for these alloys are much lower than those of the B0 base alloy, in light of their high strength.

(a)



(b)

(c)
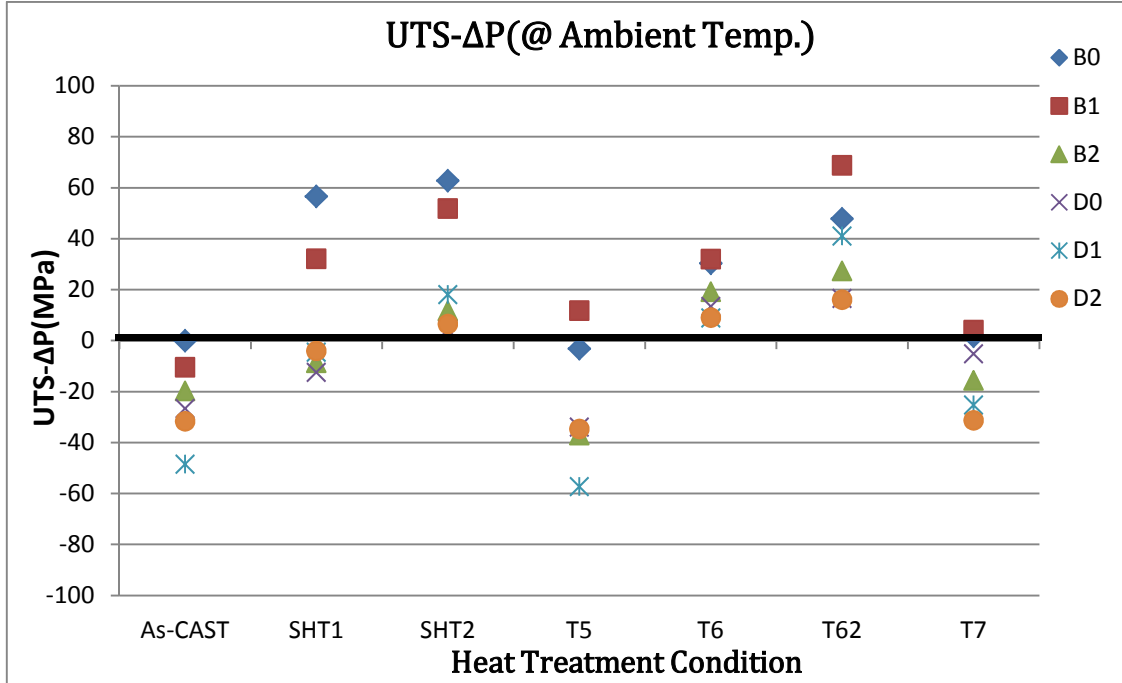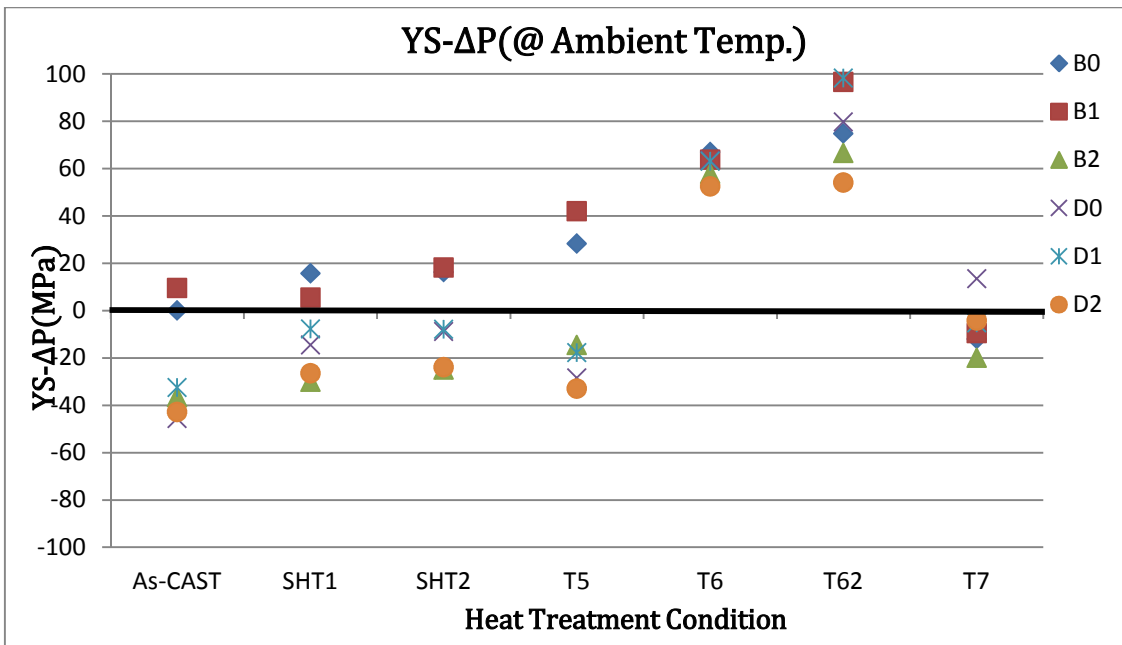
**Figure 5-23: Variation in (a) ΔP-UTS, (b) ΔP-YS and c) ΔP-%El as a function of heat treatment conditionfor the 220 alloys tested at ambient temperature.**

The variations in the high temperature tensile properties with respect to alloy B0 after 1hr stabilization at the testing temperature (250°C) are shown in Figure 5.24. It may be observed from Figure 5.24(a) that the T62-treated B2 alloy displays the highest UTS value among all the other alloys and for all heat treatment conditions. The B1, D0, D1and D2 alloys show UTS levels higher than those shown by the base alloy for most heat treatment conditions, except in the case of T7 temper, where all alloys exhibit lower strengths than the as-cast B0 alloy.

With respect to the yield strength, Figure 5.24(b) reveals that the B2 and/or D2 alloys show higher YS values compared to the other alloys for most conditions with the

exception of the T62-tempered B0 alloy which displays the highest yield strength. In accordance with these observations, Figure 5.24(c) shows that the ductilities of the T62-tempered alloys are the lowest among all conditions, followed by the T5-tempered alloys. Apart from these tow general observations, the ductility values of the individual alloys fluctuate from higher to lower and again to higher values with respect to the as-cast base alloy. While the T7-tempered B0 alloy shows the highest ductility, with the B1 and B2 alloys also showing high ductilities, as expected, the D-series alloys do not follow the same trend. This may be attributed to their higher Si content compared to the B-series alloys.

Figure 5.25 compares the tensile properties obtained for the B-series and D-series alloys tested at 250°C after 200 hrs stabilization at the testing temperature, relative to the values obtained for the as-cast B0 base alloy - represented by the X-axis base line. Figure 5.25(a) shows that the highest UTS values are exhibited by all alloys in the T5 heat-treated condition, with alloy B2 exhibiting the highest improvement relative to the as-cast base alloy. The values start to decrease with the T6, T62, and T7 conditions, the B0 and B1 alloys showing the highest decrease in UTS, and the D2 alloy showing the least decrease over these three tempers.

The same trend is observed in the case of yield strength, where all alloys in the T5 heat-treated condition exhibit the highest YS values, with the T5-tempered B2 alloy again exhibiting the highest improvement relative to the as-cast base alloy. As in the case of the UTS values, the YS values also start to decrease with the T6, T62, and T7 conditions, the variation in YS values for the T6-treated alloys lying within a closer range than that observed in the case of the UTS values, as may be seen from Figure 5.25(b).

Figure 5.25(c) shows that the percentage elongation values for all alloys in the as-cast and T5-tempered conditions are lower than that of the as-cast base alloy, which may be understood in light of the results shown in Figure 5.25(a). The ductility values observed in the T6, T62 and T7 conditions vary from about 6 to 13% for the B-series alloys, while the D-series alloys exhibit ductility values that lie between 1 and 4%, depending on the alloy and heat treatment condition. These ductility values exhibited by the B- and D-series alloys may be attributed to their low and high silicon content, respectively

(a)



(b)

136
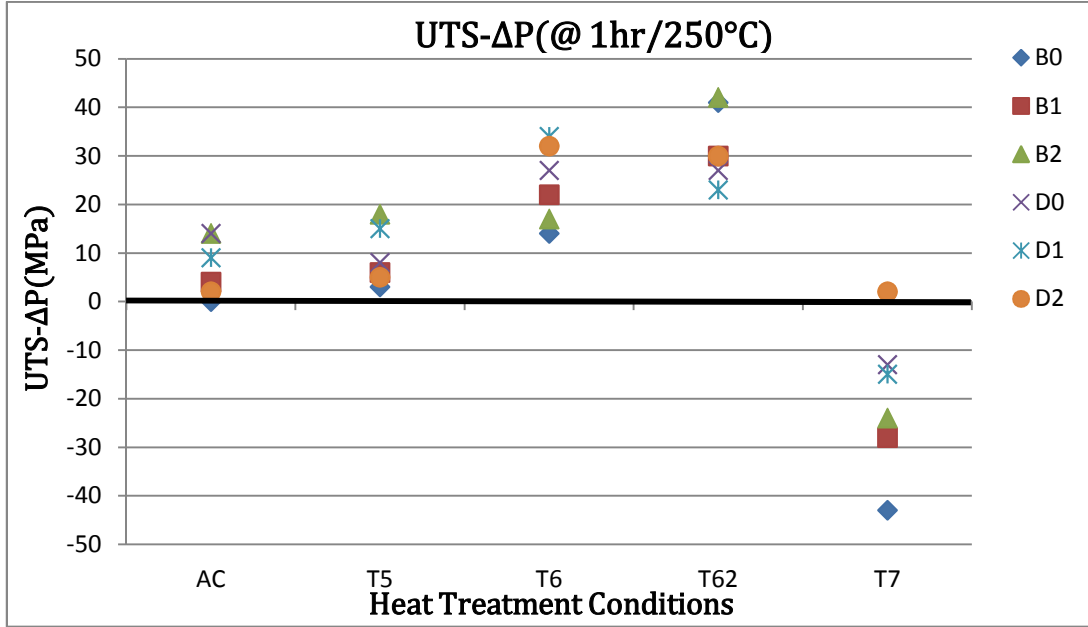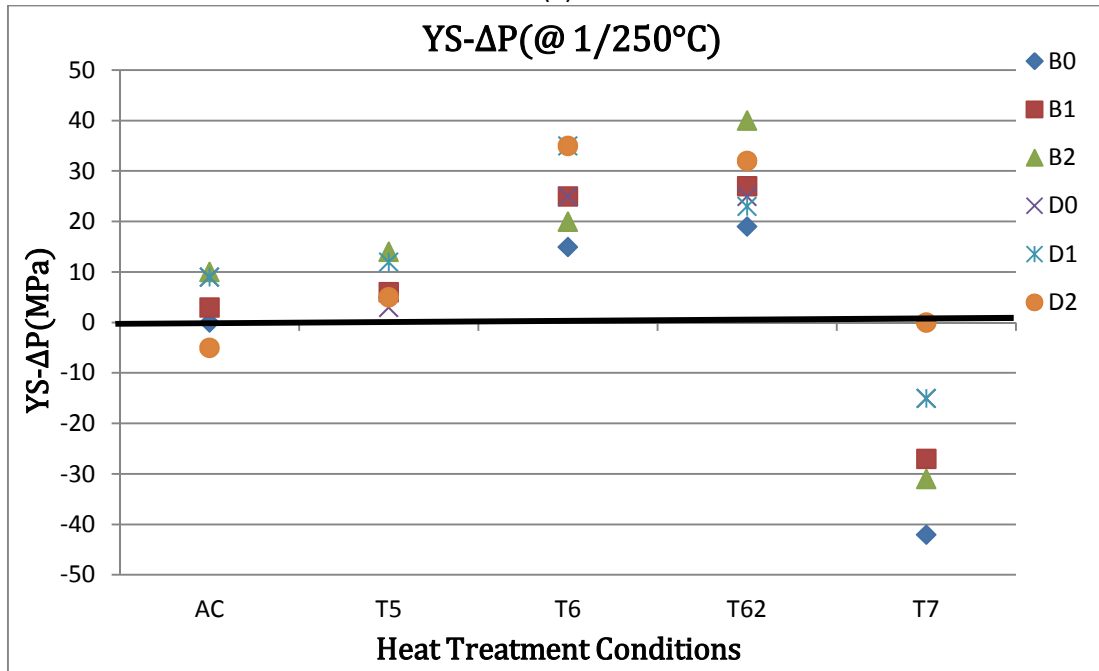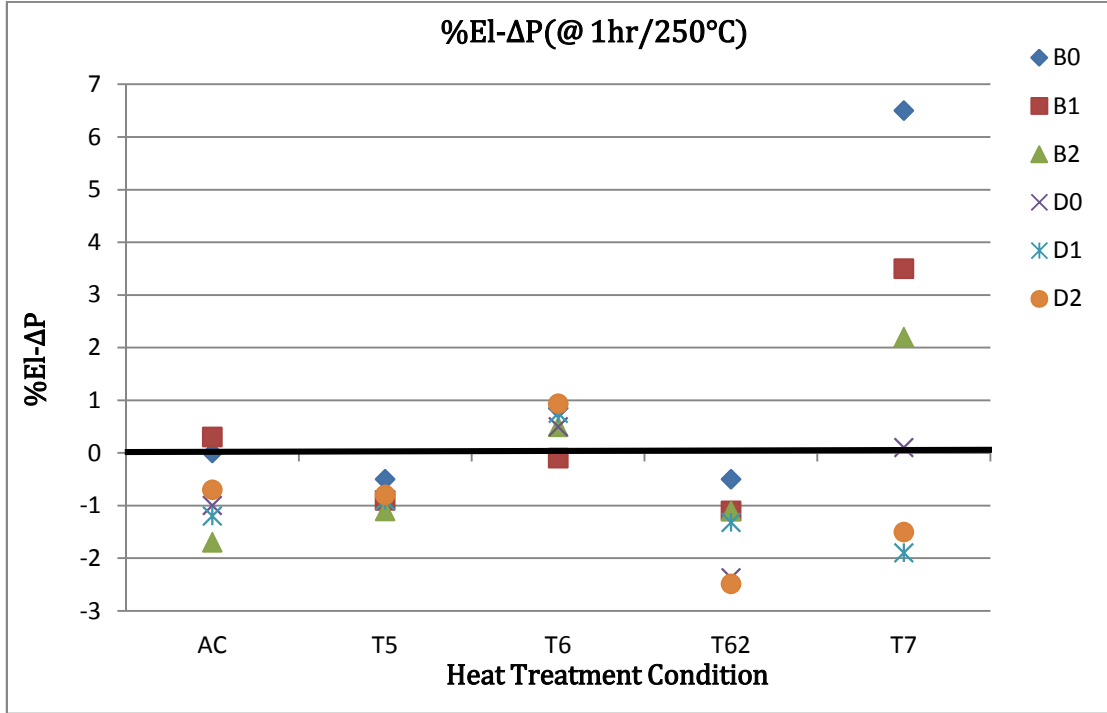
(c)

**Figure 5-24: Variation in (a) ΔP-UTS, (b) ΔP-YS and (c) ΔP-%El as a function of heat treatment condition for the 220 alloys tested at 250°C after 1 hr stabilization at testing temperature.**
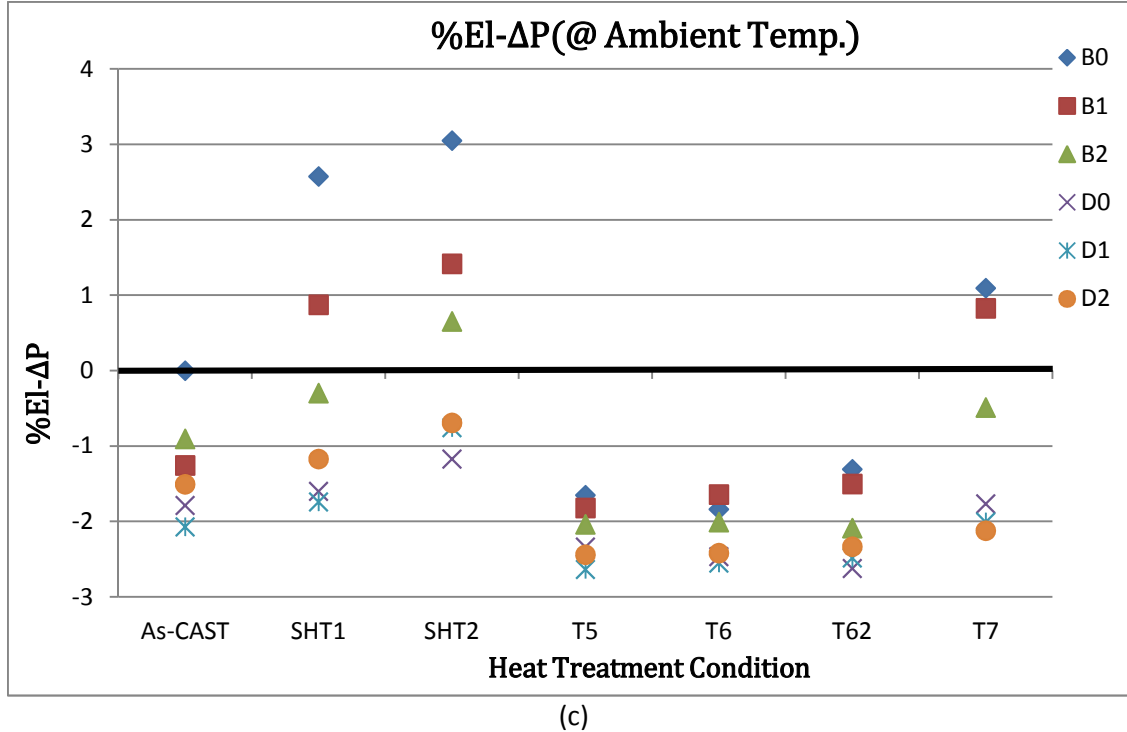
(a)



(b)

138
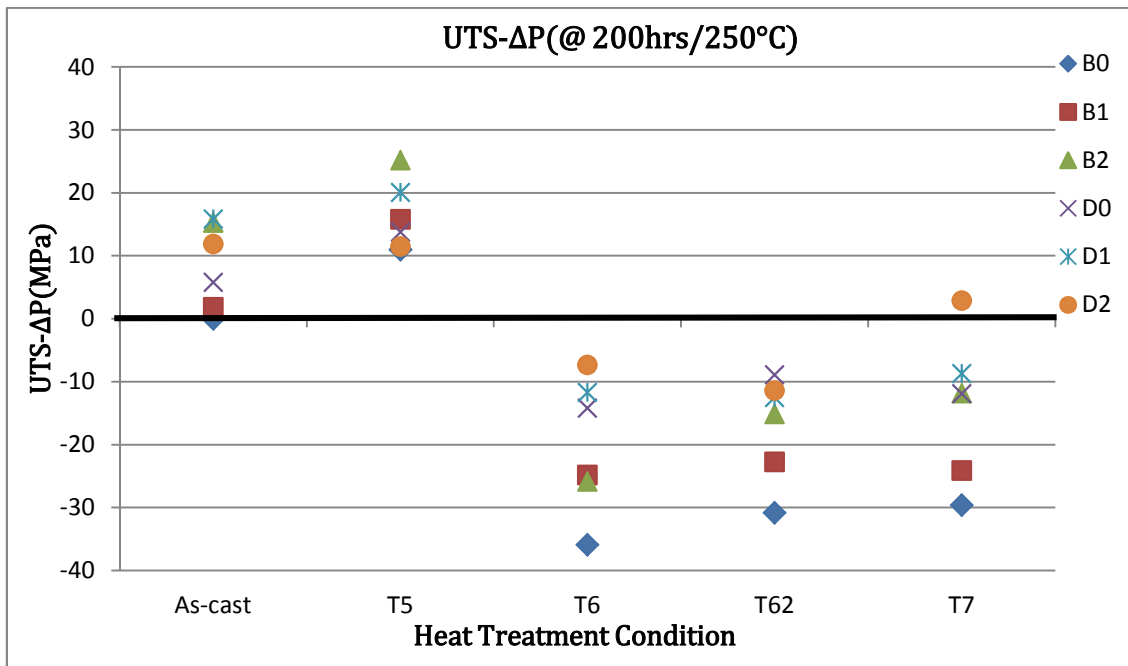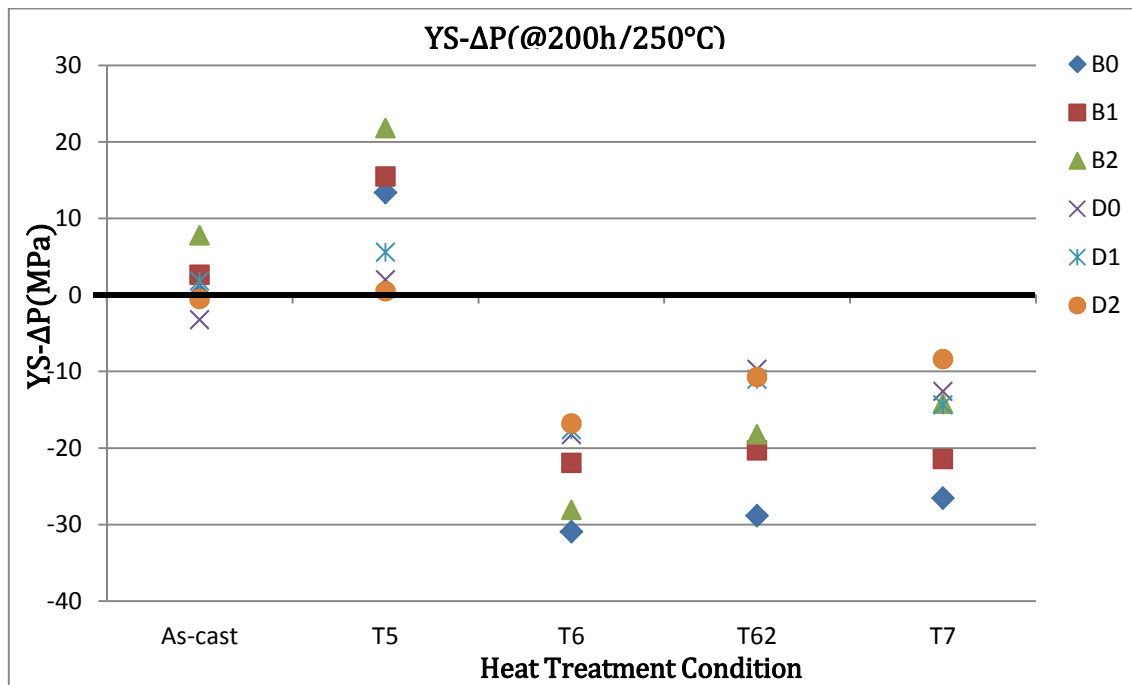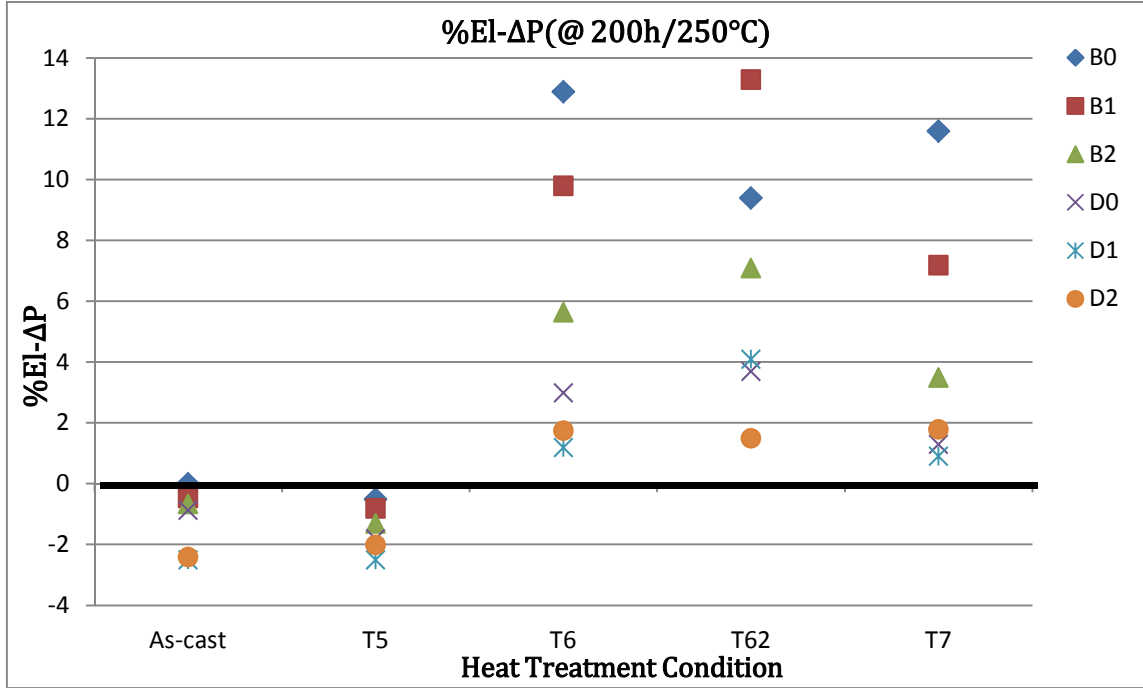
**Figure 5-25: Variation in (a) ΔP-UTS, (b) ΔP-YS and (c) ΔP-%El as a function of heat treatment condition for the 220 alloys tested at 250°C after 200 hrs stabilization at testing temperature.**

# CHAPTER SIX

# CONCLUSIONS AND RECOMMENDATIONS

# CHAPTER 6

# CONCLUSIONS AND RECOMMENDATIONS

An investigation was carried out of the effects of different alloying additions and heat treatments on the mechanical properties of 220-type Al-2.4%Cu-1.2%Si-0.4%Mg-0.4%Fe-0.6%Mn alloys at ambient and high temperatures. Six alloys were investigated, covering the grain refined (0.15% Ti) base 220 alloy (coded B0) and B1 and B2 alloys comprising B0 alloy with 0.15% Zr, 0.2% V and 0.3% Ni additions, and 0.15% Zr, 0.2% V, 1% Ni, 0.015%Sr, 0.2% La and 0.2% Cr additions, respectively, and three other alloys where the silicon content of the 220 alloy was increased to 8 wt% (coded D0 alloy) from which D1 and D2 alloys were obtained, containing the same alloying additions as B1 and B2 alloys. The heat treatments applied covered those commonly used in the case of cast aluminum alloys, namely T5, T6, T62, and T7 treatments which consisted of a single-stage solution heat treatment (495°C/5h) for T6 and T7 tempers, and a multi-stage solution treatment (495°C/5h + 515°C/2h + 530°C/2h) for the T62 temper, followed by quenching in warm water, and then artificial aging at 180°C/8h for T5, T6 and T62 tempers, and at 240°C/4h for the T7 temper.

From the analysis and discussion of the results presented in Chapters 4 and 5 of this dissertation, the following conclusions may be drawn.

## 6.1    MICROSTRUCTURE

1- The thermal analysis experiments provide evidence of the solidification sequence i.e., the reactions taking place and the corresponding phases formed during solidification under close-to equilibrium cooling conditions.

2- The $\theta$-Al$_2$Cu, Q-Al$_5$Mg$_8$Si$_6$Cu$_2$, and the Chinese script-like $\alpha$-Al$_{15}$(Fe,Mn)$_3$Si$_2$ phases were identified as the main microstructural constituents of the 220 alloy.

3- Three main reactions are detected during the solidification of the 220 base alloy: (i) formation of the $\alpha$-Al dendritic network at 640°C, followed by (ii) the precipitation of the $\alpha$-iron Al$_{15}$(Fe,Mn)$_3$Si$_2$ intermetallic phase at 620°C; and then (iii) Al$_2$Cu and Al$_5$Mg$_8$Si$_6$Cu$_2$ phases which precipitate simultaneously as the final reaction at 495°C.

4- One more reactions is observed in the B2 alloy with the addition of Zr and V, accompanying the formation of AlSiTiZrV phases.

5- The addition of Cr (0.2%) in Alloys B2 and D2 helped in reducing the detrimental effects of the platelet morphology of the $\beta$-iron Al$_5$FeSi phase by replacing it with the more compact and hence less detrimental $\alpha$-Al$_{15}$(Fe,Mn)$_3$Si$_2$ phase with its Chinese script morphology and sludge particles ($\alpha$-Al$_{15}$(Fe,Mn,Cr)$_3$Si$_2$).

6- The increased Si content (8 wt.%) in the D-series alloys compared to the B-series alloys (1.2 wt% Si), resulted in the precipitation of the eutectic Al-Si phase in addition to the $\alpha$-iron phase at 570°C.

7- The eutectic Si morphology changed from coarse brittle flakes to a finer fibrous form with the addition of 0.02 wt% Sr addition in D2 alloy, that led to an enhancement in the tensile properties; also, the presence of chromium led to the formation of another version of the α-Fe phase, commonly known as sludge $\alpha$-$Al_{15}(Fe,Mn,Cr)_3Si_2$.

8- Three new reactions were observed in the D2 alloy, with the addition of Zr, Cr, Ni, V and La, corresponding to the formation of AlSiCuNiLa, AlNiSiZrCuFe and AlFeMnCrSiVNi phases.

9- When the as-cast alloys are subjected to the multi-step solution treatment – involving higher solution temperatures and longer durations, an increased amount of incipient melting is expected to occur.

10- The D alloys (containing a higher Si content) showed much smaller porosity/incipient melting in the as-cast condition compared to the B alloys. The eutectic Si regions which are dispersed in the matrix of the as-cast D0 alloy (with almost no porosity) undergo the process of Si particle necking, fragmentation and spheroidization during single stage or SHT-1 solution heat treatment of the alloy, followed by coarsening of the spheroidized Si particles during the extended duration of the multi-step or SHT-2 solution treatment.

11. With the exception of the Cu-rich $CuAl_2$ phase, most of the other intermetallic phases formed in the alloys did not dissolve upon solution heat treatment.

## 6.2    TENSILE PROPERTIES

12. The UTS values improved considerably after solution heat treatment, resulting from the dissolution of the Cu-rich phase, with solid solution strengthening being the main operating mechanism.

13- The UTS of the as-cast alloy B0 improves by ~ 18% following solution heat treatment (495°C/5h) compared with other alloys; the T62-tempered B1 alloy showed maximum improvement in the B-series alloys with a UTS of ~401.55 MPa, with the greatest response to the multi-stage solution heat treatment (495°C/5h+515°C/2h+530°C /2h), which may be attributed to the addition of Ti and Zr. In the D-series alloys, the T62-tempered D1 alloy displayed the highest improvement, with a UTS of ~293.5 MPa at ambient temperature.

14- The use of the T62 heat treatment allows for maximum dissolution of the copper phases in the two stages of solution treatment; such dissolution produces the greatest improvement in both UTS and YS values.

15- At ambient temperature tensile testing, T6 and T62 treatments provide the best improvements in both UTS and YS values for all alloys.

16- After T62 treatment, alloy B1 (containing 0.15wt% Zr + 0.20wt% V + 0.3wt% Ni) showed the maximum increase in tensile properties, with the UTS and YS values increasing by ~115 MPa and ~150 MPa, respectively.

17- The yield strength values improved overall after solution treatment; moreover, the yield strength values followed the same trend as the ultimate tensile strength at both ambient and high temperature testing.

18- Increasing the amount of added elements increased the volume fraction of the intermetallic phases formed in the alloys which reflected upon the alloy mechanical properties and quality.

19- At high temperature testing at 250°C after one hour stabilization, the ultimate tensile strength of the alloy increased with the T6 and T62 heat treatment conditions, but remained the same after T5 heat treatment; the highest UTS value was exhibited by the T62-tempered B2 alloy with ~195 MPa. All alloys displayed tensile strength values that are higher than those exhibited by the base alloy B0 in the T7-tempered condition. The lowest ductility values were observed for the T62-tempered alloys, while all T7-tempered alloys show maximum ductility.

20- At 250°C, after one hour stabilization, the D2 alloy showed unchanged UTS and improved YS values in the T7-treated condition compared to the corresponding strength values in its as-cast condition; this behavior is opposite to the general trend followed by the other alloys (B0 through D1) which showed a noticeable decrease in their strength values in the T7-treated condition in comparison to their as-cast values in each case.

21- At high temperature testing at 250°C after 200 hours stabilization, the alloy strength increased after the T5 heat treatment but decreased in the T6 and T62-tempered conditions; the alloy B2 showed maximum strength in the T5-tempered condition (B-series) with ~ 135

MPa, followed by the T5-tempered D1 alloy, with ~130 MPa. The highest ductility values were observed in the T6 and T62 conditions whereas the T5-treated alloys exhibited the lowest ductility values, with the D1 and D2 alloys showing the same ductility as in the as-cast condition.

22- Quality charts, color contour maps and plots of ΔP constructed from the tensile test data may be used for selecting the appropriate metallurgical conditions for tailoring the alloy properties to those required for a specific application.

23- The quality index charts revealed that, for ambient temperature testing, the best alloy quality for the B-series alloys was provided by the B1 alloy in the T62- and T7-tempered conditions, i.e., ~444 MPa and ~430 MPa, respectively. For the D-series alloys, the highest Q values were obtained for the T62-tempered D1 alloy, with ~368 MPa, and the T7-tempered D0 alloy, with ~360 MPa.

24- In the case of high temperature testing, after one hour stabilization time at the testing temperature (250°C), the highest Q values were obtained for the T62-tempered B2 alloy and the T6-tempered D2 alloy i.e., ~270MPa and ~290MPa, respectively when aged at 180°C for 8 hrs. After stabilization for 200 hours at the testing temperature (250°C), the highest quality index in the B-series alloys was achieved by the alloy B1 in the T7-tempered condition i.e., ~260MPa.

25- Plots of ΔP provided a better visualization of the effects and interactions of the various additions used and the different heat treatment conditions. They also revealed at a glance

how the different 220 alloys stand with respect to the base alloy B0 after the various additions and application of the different heat treatments commonly used in the case of aluminum alloys.

## 6.3    RECOMMENDATIONS FOR FUTURE WORK

The focus of this study was on determining the tensile properties of the Al-2%Cu based 220 type alloys. Based on the results obtained in this project, it would be interesting to extend the work to investigate:

(i)      the effects of the different heat treatment used on other mechanical properties such as (the hardness, impact, and fatigue properties) of these alloys, and

(ii)     follow the precipitation behavior of the various precipitates formed using transmission electron microscopy, this would enable a deeper understanding of the role played by these precipitates on the alloy properties

# REFERENCES

[1]     Emma Sjölander," Heat Treatment of Al-Si-Cu-Mg Casting Alloys", Department of Mechanical Engineering, Materials and Manufacturing – Casting, Chalmers University of Technology, 2011.

[2]     ASM Handbook, "Heat Treating of Aluminum Alloys", 10th Edition, American Society for Metals, Materials Park, Ohio, vol. 4, 1991.

[3]     A. Hossain, A. S. W. Kurny, M. A. Gafur, "Effect of 2wt% Cu Addition on the Tensile Properties and Fracture Behavior of Peak Aged Al-6Si-0.5Mg-2Ni Alloy at Various Strain Rates", International Journal of Chemical, Nuclear, Metallurgical and Materials Engineering, vol: 8 No: 5, 2014, pp. 356-364.

[4]     I.N. Fridlyander, "Aluminum Alloys in Aircraft in the Periods of 1970-2000 and 2001-2015," *Metal Science and Heat Treatment*, vol. 43(1-2), 2001, pp. 6-10.

[5]     F. Paray and J.E. Gruzleski, "Factors to Consider in Modification," *AFS Transactions*, vol. 102, 1994, pp. 833-842.

[6]     L. Bäckerud, G. Chai and J. Tamminen, Solidification Characteristics of Aluminum Alloys, vol. 2: Foundry Alloys, AFS/Skanaluminium, Des Plaines, IL, 1990, pp. 71-84.

[7]     A.M.A. Mohamed, F.H. Samuel, A.M. Samuel and H.W. Doty, "Influence of Additives on the Impact Properties of Al-10.8%Si Near-Eutectic Al-Si Alloys," *Materials and Design*, vol. 30(10), 2009, pp. 4218-4229.

[8]     G.E. Totten and D.S. MacKenzie (Eds.), Handbook of Aluminum, vol. 1: Physical Metallurgy and Process, Marcel Dekker Inc., New York, 2003, pp. 114-168.

[9]     A.M. Samuel, F.H. Samuel and H.W. Doty, "Observations on the Formation of $\beta$-$Al_5FeSi$ Phase in 319 Type Al-Si Alloys," *Journal of Materials Science*, vol. 31(20), 1996, pp. 5529-5539.

[10]    S.G. Shabestari and J.E. Gruzleski, "Modification of Iron Containing Precipitates in $AlSi_2$ Alloys with Strontium," *Giesserei-Praxis*, vol. 17, 1997, pp. 385-394.

[11]    K. Wojciech, S. A. Babak and M. Niewczas, "Structure and properties of cast Al–Si based alloy with Zr–V–Ti additions and its evaluation of high temperature performance," Journal of Alloys and Compounds, vol. 595, 2014, pp. 67-79.

[12]    V. I. Elagin, "Ways of Developing high-Strength and high-Temperature Structural Aluminum alloys in the 21st Century," *Metal Science and Heat Treatment,* vol. 49, no. 9-10, 2007, pp. 427-434.

[13]    A. Tolley, V. Radmilovic and U. Dahmen, "On the effect of Zr on precipitate evolution in Al-Sc-Zr alloys," in *Congress CONAMET/SAM 2004 Proceedings*, La Serena, Chile, 2004.

[14]    D. Emadi, J.E. Gruzleski, "Effects of Casting and Melt Variables on Porosity in Directionally-Solidified Al-Si Alloys," *AFS Transactions*, vol. 95, 1994, pp. 307-312.

[15]    Davis, J.R. (Ed.), *ASM Speciality Handbook: Aluminum and Aluminum Alloys,* ASM International, Materials Park, OH, 1993.

[16] J.G. Kaufman, Introduction to Aluminum Alloys and Tempers: Surface Treatments and Coating, "Materials Park, OH: ASM International, 2000.

[17] Brick, R.M., Gordon, R.B., Phillips, A., *Structure and Properties of Alloys,* 3rd Edition, McGraw-Hill, 1965.

[18] A. Mohamed and F. Samuel, "A Review on the Heat Treatment of Al-Si-Cu/Mg Casting Alloys," in *Heat Treatment - Conventional and Novel Applications*, Dr. Frank Czerwinski (Ed.), ISBN: 978-953-51-0768-2, InTech, DOI: 10.5772/50282, 2012.

[19] J. E. Hatch, Aluminum: Properties and Physical Metallurgy, American Society for Metals, Materials Park, OH, 1984, p.135.

[20] Emma Sjölander, Salem Seifeddine, "The Heat Treatment of Al–Si–Cu–Mg Casting Alloys", Journal of Materials Processing Technology 210, 2010 pp.1249–1259.

[21]  Srecko Manasijevic, Srdjan Markovic, "Effect of Heat Treatment on The Microstructure and Mechanical Properties of Piston Alloys", Materials Science and Engineering, 2013, pp.396-402.

[22] Salem Seifeddine, Sten Johansson and Ingvar L. Svensson, "The influence of cooling rate and manganese content on the β-Al5FeSi phase formation and mechanical properties of Al–Si-based alloys," *Materials Science and Engineering: A,* vol. 490, no. 1-2, , 2008, pp. 385-390.

[23]    L. A. Abel, R. T. Kiepura, P. Thomas, H. F. Lampman, N. D. ASM Handbook, Properties and Selection: Nonferrous Alloys and Special-Purpose Materials, Wheaton (Eds.), The Materials Information Society, vol. 2, 1990, p. 1328.

[24]    O. Reiso, H.G. Overlie, N. Ryum, "Dissolution and Melting of Secondary $Al_2Cu$ Phase Particles in an Al-Cu Alloy," Metallurgical Transactions A, vol. 21A, 1990, pp.1689-1695.

[25]    M. Tash, F. H. Samuel, F. Mucciardi, H. W. Doty, "Effect of Metallurgical Parameters on the Hardness and Microstructural Characterization of As-Cast and Heat-Treated 356 and 319 Aluminum Alloys," Materials Science and Engineering A, vol. 443A, 2007, pp. 185-201.

[26]    Z. Ma, A. M. Samuel, F. H. Samuel, H. W. Doty, and S. Valtierra, "A Study of Tensile Properties in Al-Si-Cu and Al-Si-Mg Alloys: Effect of β-iron Intermetallic and Porosity", Materials Science and Engineering A, vol. 490, 2008, pp. 36-51.

[27]    Jerry H. Sokolowski, X-C. Sun, G. Byczynski, D.E. Penord, R. Thomas, and A. Esseltine, "The Removal of Copper-Phase Segregation and the Subsequent Improvement in Mechanical Properties of Cast 319 Aluminum Alloys by a Two-Stage Solution Heat-Treatment," Journal of Materials Processing Technology, vol. 53, 1995, pp. 385-392.

[28]    Chen Song-yi, Chen Kang-hua, Peng Guo-sheng, Liang Xin and Chen Xue-hai, "Effect of quenching rate on microstructure and stress corrosion cracking of 7085

aluminum alloy," *Transactions of Nonferrous Metals Society of China,* vol. 22, no. 1,  2011, pp. 47-52.

[29]     A. Cuniberti, A. Tolley, M.V. Castro Riglos and R. Giovachini, "Influence of natural aging on the precipitation hardening of an AlMgSi alloy," *Materials Science and Engineering: A,* vol. 527, no. 20, 2010,  pp. 5307-5311.


[30]     G. E. Totten, and D. S. Mackenzie (Eds), Handbook of Aluminum, Marcel Dekker, Inc., New York, Basel, 2003, p. 1296.

[31]   H. Sehitoglu, T. Foglesong, H.J. Maier, "Precipitation Effects on the Mechanical Behaviour of Aluminum Copper Alloys: Part I. Experiments," *Metallurgical and Materials Transactions A*, vol. 36A, 2005,  pp. 749-761.

[32]   R. N. Lumley, J.Buha, I.J. Polmear, A.J. Morton, A.G. Crosky, "Secondary Precipitation in Aluminum Alloys & Its Role in Modern Heat Treatment," *Materials Science Forum*, vol. 519, 2006, pp. 283-290.

[33]   Reif, W., Yu, S., Dutkiewicz, J., Ciach, R., Krol, J., "Pre-Ageing of AlSiCuMg Alloys in Relation to Structure and Mechanical Properties," *Materials and Design,* vol. 18(4), 1997, pp. 253-256.

[34]   Mishra, R.K., Smith, G.W., Baxter, W.J., Sachdev, A.K., Franetovic, V., "The Sequence of Precipitation in 339 Aluminum Castings," *Journal of Materials Science,* vol. 36(2), 2001,  pp. 461-468.

[35]  Suzuki, H., Arai, I., Kanno, M., Itoi, K., "Effect of Silicon Addition on the Aging Behavior of an Al-2%Cu-0.9%Mg Alloy," *Journal of the Japan Institute of Metals,* vol. 27(5), 1977, pp. 239-245.

[36]  Li, Y.J., Brusethaug, S., Olsen, A., "Influence of Cu on the Mechanical Properties and Precipitation Behavior of AlSi7Mg0.5 Alloy During Aging Treatment," *Scripta Materialia,* vol. 54(1), 2006,  pp. 99-103.

[37]  G. G. Elizondo, S. Alkahtani, A. Samuel and F. Samuel, "Role of Ni and Zr in Preserving the Strength of 354 Aluminum Alloy at High Temperature," in *Light Metals 2014*, Hoboken, NJ, USA, J. Grandfield (ed.), John Wiley & Sons, Inc., 2014.

[38]  J. A. Lee, "Cast Aluminum Alloy for High Temperature Applications," in *TMS 2003*, San Diego, California, 2003.

[39]  R. S. Rana, R. Purohit and S. Das, "Reviews on the Influences of Alloying elements on the Microstructure and Mechanical Properties of Aluminum Alloys and Aluminum Alloy Composites," *International Journal of Scientific and Research Publications,* vol. 2, no. 6, 2012.

[40]  Lumley, R. N., et al., "The role of alloy composition in the heat treatment of aluminium high pressure die castings," *Metallurgical Science and Technology,* vol. 26.2, 2013, pp. 283-290.

[41]  H. G. E. Guillermo, "Ambient and High Temperature performance of Al-Si-Cu-Mg Based Alloys," *Metallurgical Science and Technology,* November 2014, pp.67-79.

[42]    D.H. Xiao, J.N. Wang, D.Y. Ding, S.P. Chen, "Effect of Cu content on the mechanical properties of an Al–Cu–Mg–Ag alloy," Journal of Alloys and Compounds, no. 343, 2002, pp. 77-81.

[43]    http://wpedia.goo.ne.jp/enwiki, "Reviews on the influences of alloying elements on microstructure and mechanical properties of aluminum alloys", International Journal of Scientific and Research Publications, 2012.

[44]    H. R. Ammar, C. Moreau, A. M. Samuel, F. H. Samuel and H. W. Doty, "Influences of alloying elements, solution treatment time and quenching media on quality indices of 413-type Al–Si casting alloys," *Materials Science and Engineering A,* vol. 489, no. 1, 2008, pp. 426-438.

[45]    P. Ouellet, F.H. Samuel, D. Gloria and S. Valtierra, "Effect of Mg content on the dimensional stability and tensile properties of heat treated Al-Si-Cu (319) type alloys", Ibid International Journal of Cast Metals *Res.,* vol. 10, 1997, pp. 67-78.

[46]    F.Tavitas-Medrano,J.Gruzleski,F.Samuel,S.Valtier and H.W. Doty, "Effect of Mg and Sr-modification on the mechanical properties of 319-type aluminum cast alloys subjected to artificial aging," *Materials Science and Engineering A,* no. 480, pp. 356-364, 2008.

[47]    A.M.A. Mohamed, F.H. Samuel, A.M. Samuel and H.W. Doty, "Influence of Additives on the Impact Properties of Al-10.8%Si Near-Eutectic Al-Si Alloys," Materials and Design, vol. 30(10), 2009, pp. 4218-4229.

[48]    R. Molina, P. Amalberto and M. Rosso, "Mechanical characterization of aluminium alloys for high temperature applications Part1: Al-Si-Cu alloys," *Metallurgical Science and Technology,* vol. 29-1, 2011 pp. 5-15.

[49]    G.K. Sigworth and T.A. Kuhn, "Grain Refinement of Aluminum Casting Alloys," American Foundry Society, Schaumburg, IL USA, 2007.

[50]    S. Zor, M. Zeren, H. Özkazanc and E. Karakulak, "Effect of Titanium Addition on Corrosion Properties of Al–Si Eutectic Alloys," *Protection of Metals and Physical Chemistry of Surfaces,* vol. 48, no. 5, 2012, pp. 568-571.

[51]    S.C. Bergsma, M.E. Kassne, X. Li, in: 3rd Int. Conf. on Processing and Manufacturing Advanced Mater, U.S. Department of Energy, Inc., 2000, pp.12–17.

[52]    Crepeau, P.N., "Effect of Iron in Al-Si Casting Alloys: A Critical Review," *AFS Transactions,* vol. 103, 1995, pp. 361-366.

[53]    Couture, A., "Iron in Aluminum Casting Alloys," *AFS International Cast Metals Journal,* vol. 6(6), 1984, pp. 9-17.

[54]    Bonsack, W., "Discussion on the Effect of Minor Alloying Elements on Aluminum Casting Alloys," *ASTM Bulletin,*1942, pp 45-51.

[55]    S.C. Bergsma, M.E. Kassne, The new aluminium alloy AA6069, Mater. Sci. Forum. (217–222), 1996, pp 1801–1806.

[56]    F.J. MacMaster, K.S. Chan, S.C. Bergsma, M.E. Kassner. Aluminum alloy 6069 part II: fracture toughness of 6061-T6 and 6069-T6. Materials Science and Engineering A289, 2000, pp 54–59.

[57]    R. Sharan and S.N. Prasad, "Development of aluminum alloys with rare earth additions", *Light Metal Age,* vol. 47, 1989, pp. 23-26.

[58]    R. Sharan and N.P. Saksena, "Rare earth additions to aluminum silicon alloys", *Castings,* Jan.-Feb., 1978, pp. 37-41.

[59]    R. Sharan and N. P Saksena, "Rare earth additions as modifiers of aluminum silicon alloys", *AFS Transactions,* vol. 3(1), 1978, pp. 29-33.

[60]    S.N. Prasad and R. Sharan, "Rare earth additions as modifiers to hypereutectic aluminum-silicon alloys", *Indian Foundry Journal,* June, 1985, pp. 15-18.

[61]    J.G Kaufman, Elwin L.Rooy, ASM Speciality Handbook: Aluminum Casting Alloys, ASM International, Materials Park, OH, 2004.

[62]    M. Ravi, U.T.S. Pillai, B.C. Pai, A.D. Damodaran and E.S. Dwarakadasa, "A study of the influence of mischmetal additions to Al-7Si-0.3Mg (LM 25/356) alloy", *Metallurgical and Materials Transactions A,* vol. 27(A), 1996, pp. 1283-1292.

[63]    Z. Nie, T. Jin, J. Fu, G. Xu, J. Yang, J. Zhou and T. Zuo, "Research on rare earth in aluminum", *Materials Science Forum,* vol 396-402, 2002, pp. 1731-1736.

[64]    Taylor, J.A., Schaffer, G.B., StJohn, D.H., "The Role of Iron in the Formation of Porosity in Al-Si-Cu-Based Casting Alloys: Part I. Initial Experimental

Observations," *Metallurgical and Materials Transactions A,* vol. 30(6), 1999, pp. 1643-1650.

[65]   J. Gobrecht, "Ségrégation par Gravité du Fer, du Manganèse et du Chrome dans les Alliages Al-Si de Fonderie," *Fonderie,* No. 367, 1977, pp. 171-173.

[66]   J.L. Jorstad, Understanding "Sludge", *Die Casting Engineer,* Nov-Dec 1986, pp. 30- 36.

[67]   Lakshmanan, A.N., Samuel, F.H., Gruzleski, J.E., "Crystallization Behavior of Iron Containing Intermetallic Compounds in 319 Aluminum Alloy," *Metallurgical and Materials Transactions,* vol. 25(8), 1994, pp. 1761-1774.

[68]   Triveno Rios, C, Caram, R., Bolfarini, C, Botta F., W.J., Kiminami, C.S., "Intermetallic Compounds in the Al-Si-Cu System," *Acta Microscopica,* vol. 12(1), 2003, pp. 77-81.

[69]   Dinnis, C.M., Taylor, J.A., Dahle, A.K., "Iron-Related Porosity in Al-Si-(Cu) Foundry Alloys," *Materials Science and Engineering A,* vol. 425, 2006, pp. 286-296.

[70]   J.D. Robson and P.B. Prangnell, "Dispersoid Precipitation and Process Modelling in Zirconium Containing Commercial Aluminum Alloys," *Acta Materialia*, vol. 49, 2001, pp. 599-613.

[71]   J.D. Robson, "Optimizing the Homogenization of Zirconium Containing Commercial Aluminum Alloys Using a Novel Process Model," *Materials Science and Engineering A*, vol. 338A, 2002, pp. 219-229.

[72]   C.H. Câceres, "A Rationale for the Quality Index of AI-Si-Mg Casting Alloys," *International Journal of Cast Metals Research,* vol. 10, 1998, pp. 293-299.

[73]   C.H. Câceres, "A Phenomenological Approach to the Quality Index of AI-Si-Mg Casting Alloys," *International Journal of Cast Metals Research,* vol. 12, 2000, pp. 367-375.

[74]   Z. Ma, A.M. Samuel, F.H. Samuel, H.W. Doty, and S. Valtierra, "A Study of Tensile Properties in Al-Si-Cu and Al-Si-Mg Alloys: Effect of $\beta$-iron Intermetallics and Porosity," *Materials Science and Engineering A*, vol. 490, 2008, pp. 36-51.

[75]   M.B. Durdjevic, B. Duric, A. Mitrasinoniv, and J.H. Sokolowski, "Modeling of Casting Processes Parameters for the 3xx Series of Aluminum Alloys Using the Silicon Equivalency Algorithm," *Association of Metallurgical Engineers Serbia and Montenegro*, vol. 9, 2003, pp. 91-106.

[76]   F.H. Samuel, A.M. Samuel, and H.W. Doty, "Factors Controlling the Type and Morphology of Cu-Containing Phases in 319 Al Alloy," *AFS Transactions*, vol. 104, 1996, pp. 893-901.

[77]   F.H. Samuel, A.M. Samuel, and H. Liu, "Effect of Magnesium Content on the Aging Behaviour of Water-Chilled Al-Si-Cu-Mg-Fe-Mn (380) Alloy Castings," *Journal of Materials Science*, vol. 30, 1995, pp. 1-10.

[78]   A.M. Samuel and F.H. Samuel, "Review: Various Aspects Involved in the Production of Low Hydrogen Aluminum Castings," Journal of Materials Science, vol. 27, 1992, pp. 6533-6563.

[79]    J. Campbell, "The Solidification of Metals," Iron and Steel Institute, Publication No. 110, London, 1967, pp. 18-26.


[80]    K. Kubo and R.D Pehlke, "Mathematical Modeling of Porosity Formation in Solidification," Metallurgical Transactions B, vol. 16B, 1985, pp. 359-366.

[81]    N. Roy, A.M. Samuel and F.H. Samuel, "Porosity Formation in Al-9 Wc Pet Si-3 Wt Pet Cu Alloy Systems: Metallographic Observations", *Metallurgical and Materials Transactions A,* vol. 27A, 1996, pp. 415-429.

[82]    N. Roy, "Etude parametrique de revolution de la porosite dans le system Al-9%Si-3%Cu", M. Eng. Thesis, UQAC, Chicoutimi, QC, Canada, December 1994.

[83]    G.A. Edwards, G.K. Sigworth, C.H. Caceres, D.H. StJohn, and J. Barresi, "Microporosity Formation in Al-Si-Cu-Mg Casting Alloys", AFS *Transactions,* vol.105,1997, pp. 809-818.

[84]    G. E. Dieter, *Mechanical Metallurgy*, Third Ed., McGraw-Hill, Boston, 1986, p.751.

[85]    Z. Jia, G. Hu, "Effect of Homogenization and Alloying Elements on Resistance of Al- Zr Mn Alloys," *Materials Science and Engineering A*, vol. 444A, 2007, pp.284-290.

[86]    H. Liao, Y. Sun and G. Sun, "Effect of Al-5Ti-1B on the microstructure of Near-Eutectic Al-13%Si Alloys Modified with Sr," *Materials Science*, vol. 37, 2002, pp. 3489-3495.

[87] R. Mahmudi, P. Sepehrband and H.M. Ghasemi, "Improved properties of A319 aluminum casting alloy modified with Zr," *Materials Letters,* vol. 60, 2006, pp. 2606-2610.

[88] K. Yu, W. Li, S. Li and J. Zhao, "Mechanical Properties and Microstructure of Aluminum Alloy 2618 with Al3(Sc,Zr) Phases," *Materials Science and Engineering A*, vol. A368, 2004, pp. 88-93.

[89] P. Sepehrband, R. Mahmudi and F. Khomamizadeh, "Effect of Zr Addition on the Aging Behavior of A319 Aluminum Cast Alloy," *Scripta Materialia*, vol. 52, 2005, pp. 253-257.

[90] R. Mahmudi, P. Sepehrband and H.M. Ghasemi, "Improved properties of A319 aluminum casting alloy modified with Zr," *Materials Letters,* vol. 60, 2006, pp. 2606-2610.

[91] E. Rincon, H.F. Lopez, M.M. Cisneros, H. Mancha, and M.A. Cisneros, "Effect of temperature on the tensile properties of an as-cast aluminum alloy A319," *Materials Science and Engineering A*, vols. 452-453, 2007, pp. 682-687.

[92] Z. Li, A.M. Samuel, F.H. Samuel, C. Ravindran, S. Valtierra, and H.W. Doty, "Parameters controlling the performance of AA319-type alloys Part I: Tensile Properties," *Material Science and Engineering A*, vol. A367, 2004, pp. 96-110.

[93] M. Drouzy, S. Jacob and M. Richard, "Interpretation of Tensile Results by Means of Quality Index and Probable Yield Strength," *AFS International Cast Metals Journal,* vol. 5, 1980, pp. 43-50.

[94]    S. Jacob, "Quality Index in Predicting of Properties of Aluminum Castings-A Review," *AFS Transactions,* vol. 108, 2000, pp. 811-818.

[95]    A.L. Dons, G. Heiberg, J. Voje, J.S. Maeland, J.O. Loland and A. Prestmo, "On the Effect of Additions of Cu and Mg on the Ductility of Al-Si Foundry Alloys Cast with a Cooling Rate of Approximately 3 K/s," *Materials Science and Engineering A*, vol. 413-414, 2005, pp. 561-566.

[96]    S. Abis, M. Massazza, P. Mengucci, and G. Tiontino, "Early Ageing Mechanisms in a High-Copper AlCuMg Alloy," *Scripta Materialia*, vol. 45, 2001, pp. 685-691.

[97]    S.C. Wang, M.J. Starink, and N. Gao, "Precipitation Hardening in Al-Cu-Mg Alloys Revisited," *Scripta Materialia*, Vol. 54, 2006, pp. 287-291.

[98]    P. Ratchev, B. Verlinden, P. De Smet, and P. Van Houtte, "Effect of Cooling Rate and Predeformation on the Precipitation Hardening of an Al-4.2wt%Mg-0.6wt%Cu Alloy," *Scripta Materialia*, vol. 38(8), 1998, pp. 1195-1201.

[99]    P. Ratchev, B. Verlinden, P. De Smet, and P. Van Houtte, "Precipitation Hardening of an Al-4.2wt%Mg-0.6wt%Cu Alloy," *Acta Materialia*, vol. 46(10), 1998, pp. 3523-3533.

[100]   G.K. Sigworth and C.H. Cáceres, "Quality Issues in Aluminum Net Shape Castings," *AFS Transactions*, vol. 112, 2004, pp. 1-15.

[101]   N.D. Alexopoulos, "Generation of Quality Maps to Support Material Selection by Exploiting the Quality Indices Concept of Cast Aluminum Alloys," *Materials and Design*, vol. 28, 2007, pp. 534-543.

[102] H. Ammar, "Influence of Metallurgical Parameters on the Mechanical Properties and Quality Indices of Al-Si-Cu-Mg and Al-Si-Mg Casting Alloys," PhD. Thesis, university of Quebec, Chicoutimi, Canada (2010).

[103] S.A. Musmar, "In-situ Thermal Analysis Probe," Ph.D Thesis, McGill University, Montreal, Canada (2006).

[104] T. Gladman, "Precipitation Hardening in Metals," *Materials Science and Technology*, Vol. 15, 1999, pp. 30-36.

[105] F.J. Tavitas-Medrano, "Artificial Aging Treatments of 319-Type Aluminum Alloys," PhD. Thesis, McGill University (2007).

[106] De la Sablonnière, H. and F.H. Samuel, "Solution heat treatment of 319 aluminum alloy containing ~ 0.5wt%Mg", Part2-microstructure and fractography, International Journal of Cast Metals Research, 9(4), 1996, pp.213-225.